INNOVATIVE POLYMERS FOR LITHIUM-O2 RECHARGEABLE BATTERIES

Marta Alvarez Tirado | PhD Thesis 2022

Innovative Polymers for Lithium-O₂ Rechargeable Batteries

Marta Alvarez Tirado

PhD Thesis 2022

Supervised by:

Professor David Mecerreyes (UPV/EHU)
Dr Laurent Castro (Toyota Motor Europe)

OUTLINE

CHAPTER 1.- INTRODUCTION

CHAPTER 2.- DESIGNING SINGLE-ION GEL POLYMER ELECTROLYTES BY PHOTOPOLYMERIZATION SUITABLE FOR LI-O₂ BATTERIES

CHAPTER 3.- 1,2,3 – TRIMETHOXYPROPANE: A GLYCEROL-DERIVED GLYME WITH LOW TOXICITY AS ELECTROLYTE FOR LITHIUM-O$_2$ BATTERIES

CHAPTER 4.- DESIGNING HIGHLY CONDUCTIVE IONGEL SOFT SOLID ELECTROLYTES SUITABLE FOR LI-O₂ BATTERIES

CHAPTER 5.- VERSATILE HIGH RATE PYRROLIDINIUM-BASED BINDERS FOR LI-O$_2$ AIR ELECTRODES

Chapter 1

Introduction

1.1 Global energy needs

We live in a world with increased population in which thousands of devices improve the quality of our lives in many ways. However, they require energy to work. This high demand of energy (both production and use) pushes our natural ecosystem as, so far, we have a high dependency on fossil fuels and there is a poor energy management[1].

The production and use of energy account for more than 75% of the EU's greenhouse gas emissions. Decarbonizing the EU's energy system is therefore critical to reach our 2030 climate objectives and the EU's long-term strategy of achieving carbon neutrality[2]. Beyond gas emission to the atmosphere and their impact in the climate, the society also pays an important penalty in terms of pollution (with an impact on human health) or loses in biodiversity[3]. Hence, the importance of these initiatives and their implementation.

Without any doubt, climate change is - and will be - the biggest challenge of our society.

Therefore, there is an urgent need to take actions against climate change. In 2015, the Paris Agreement was born during the COP21 international climate summit. On that event, every country brought by the United Nations (UN) agreed to work together to limit global warming below 2 degrees, with an ideal case of 1.5. The last global summit, COP26, took place in Glasgow (UK) in October 2021. Nearly 200 countries participated and some details of the Paris Agreement were finalized[4].

As part of its climate-fight strategy, the 27 EU Member States outlined the *European Green Deal*, a proposal committed to turn the EU into a climate neutral continent by 2050[2]. To achieve this, emissions need to be reduced by at least 55 % by 2030 (compared to 1990 levels). In fact, transport accounts for ~ 25% of greenhouse gas

emissions. Within these transport emissions, *road transport* emits the 72 % (as per data of 2019 of all domestic and international transport)[5].
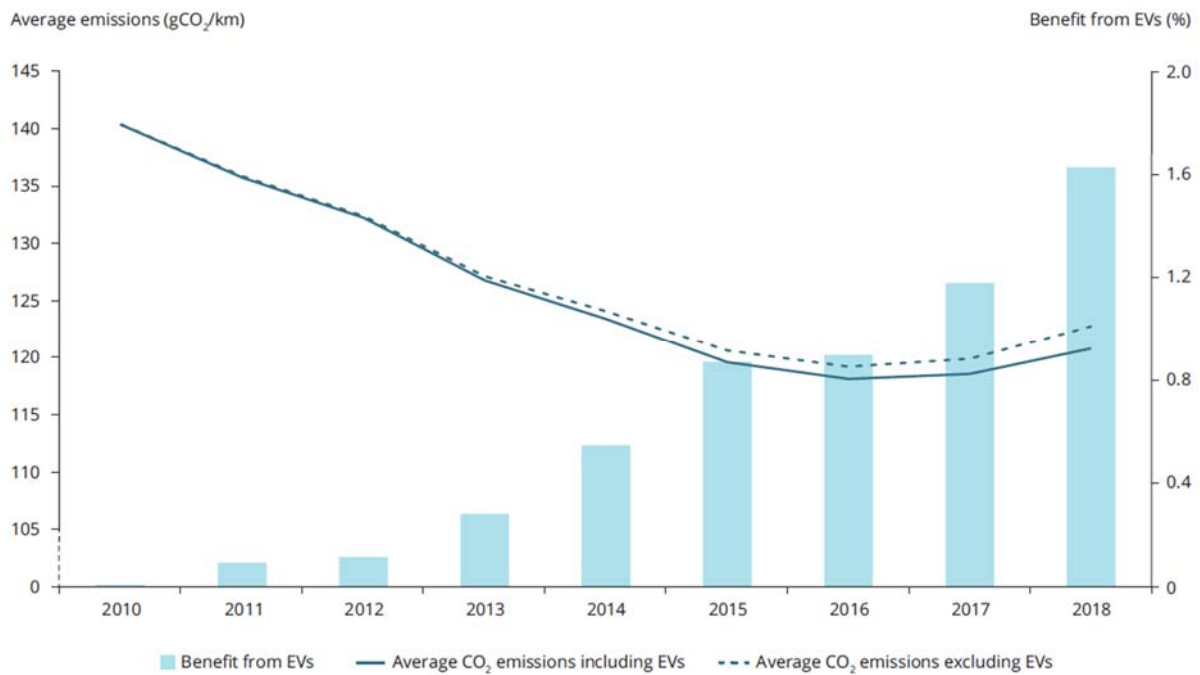
Figure 1. 1. Average CO_2 emissions (gCO_2/km) in the EU from 2010 to 2018 (with/without electric cars). Reproduced with permission from literature[6].

Hence, one key change is to make transport sustainable. For that, the EU proposes to reduce 50-55 % CO_2 emissions from cars and vans by 2030 and eliminate them from new cars by 2035. And, by 2050, the transport sector has to reduce these emissions by 90 %[7].

However, this target seems contradictory with actual data[8] (Figure 1.1). The reality is that transport emissions have steadily risen in recent years by 0.8%, with the exceptional case of 2020 (dropped of 12.7 %) due to the decreased activity inflamed by the COVID-19 pandemic[5]. Only Finland, Sweden and the Netherlands reported a 5.8-6 % reduction[5].

To push the strategy on the transport sector, the EU announced on December 2020 a *Sustainable and Smart Mobility Strategy*[3]. This strategy relays in three pillars: reduce the dependency on fossil fuels, shift freight transports from road to rail or inland waterways and, finally, reduce costs by internalising external costs[9].

"National projections compiled by the EEA indicate that even with measures currently planned in the Member States, domestic transport emissions will only drop below their 1990 level in 2029. International transport emissions (aviation and maritime) are projected to continue increasing." [5]

To reduce the dependency on fossil fuels the EU proposes to increase the use of energy from renewable sources or low-carbon fuels (e.g. bio-fuels) and use low and zero-emission vehicles, tightening the use of combustion engine vehicles. By 2030, it is aimed to have at least 30 million zero-emission cars on the road. By 2050, almost all vehicles (cars, vans, buses, trucks) will be zero-emission.

Therefore, electrochemical energy storage devices are, and will be, essential key technology enablers not only in the energy storage (electricity grids) and consumer electronics[10], but also in the transport sector.

1.1.1 Example of Toyota Global strategy towards climate change

Following the significant environmental issues declared by the *United Nations (UN) 2030 Agenda* and the *17 Sustainable Development Goals* program, Toyota Motor Corporation announced in 2015 the *Toyota Environmental Challenge 2050*, a set of six challenges seeking to make an environmental commitment in which Toyota aims to become carbon neutral by 2050 (Figure 1.2).
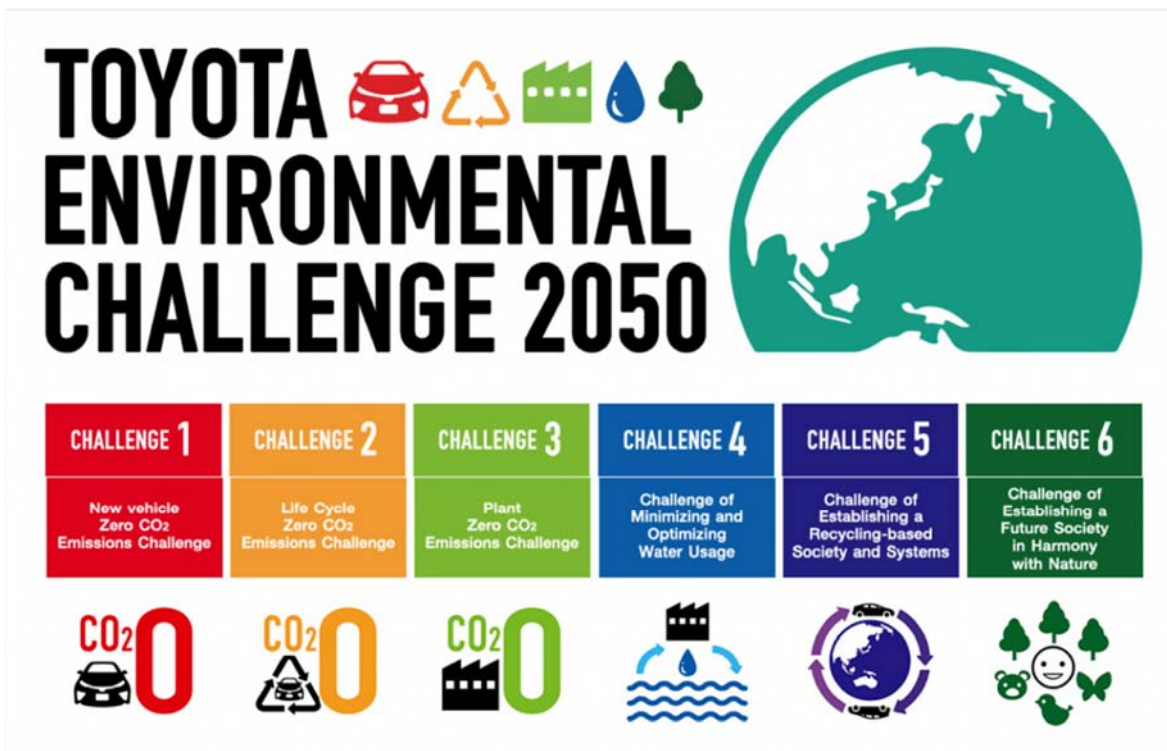
Figure 1. 2 Toyota environmental challenge 2050. *Source: Toyota Global* [11].

The first challenge aims to reduce or eliminate CO_2 emissions from new vehicles by 90%. Challenge 2 and 3, aims to eliminate CO_2 emissions from operations and suppliers. Challenge 4 and 5 supports the protection of water resources and supports a RRRR society (Reduce, Reuse, Recycle, Recover). The last one, Challenge 6, aims to establish a society in harmony with nature.

1.1.2 Electrochemical energy storage devices

Energy storage devices (either chemical, electrochemical, electrical, mechanical or thermal technologies) can significantly contribute to the implementation of these strategies. Within all these possibilities, the electric and electrochemical energy storage devices are the most known, including systems such as rechargeable batteries, fuel cells, flow batteries, or capacitors and supercapacitors[12].

Rechargeable batteries are able to store energy on an electrochemical cell from an external electrical source and supply it on demand. Examples include from lead-acid systems (operating for over 150 years) or more advanced nickel-metal hydride or

lithium-based systems. Fuel cells are also able to supply energy, but key components are continuously supplied from an external source, instead of being on the cell itself. Possibly the most known example is the hydrogen-oxygen fuel cell. Flow batteries work similarly to a rechargeable battery, but key components for the energy storage are stored externally in tanks. Some examples include vanadium flow batteries or zinc-bromide hybrid flow batteries. Conventional capacitors can store the energy by electrostatic interactions in the electric fields; and the supercapacitors can store it at the electrode-electrolyte interface, where ions are adsorbed into the electrode. This is why these devices are also called double-layer capacitors[12].

Overall, the choice of the device relies on the needs of the requirement. For example, batteries and fuel cells can store a high amount of energy by mass (gravimetric energy density), but they can only release it in long times (low power density). Capacitors seat on the opposite side, where they can liberate the energy in very short times but in short quantities. This information is typically visually plotted on the so-called *Ragone* plots (Figure 1.3)[13–15].
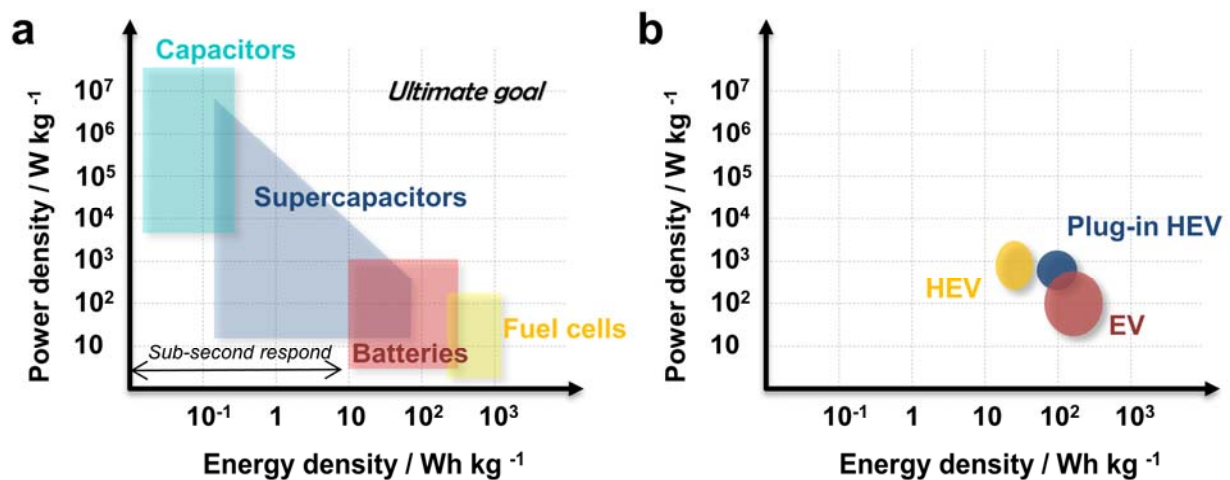
Figure 1. 3. a) Ragone plot of electrochemical energy devices. Figure adapted from literature[12]; and b) Ragone plot for various types of electrified vehicles (EV, electric vehicle; HEV, hybrid electric vehicle). Figure adapted from literature[15,16].

Within the automotive world, there are four main types of electrified vehicles aligned: hybrid electric vehicles (HEV), plug-in hybrid electric vehicles (PHEV), full electric vehicles (EV, also called sometimes battery electric vehicles (BEV)); and the very recently commercialized, fuel cell electric vehicles (FCEV).

More particularly, rechargeable batteries with a very high round-trip efficiency have a tremendous potential on full electric vehicles, possibly being one of the key technologies help achieving the 2 °C Paris Agreement and the European Green Deal targets. According to the Global Battery Alliance[17], batteries could enable 30 % of the required reductions in energy.

"Batteries are among the key technologies enabling a climate-neutral Europe by 2050" [18]

Current rise on batteries demand is stunning, and it is growing even faster (Figure 1.4). Actually, global battery demand is expected to grow by 25 % every year and reach 2600 GWh in 2030[10,17]. Predictions shared that only Europe alone will need 200 GWh of annual cell production in the next five years[18] and it is expected that around 34 million of electrified vehicles (HEVs, PHEVs and BEVs) will be sold globally by 2030[17].
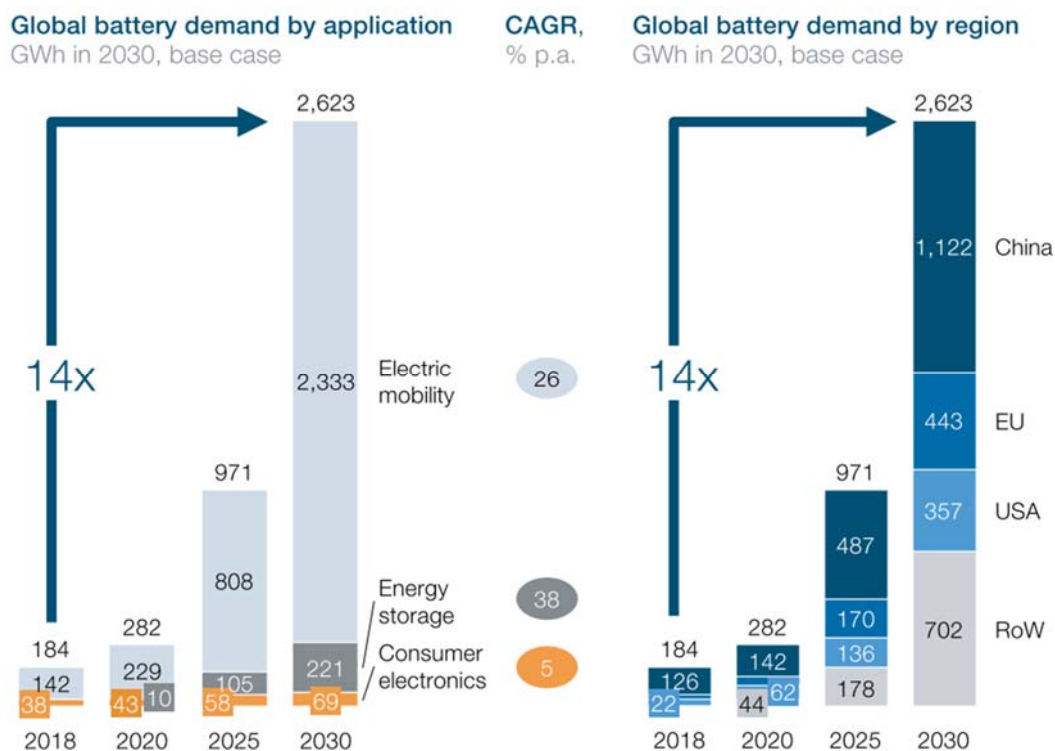
Figure 1. 4. Global battery growth until 2030, divided by industry application and regions. Reproduced with permission from literature[17].

Despite the full range of battery technologies available, the absolute ruler of the high energy density market are the lithium-ion batteries (LIB)[19,20], further recognized by the Noble Prize in Chemistry in 2019[21]. Its huge success is strongly related to the balance of lifetime, safety, power, costs or energy density; key parameters in the EV economy[20].

"It is a major paradox of the digital era that some of the world´s richest and most innovative companies are able to market incredibly sophisticated devices without being required to show where they source raw materials"
– Emmanuel Umpula, Afrewatch Executive Director

Overall, it is clear that LIBs are a key enabler technology in terms of road transport sustainability. However, it is fundamental to understand that the metals and materials demand for LIB packs in EVs is also raising tremendously. LIB´s most popular cathodes (positive active materials) and anodes (negative active materials), such as $LiNi_xCo_yAl_zO_2$ (NCA), $LiCoO_2$ (LCO), $LiMn_2O_4$ (LMO), $LiFePO_4$ (LFP), $LiNi_xMn_yCo_zO_2$ (NMC) or graphite[20], are obtained from ores (lithium, cobalt, manganese, etc) that are concentrated only in few countries worldwide (i.e. ~60-65% of the world´s cobalt or flake graphite production is in Congo and China, respectively)[20,22]. This might lead to geopolitical challenges as well as limitations in the production capacity of the mining. Actually, there are already important concerns about unethical mining practices, in which child labour has been alarmed [22,23].

1.1.3 Beyond lithium-ion batteries

This outlook in materials resourcing and global demand is forcing the research community to look into other battery chemistries; and to put efforts in the development of new materials and batteries that are more sustainable (recycling cycle implementation or batteries based on naturally abundant elements) and efficient (longer lives, higher energy densities, etc)[20,22]. Moreover, safety, cost, lifetime, energy and power densities need to be taken into account in this development.

Beyond lithium-ion batteries, there are several chemistries based on other active metals such as sodium, potassium, aluminium, magnesium or calcium that can be

used as potential candidates (Figure 1.5). Lithium-based batteries can be further exploited in more efficient technologies that show superior properties than other chemistries, unveiling a good combination of higher energy and specific power than other systems[13]. They can be paired with positive electrodes such as sulphur (Li-S) or oxygen (Li-O$_2$) (conversion type), or intercalating cathodes (metal oxides, e.g. LiCoO$_2$); exhibiting energy densities as high as ~400 - 500 Wh/ kg, overtaking LIBs (~280 Wh/ kg)[24].
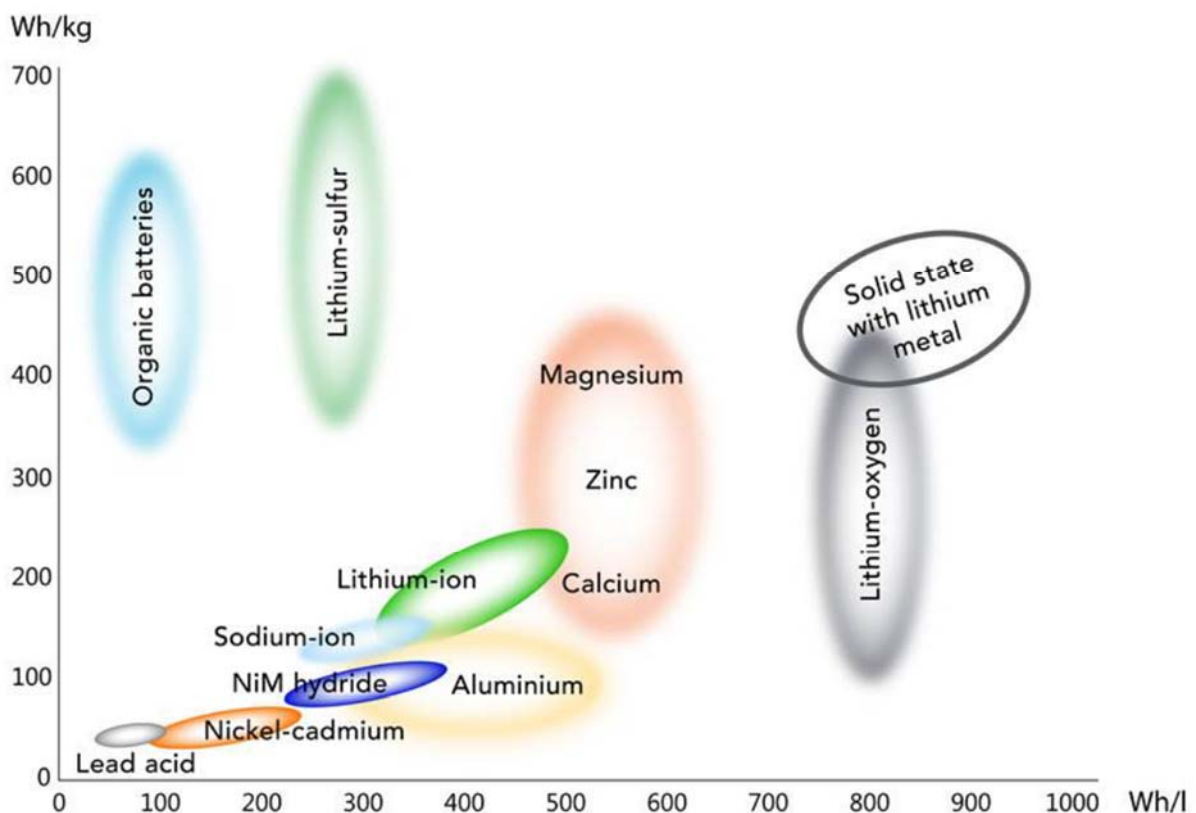
Figure 1. 5. Specific against volumetric energy density of current battery technologies. Note from the original author: there is a large uncertainty of their respective position in the graph. Reproduced with permission from literature[18].

Amongst all of them, rechargeable lithium−air/Li−O$_2$ batteries are possibly one of the most attractive candidates due to their remarkable theoretical specific energy density (~11,000 Wh/ kg; considering a theoretical capacity of ~3800 Ah/ kg and a potential of ~ 3V versus lithium metal)[25], which is directly comparable to that of gasoline (~13,000 Wh/ kg)[26].

Some metal-air primary batteries are already commercialized. For example Zn-air cells have been sold for consumer applications such as hearing aids for decades[27]. Rechargeable Li−O$_2$ batteries are on another technology readiness level, though. As described, practical and theoretical energies are still far from each other, but the research community is putting many efforts to shrink this gap.

1.2 Lithium-air/ Lithium-O$_2$ batteries

1.2.1 Working principles

The metal-air batteries family, recently denoted as "post lithium-ion batteries" [28], have a hybrid architecture between batteries and fuel cells because they couple a metal negative electrode with an air positive electrode. This configuration differs from other systems such as LIBs or Nickel-metal hydride (NiMH) because the oxygen is one of the active materials and it is brought from the atmosphere to the cell through the air electrode, functioning as an *open* system[29]. If lithium metal is used, they are called Li-air. Actually, they are also frequently named Li-O$_2$ due to practical testing conditions as, so far, they are usually operated under pure oxygen gas flows, or oxygen flows with controlled humidity or CO$_2$ traces.

The first workable Li-air system was presented 25 years ago by Abraham et al.[30], and, nowadays, the cell configuration revealed by them remains very similar.
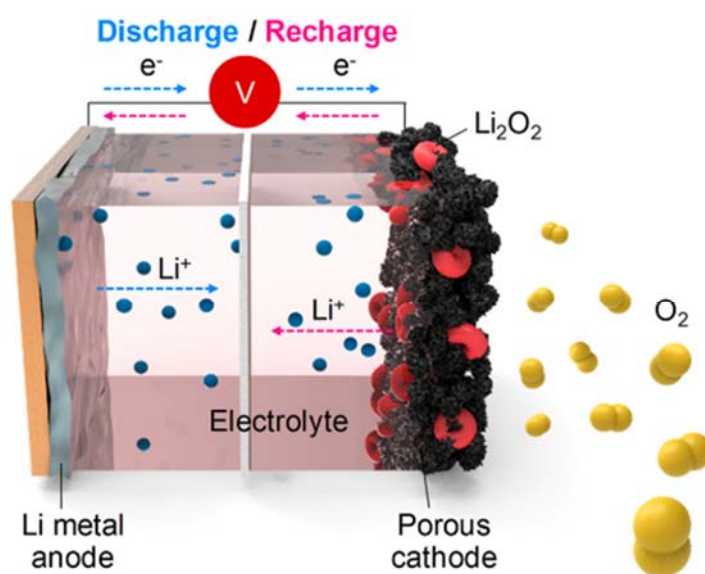
Figure 1. 6. Representation of a Li-O$_2$ battery. Reproduced with permission from literature[28].

Generally, it is formed by three basic parts: two electrodes and an electrolyte. A metallic lithium film is used as the negative electrode (also named as *anode*) and it is assembled together with a composite positive electrode (also named as *cathode, air-cathode* or *air-electrode*). This electrode is usually formed by a conducting and porous gas diffusion layer that allows electrochemical contact between the oxygen gas and the lithium ions, active materials of this cell. Between the negative and positive electrodes, there is a Li$^+$ containing electrolyte that isolates them electronically (Figure 1.6)[28].

Primarily, the electrolyte plays an essential role on Li-O$_2$ batteries as it determines the electrochemical reactions of the cells (Figure 1.7). Depending on the chemistry, Li-O$_2$ cells currently classify in four categories: non-aqueous (or aprotic), aqueous, hybrid and solid state [28,31].
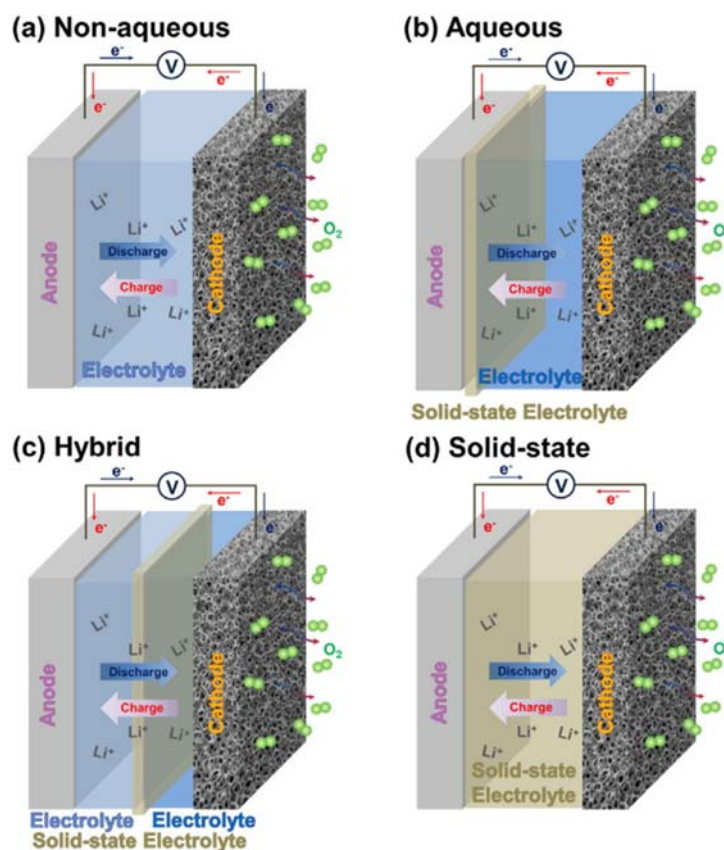
Figure 1. 7 Four possible configurations of Li-O$_2$ batteries. Reproduced with permission from literature[32].

Conventional non-aqueous or aprotic electrolytes are usually formed by a lithium salt dissolved in an aprotic organic solvent. Non-aqueous or aprotic electrolytes are, by

far, the most popular ones due to their highest capacities and wider stabilities against lithium.

Aqueous electrolytes are non-flammable, low-cost and have a high ionic conductivity. However, they have more corrosive environments than organic solutions, and a limited electrochemical/ temperature window due to water properties. The solutions are usually alkaline; otherwise there will be large amounts of H^+ reacting with the lithium metal[31].

In order to improve aqueous systems, hybrid electrolyte cells were developed. The cell has two compartments, one aqueous-based facing the air electrode (catholyte); and one aprotic-based facing the lithium metal (anolyte). These sections are separated by a solid membrane, such as NASICON[28], available on the Ohara catalogue for example[33]. These cells improve lithium conductivity but the diffusion kinetics and the overall system turn them too complicated.

Solid-state cells do not use a liquid electrolyte. Instead, they use as a electrolyte solid-state lithium ion conducting materials that can be polymers, oxide or glass-ceramics or single-crystalline silicon. Oxide ceramics such as NASICON-type, e.g. $Li_{1+x} Al_x Ti_{2-x} (PO_4)_3$ (LATP) or $Li_{1+x} Al_x Ge_{2-x} (PO_4)_3$ (LAGP) [34] have been most widely studied thanks to their lower air – sensitivity, despite their lower conductivity. On the other hand, in the last years polymer-based electrolytes are becoming increasingly popular as reported in the next section.
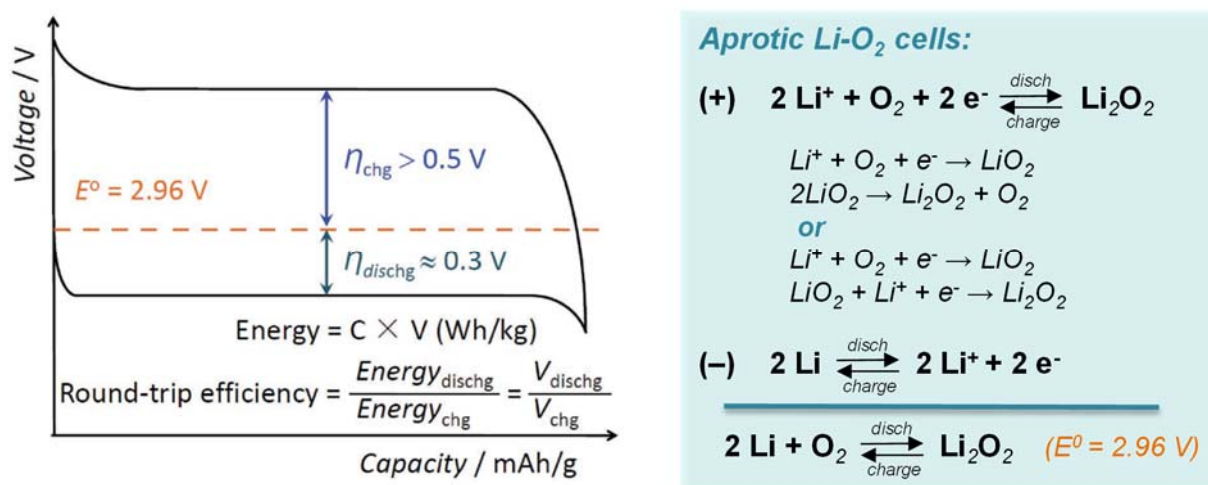
Figure 1. 8. Typical potential profile during discharge/charge of a Li-O$_2$ cells and electrochemical reactions involved. Figure adapted from literature [35].

The electrochemical reactions of Li-O_2 cells involves the oxygen and lithium redox reactions. The lithium metal is dissolved/deposited at the negative side, whilst the oxygen-evolution reaction (OER) and the oxygen-reduction reaction (ORR) occur at the positive side[28].

The typical reactions in aprotic Li-O_2 cells were first proposed by Abraham and co-workers in 1996[36]. During discharge, the ORR process leads to the formation of lithium peroxide (Li_2O_2) at the cathode side, which is the main discharge product. The formation of this insoluble peroxide is not direct and it can involve one or two electrons transfer processes (Figure 1.8). In both cases, a lithium ion first reacts with an oxygen radical (O_2^-) to form lithium superoxide (LiO_2). This superoxide is very unstable; hence, it can either disproportionate and form Li_2O_2 (one electron transfer); or it can either go through another electron transfer process (two electron transfer)[28,32].

During discharge (Figure 1.8), the cells first experiment an Ohmic drop (iR), reaching quickly a plateau at around 2.7 V vs Li^0/Li^+, which corresponds to the practical redox potential of the spontaneous reaction $2Li + O_2 + 2e^- \rightarrow Li_2O_2$[37]. This potential is around 0.3 V (η_{dischg}) below the redox equilibrium potential (2.96 V vs Li^0/Li^+). Charge overpotentials (η_{chg}) are, bare minimum, 0.5 V above O_2/O_2^- redox potential[35]. This leads to a drop in the round-trip efficiency, even that part of the energy during charge or discharge will be lost.

1.2.2 Challenges of Li−O_2 cells and prospects

Li-O_2 batteries have been investigated for a long period of time due to their huge potential, but practical deployment is still limited due to a number of unsolved challenges that can be summarized in Figure 1.9.

These unresolved challenges are related to the high reactivity of the electrolyte and the carbon-base electrode with the oxygen superoxide radicals (O_2^-); the limited rate capability (applied current densities are 1-2 orders of magnitude below LIBs); the growth of lithium dendrites at the lithium surface; and/or the relatively high polarization overpotentials achieved during cycling[38].
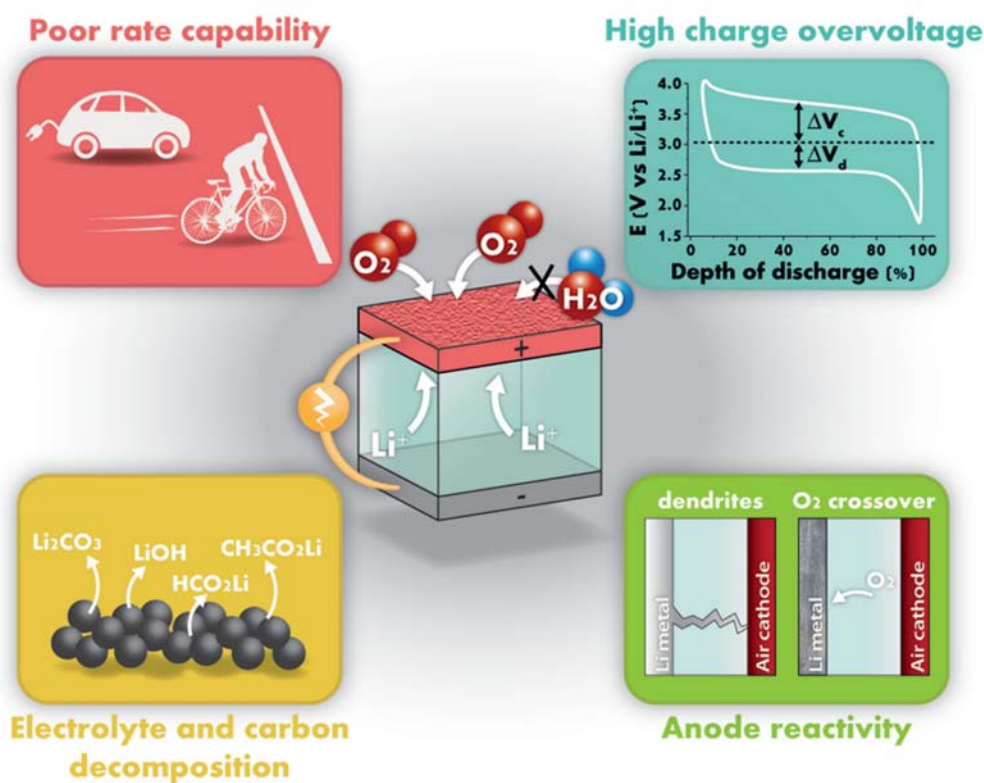
Figure 1. 9. Main challenges encountered by Li-air/Li-O_2 batteries. Reproduced with permission from literature [38].

To mitigate this, researchers are focusing efforts in different directions, including strategies to protect lithium metal or achieve lower polarization overpotentials allowing a higher round-trip efficiencies and rate capability. One of the most plausible approaches is based on the development of solid/quasi-solid Li-O_2 batteries [39]. By using them, the volatility of liquid electrolytes will be avoided, enlarging operating cell live and avoiding potential safety hazards caused by the leak of toxic organic solvents. Even further, lithium dendrites growth could be mitigated.

1.3 Electrolytes for Li-O₂ batteries

1.3.1 Non-aqueous liquid electrolytes
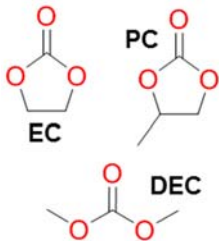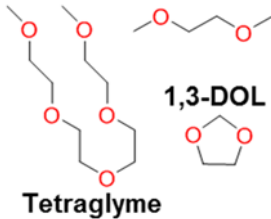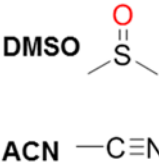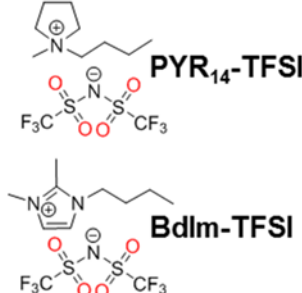
Conventional non-aqueous liquid electrolytes are formed by a lithium salt dissolved in an organic aprotic solvent. Some desirable properties of these electrolytes are[40]:

- Low volatility and moisture absorption as well as non-flammability; due to the open-cell configuration.
- Formation of a stable solid electrolyte interphase (SEI), in order to protect the lithium metal.
- High oxygen solubility and diffusivity, especially on the catholyte side in order to improve oxygen availability.
- High electrochemical stability to oxygen reduction species, such as the highly reactive superoxide radical (O_2^-).
- High donor number, in order to promote solution mediated pathways for the formation of toroidal Li_2O_2 particles, which improves the cell capacity.

Common aprotic solvents used in electrolytes are organic carbonates (e.g. ethylene carbonate (EC), propylene carbonate (PC) or dimethyl carbonate (DMC)); ethers (e.g. tetrahydrofuran (THF), 1,3-dioxolane (DOL), dimethoxyethane (DME) or diethylene glycol dimethyl ether (diglyme)); or others such as dimethyl sulfoxide (DMSO), acetonitrile (ACN) or ionic liquids [38,41]. Most common ones are reported in Table 1.1 [40].

Carbonate solvents were initially deeply studied for Li-O_2 cells, following the inertia of LIBs. However, it has been demonstrated to be dramatically unstable in the presence of oxygen radicals and form Li_2CO_3 as the main discharge decomposition product. Ether solvents have higher stability than carbonates against superoxides, but they can also experience decomposition during cycling. DMSO- and ACN- based electrolytes can have high conductivity and has a higher stability against the O_2/O_2^- redox couple. However, DMSO can react with the carbon electrodes; and ACN can be unstable against lithium metal.

Table 1. 1. Some common non-aqueous solvent electrolytes for Li-O$_2$ batteries. Adapted from literature [40].

Electrolytes	Candidates	Positive	Negative
Carbonate-based [a]	PC, EC, DEC	Relative low volatility; Wide electrochemical window; Wide temperature range	Highly unstable against O$_2^-$ radicals
Ether-based [b]	DME, 1,3-DOL, Tetraglyme	Low volatility; Higher stability than carbonates; Stable against lithium metal	Can be unstable towards O$_2^-$ radicals
DMSO, ACN [c]	DMSO, ACN	High conductivity; Low viscosity	High volatility; Can react with carbon electrodes and/or lithium metal
Ionic liquids [d]	PYR$_{14}$-TFSI, BdIm-TFSI	Wide electrochemical windows; Low volatility; Low flammability; Higher stability towards O$_2^-$ radicals	Lower conductivity; Higher viscosity

[a] EC (ethylene carbonate), PC (propylene carbonate); DEC (dimethyl carbonate)
[b] Tetraglyme (tetraehtylene glycol dimethyl ether); DME (1,2,-dimethoxyethane); 1,3-DOL (1,3- dioxolane)
[c] DMSO (dimethyl sulfoxide); ACN (acetonitrile)
[d] PYR14-TFSI (1-Butyl-1-methyl pyrrolidium bis(trifluoromethanesulfonyl) imide); BdIm-TFSI (1-Butyl-2,3-dimethyl-imidazolium bis(trifluoromethanesulfonyl) imide)

Hence, when looking to the best-in-performance, glyme-based liquid electrolytes are on the top list. Among all, tetraethylene glycol dimethyl ether (also named as tetraglyme, G4 or TEGDME) is the most used due its low volatility (requirement for the open-to-air cells), wide electrochemical window (beyond 4.5 V versus Li^0/Li$^+$) good solubility of metal alkali salts and relatively low cost [42–46]. However, it is important to keep in mind that this aprotic solvent comes from petroleum-based sources and it is highly flammable and toxic for the environment and humans in case of leaking.

On the other hand, ionic liquids (IL) seem a good alternative to conventional flammable organic solvents due to a combination of good transport properties, non-volatility, low toxicity, non-flammability and stability to superoxide radicals [47,48]. Ionic liquids are liquid salts at room temperature. The most investigated ionic liquids in Li-O$_2$ batteries are based on imidazolium- and pyrrolidinium- cations [47,49–52] and fluorine-based anions (i.e. bis(trifluoromethanesulfonyl)imide, TFSI) [53].

In the same way than in solvents, the selection of the lithium salt is important as it has a big impact in the viscosity, electrolyte degradation (oxygen and lithium superoxides can attack them) or the oxygen solubility [54]. First studies on this type of batteries revealed that the most common salts in LIBs (i.e. LiPF$_6$) were highly unstable in Li-O$_2$ batteries.
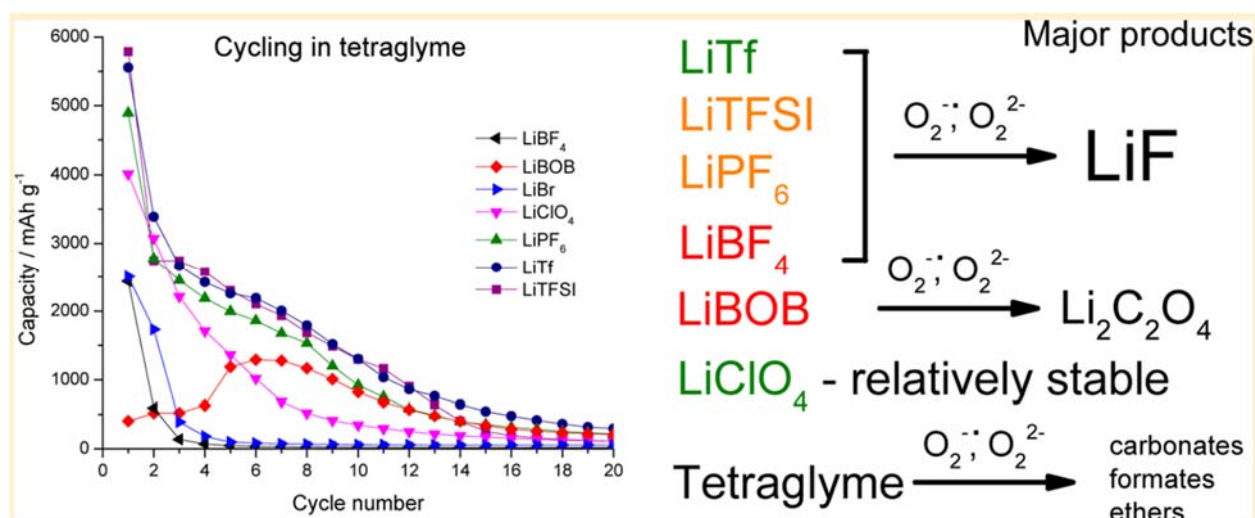
Figure 1. 10. Major degradation products during discharge of some lithium salts. Reproduced with permission from literature [43].

Since then, many efforts have been given to study the effect of electrolyte salts in the performance of Li-O$_2$ batteries and different lithium salts have been evaluated: LiCF$_3$SO$_3$, LiTFSI, LiClO$_4$, LiNO$_3$, etc. For example, a study of Zhang and co-workers [43] studied up to seven electrolytes using tetraglyme combined with different salts and they revealed that higher discharge capacities were obtained with LiTFSI > LiTf ≈ LiPF$_6$ > LiClO$_4$ > LiBF$_4$, LiBr, LiBOB; due to the contributions from the electrolyte in viscosity and oxygen solubility. However, they also discovered that these salts lead to the formation of side products, consequence of their degradation against certain currents and potentials. For example, LiTFSI, LiTf, LiPF$_6$, LiClO$_4$, and LiBr led to

produce a mixture of Li_2O_2 and side products during discharge (e.g. LiF), whereas LiBOB was found highly unstable.

1.3.2 Solid electrolytes

Currently, liquid electrolytes based on lithium salts dissolved in organic solvents are the most widely used in lithium-based batteries[55]. However, its liquid nature prompts some drawbacks related to safety issues such as the potential leaking of the toxic and flammable organic electrolyte from the cell [56]. Solid electrolytes have been proposed as one of the most feasible solutions to mitigate these safety issues (Figure 1.11).
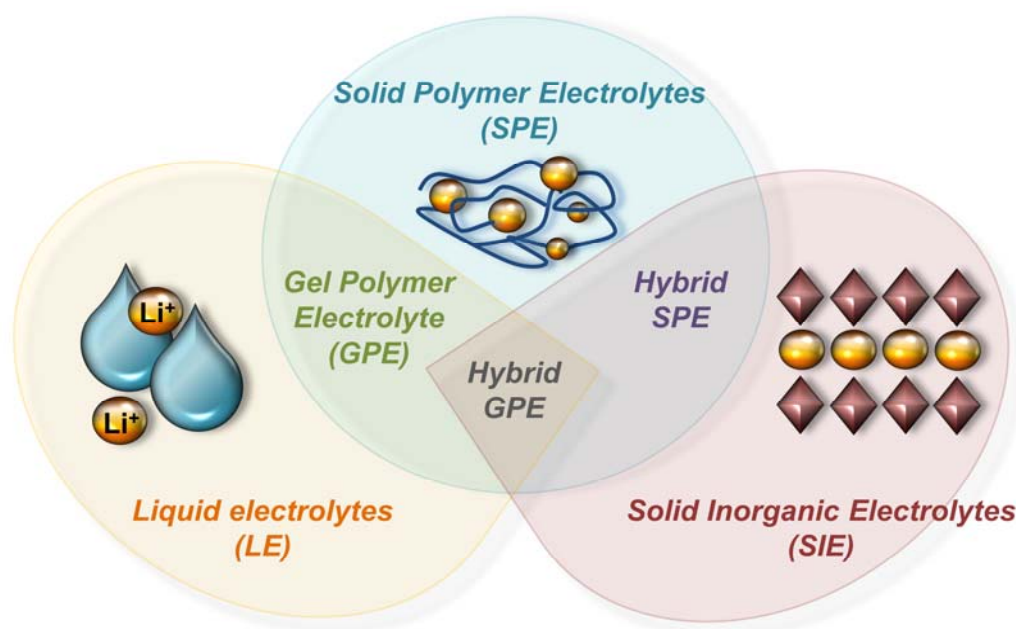
Figure 1. 11. Different types of electrolytes for batteries.

Research on solid-state Li−O_2 batteries can be divided into two main categories: pure-solid state or quasi-solid state. On the first one, the cell does not contain any liquid. In the second one, there could be mixed with liquid electrolyte solutions. These solid electrolytes could be achieved through inorganic solids, polymeric materials or a combination of both (Figure 1.11).

Solid inorganic electrolytes (SIE) are formed by mobile ions as well as metal and non-metal ions, occupying polyhedra-type positions with ligands that form the skeleton of crystal structures[57]. Amongst the crystalline inorganics used as inorganic solid

electrolyte most popular ones are lithium ion conductors (thio-) LISICON-based (e.g. $Li_{14}ZnGe_4O_{16}$), Garnets-based (e.g. $Li_7La_3Zr_2O_{12}$ (LLZO)), Perovskites-based (e.g. lithium–lanthanum–titanates, LLTO), and NASICON-based (e.g. LATP). Inorganic solid electrolytes can also be glass-based, including both glassy and glass-ceramic systems[58]. All of them are very safe candidates and provide single ion conduction properties, but they suffer from low ionic conductivities and severe interfacial contact failures [28,58].

Polymeric electrolytes represent an alternative candidate to enhance the solid-state electrolyte challenges. Depending in the way these polymers are arranged or combined with other systems (liquid electrolytes, ceramics, etc), these can be categorized in different levels, as per Figure 1.11.

Solid polymer electrolytes (SPE) were first introduced to battery applications more than 40 years ago just after P.V. Wright and M. Armand discovered the ionic conductivity in alkali metal salt complexes of poly(ethylene oxide) (PEO)[59–61]. SPEs are formed by an ideal composition of a polymer matrix and a metal salt. PEO is without any doubt the gold standard for SPE development. Its crystallinity plays an important role and drives the lithium ionic transport. At room temperature, it has a big impact on the ionic conductivity ($\sigma \leq 10^{-5}$ S cm^{-1} at 25 °C)[60]. Hence, many efforts are dedicated to tweak its crystallinity via the flexibility in design that polymers can offer.

If an SPE is combined with inorganic garnets such as LLZO, then they are named hybrid SPEs. On the other hand, when a SPE is able to entrapped/swell a liquid electrolyte, then, gel polymer electrolytes (GPEs) can be formed. The following section will provide an overview of state-of-the-art GPEs and hybrid GPEs applied to Li−O$_2$ batteries as electrolytes.

1.3.3 Gel polymer electrolytes

Beyond inorganic solid electrolytes, solid polymer electrolytes (SPEs) represent a plausible alternative solution to liquid electrolytes[59,61]. However, their ionic conductivity is still several orders of magnitude lower than the liquid electrolytes (10^{-5}-10^{-6} S·cm^{-1} for SPEs vs 10^{-2}-10^{-3} S·cm^{-1} for liquid electrolytes at room temperature)[62]. A

compromising solution could be based on the use of the so-called gel polymer electrolytes (GPEs), in which a solvent (often named plasticizer) is trapped within the polymer network. This configuration shows an intermediate ionic conductivity (~10^{-3} to 10^{-4} S·cm^{-1})[63]. In this way, GPEs can synergize the properties of high ionic conductivity (fast cation diffusion) and the good electrode/electrolyte interfacial properties of liquid electrolytes[64], with the beneficial mechanical properties (strength, flexibility, etc.) of solid polymer electrolytes[65] (Figure 1.12).
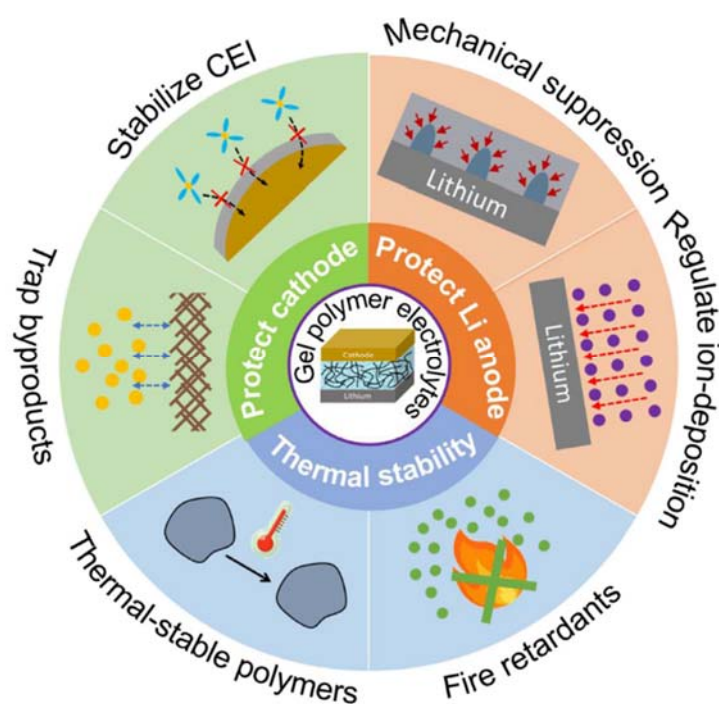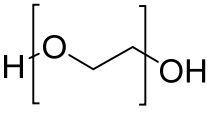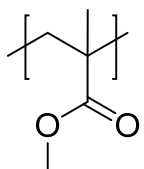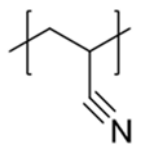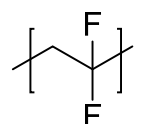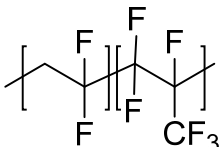
Figure 1. 12. Properties foreseen using GPEs. Reproduced with permission from literature [66].

Latest studies on polymer-based GPE electrolytes for Li-O$_2$ applications include complex hybrid composite systems, in which lithium active conductors (e.g. Li$_{7-3x}$Al$_x$La$_3$Zr$_2$O$_{12}$) or passive (e.g. Al$_2$O$_3$) inorganic fillers are also added[42]. In general, the ionic conductivities reported[67–73] in these systems are ≤10^{-3} S·cm^{-1} and lithium platting/stripping behaviors in symmetrical cells are limited to 0.1–0.2 mA·cm^{-2}, with the exception of a recently published hybrid PVDF-HFP/PMMA/SiO$_2$ system[70] that was cycled at 0.5 mA·cm^{-2}. Yu and co-workers constructed a novel ultra-dry polymer electrolyte based on P(VDF-HFP) that achieved ~2600 mAh·g^{-1} at 0.4 mA·cm^{-2} [73]. In another approach, Kim and co-workers managed to remarkably increase the

discharge capacity of their Li-O$_2$ cell from 894 mAh·g^{-1} to 4059 mAh·g^{-1} using a GPE based on PAN and tetrachloro-1,4-benzoquinone (tCl-pBQ) used as redox mediator[67].

Table 1. 2. Some common polymer matrices of polymer-based electrolytes. Adapted from literature[66].

Polymer matrix		Tg [a]	mp [b]	Advantages
PEO *Poly(ethylene oxide)*		-67 °C	65 °C	High Li+ affinity
PMMA *Poly(methyl methacrylate)*		105 °C	160 °C	Good thermal/ electrochemical stability and electrolyte affinity
PAN *Polyacrylonitrile*		125 °C	317 °C	High thermal stability and good processability
PVDF *Poly(vinylidene fluoride)*		-40 °C	177 °C	Good mechanical properties and high chemical stability
P(PVDF-co-HFP) *Poly(vinylidene fluoride- co - hexafluoropropylene*		-90 °C	143 °C	Good mechanical properties and high chemical stability

[a] Glass transition temperature, Tg
[b] Melting point

Single ion gel polymer electrolytes

All the examples shown so far are systems based on different lithium salts in combination with a polymer matrix and a plasticizer. One of the main limitations of conventional GPEs is associated with their low lithium transference number (t_{Li^+}) values, as a consequence of the dual-ion motion[74].

Recently, lithium single-ion conducting gel polymer electrolytes (SIGPE) prepared from polymerizable lithium salts such as lithium 1-[3-(methacryloyloxy)-propylsulfonyl]-1-(trifluoromethylsulfonyl)imide (LiMTFSI)[26], have been reported with high lithium transference number (close to 1) and excellent performance in lithium metal batteries[75–80]. Researches also proved that the anionic immobility decreases the

overpotential generated by anionic concentration gradients and slows down the dendritic growth rate on the negative electrode during the charge-discharge cycles of lithium metal batteries [80–82].
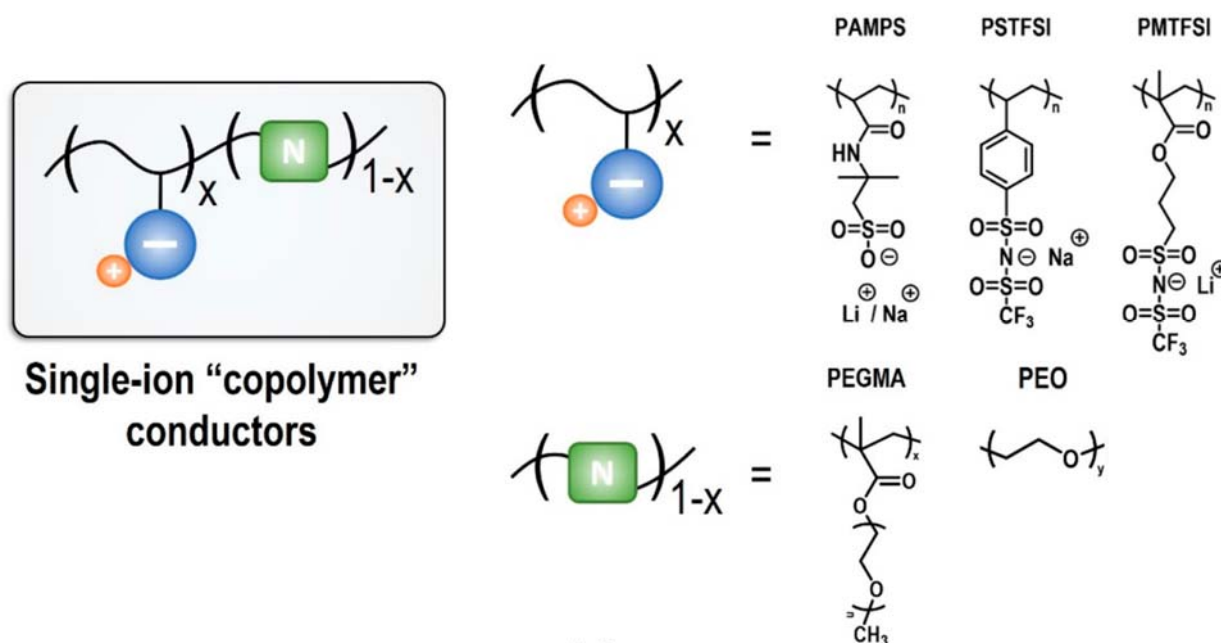
Figure 1. 13. Popular structures of single-ion conductor polymer electrolytes. Reproduced with permission from literature [83].

Although lithium single ion conductors are very popular in lithium metal batteries with different inorganic cathode materials, they have not been investigated yet in Li-O$_2$ applications. There are only three publications. Two of them were proposed by Yang and co-workers[84,85], in which a single ion GPE based on lithiated perfluorinated sulfonic ionomer (i.e. Nafion^{TM}) swollen in DMSO, and named as PFSA-Li, was developed. The last one is presented in the second chapter of this manuscript.

Iongels

When the liquid electrolyte encapsulated in a GPE is an ionic liquid-based electrolyte, these can be named as iongels, ionic liquid gels or ionogels [83].

The use of iongels is a fast-growing technology but has not been largely explored in Li-O$_2$ cells [86]. There are a few examples based on poly(methyl) methacrylate (PMMA) [87,88] or poly(vinylidene fluoride-co-hexafluoropropylene) (PVdF-HFP) [68,89] polymer-based iongels. For example, H. Zhao and co-workers[88] developed an UV-cured iongel

containing 1-Ethyl-3- methylimidazolium tetrafluoroborate ionic liquid (EMIm-BF4), dimethyl sulfoxide (DMSO) and LiTFSI, encapsulated in a polymer matrix formed by PMMA and a triacrylate. This ionogel presented overpotentials < 0.1 V for 130 hours when cycled at 0.3 mA·h^{-1} on lithium symmetrical cells.
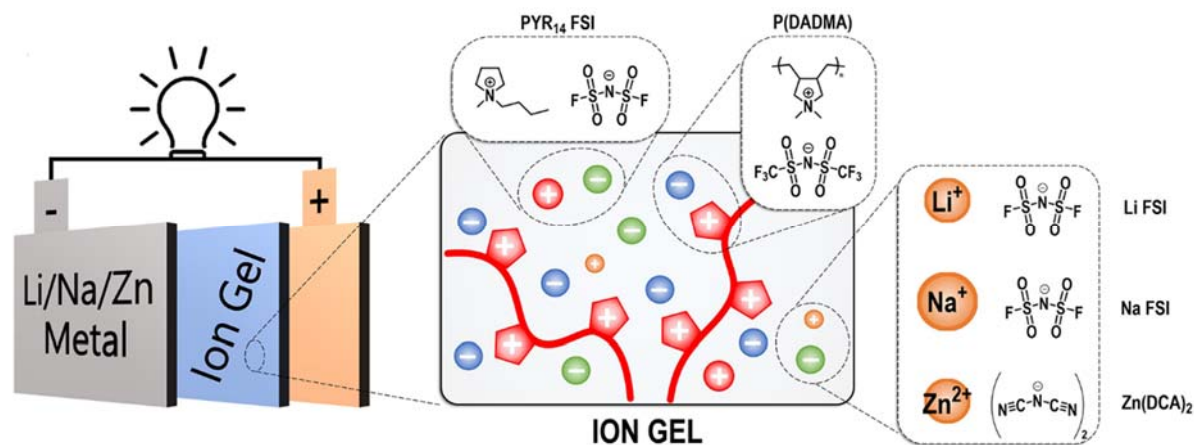
Figure 1. 14. Versatility of ion gels electrolytes. In the example, a polymer ionic liquid is selected as the polymer matrix. Reproduced with permission from literature [83].

Lately, [DEME][TFSI] was selected to form a quasi-solid-state electrolyte by the gelation of this IL when mixed with multi-wall carbon nanotubes or solidification when mixed with $Li_{6·40}La_3Zr_{1·40}Ta_{0·60}O_{12}$ (LLZTO) ceramic nanoparticles via non-covalent interactions [90].

1.4 Motivation and objectives

It is clear that energy storage systems, and more particularly batteries, are key technology enablers to fight climate change. To satisfy this upcoming huge demand, lithium-ion batteries need to be complemented with other battery technologies. Li-O$_2$ or lithium air batteries are very promising from an energy density point of view. However, this battery technology has some actual issues, and new materials need to be developed to make the technology more efficient, secure and reliable.

In this context, the main goal of the thesis is to develop new materials for greener, safer and higher performance Li-O$_2$ batteries. Our work has focused on the development of polymer-based solid electrolytes and new polymer binders for air electrodes that are suitable for this type of batteries. The work was carried out within an industry-academia collaboration where the synthesis, optimization and

characterization of novel polymeric membranes was carried out at POLYMAT - University of the Basque Country (San Sebastián, Spain). On the other hand, half of the time of this PhD thesis was spent at Toyota Motor Europe (Zaventem, Belgium) where the electrochemical characterisation on lithium symmetrical cells and Li-O$_2$ cells was carried out.

Specific objectives are:

- Synthesis and characterization of new solid electrolytes with enhanced physico-chemical and electrochemical properties:

  o Using polymerization methods that are fast and easy adoptable to industry, such as UV-photopolymerization.

  o Achieving higher thermal stabilities without a detriment in ionic conductivity.

  o Allowing lithium plating/stripping at room temperature and/or mitigating the formation of lithium dendrites.

  o Improving charge and discharge capacities of Li-O$_2$, with low overpotentials.

- Design, optimization and characterization of single-ion gel polymer electrolytes based on lithium-ion conducting monomers including lithium sulphonamide or lithium borate groups. Compare the performance of single-ion gel polymer electrolytes with conventional dual ion gel polymer electrolytes systems using tetraglyme as plasticizer within the gel formulation.

- Design, optimization of gel polymer electrolytes and characterization in Li-O$_2$ battery cells that include alternative plasticizers to tetraglyme based on greener and lower toxicity glymes.

- Design and optimization of new iongel polymer electrolytes and characterization in Li-O$_2$ battery cells. Investigate the effect of the chemical composition of the ionic liquid component in the ionic conductivity and electrochemical performances.

- Synthesis and performance evaluation of new poly(ionic liquid) binders for air cathodes in Li-O$_2$ alternative to the currently used lithiated NAFION-type binders.

Contribution to the Toyota Environmental Challenge 2050

As part of the collaboration with Toyota Motor Europe, the work presented in this manuscript aims to contribute to – specially – two *Toyota Environmental 2050 Challenges*, Challenge 1 and 5.

- *Challenge 1. New vehicle zero CO2 emissions.* The aim of this challenge is to reduce CO$_2$ emissions by 90% by 2050, compared to 2010 levels. The approach is based on promoting the development of next-generation vehicles, including hybrid electric (HEV), plug-in hybrid electric (PHEV), battery electric (BEV) and fuel cell electric vehicles (FCEV).

  As part of this strategy, new BEV materials and solid-state batteries need to be developed and evaluated in the near future (Figure 1.15). This thesis aims to contribute to this challenge by proposing alternative solid polymer-based electrolytes that could be used in lithium-O$_2$ batteries.
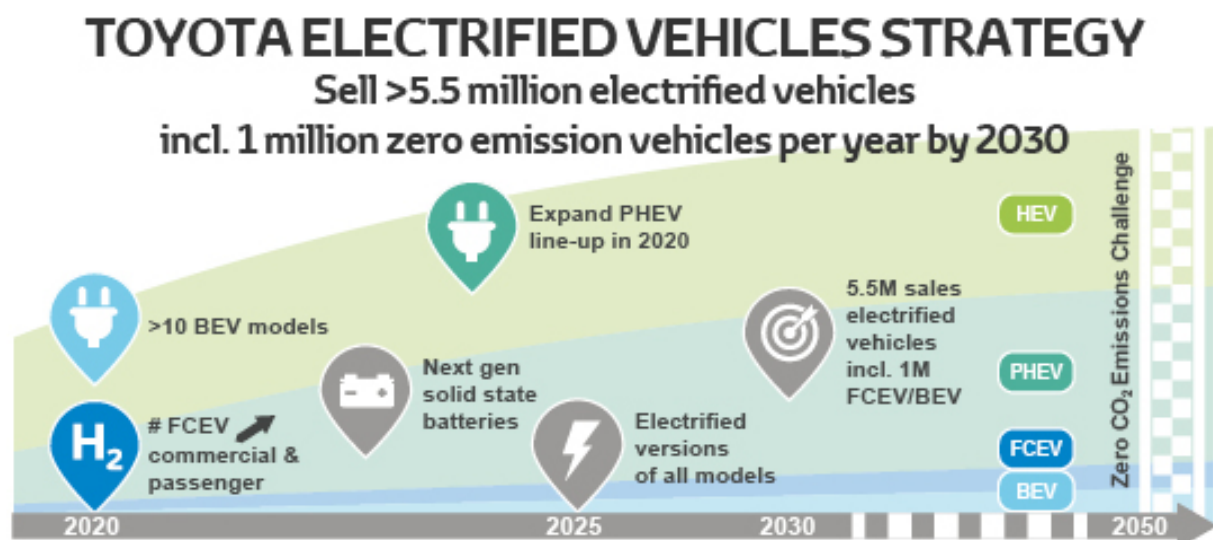
Figure 1. 15. Challenge 1 – New vehicle zero CO$_2$ emissions. *Source: Toyota Global* [11].

- *Challenge 5. Establishing a recycling-based society.* The key aim is to reduce waste and contribute to a sustainable resource consumption. Some strategies involve the use of more eco-friendly materials or develop recycling technologies.

This thesis aims to contribute to this challenge by proposing alternative greener materials that could be use as part of liquid or polymer-based electrolytes in lithium metal batteries.

1.5 Outline of the thesis

This thesis is shaped by six chapters, including this introduction.

In **Chapter 2**, the performance of Li-O$_2$ batteries using a single-ion and an equivalent dual-ion conducting gel polymer electrolyte is compared for the first time. These gels are designed by combining UV-based techniques already reported on other battery technologies with state-of-the-art solvents/ plasticizers used in Li-O$_2$ batteries such as tetraethylene glycol dimethyl ether (tetraglyme). Moreover, a new family of lithium single-ion polymer electrolytes (SIGPEs) based on tailored-designed borate-based lithium conducting monomers (single-ion monomers, SIMs) is evaluated. The ether-based functionalities added to the SIMs aimed to reduce the amount of organic solvent used in the gel formulation. In addition, we will also show for the first time, the versatility of boron-based chemistry by the evaluation in lithium metal batteries of a new set of lithium molten salts at room temperature.

In **Chapter 3**, we propose a greener and low toxicity glyme derived from bio-sourced glycerol (1,2,3 – trimethoxypropane (TMP)) as alternative aprotic solvent to toxic glymes. It will be evaluated for the first time as a plasticizer in liquid and gel polymer electrolytes for Li-O$_2$ batteries.

In **Chapter 4**, a tetra-alkyl ammonium based ionic liquid is evaluated as plasticizer to prepare iongel soft solid electrolytes. A full study to obtain optimized solid polymer electrolytes for Li-O$_2$ batteries based on a low polarization ionic liquid ([DEME][TFSI]) will be presented; including an evaluation on the effects of salt concentration on the polymer-based electrolyte. Furthermore, [DEME][TFSI] cation and anion will be tuned

to increase the presence of fluorine moieties with highly delocalized charge. Up to five different ionic liquids are designed and used as plasticizers in iongel electrolytes. Synergy between IL and salts cations / anions will be explored through the iongel electrolyte properties.

In **Chapter 5**, instead of electrolytes as in the previous chapter, new binders for air electrodes will be investigated. Thus, polymeric binders based on a poly(ionic liquid) (PDADMA-type) with different anions are investigated as components in the air-electrode. Poly(ionic liquid)s will be evaluated as binders for the first time in Li-O$_2$ cells and compared to the lithiated Nafion^{TM} reference binder used on the other chapters.

In **Chapter 6**, overall conclusions of the work will be presented as well as a discussion on the properties and results achieved by the different polymeric materials developed in this PhD thesis.

1.6 References

(1)   Agency, E. E. Energy — Renewable energy.

(2)   European Commission. Energy and the Green Deal | European Commission https://ec.europa.eu/info/strategy/priorities-2019-2024/european-green-deal/energy-and-green-deal_en (accessed Jan 12, 2022).

(3)   Deutsche Gesellschaft für Internationale Zusammenarbeit (GIZ). The Sustainable and Smart Mobility Strategy of the European Commission - A Critical Assessment https://www.changing-transport.org/wp-content/uploads/EU-Mobility-Strategy.pdf (accessed Jan 12, 2022).

(4)   Nations, U. COP26 - A pivotal moment in the fight against climate change.

(5)   European Environment Information and Observation Network (Eionet). Greenhouse gas emission intensity of fuels and biofuels for road transport in Europe https://www.eea.europa.eu/data-and-maps/indicators/greenhouse-gas-emissions-intensity-of-1/assessment.

(6)   European Environment Agency. *Monitoring Carbon Dioxide Emissions from Passenger Cars and Vans in 2014*; 2015.

(7)   Delivering the European Green Deal | European Commission. Delivering the European Green Deal | European Commission https://ec.europa.eu/info/strategy/priorities-2019-2024/european-green-deal/delivering-european-green-deal_en (accessed Jan 12, 2022).

(8)   Eurostat. *News Release - Early Estimates of CO2 Emissions from Energy Use*;
        2018.

(9)   EPRS | European Parliamentary Research Service. BRIEFING - Sustainable
        and Smart Mobility Strategy. 2021.

(10)   Zhao, Y.; Pohl, O.; Bhatt, A. I.; Collis, G. E.; Mahon, P. J.; Rüther, T.;
        Hollenkamp, A. F. A Review on Battery Market Trends, Second-Life Reuse, and
        Recycling. *Sustain. Chem.* **2021**, *2* (1), 167–205.

(11)   Toyota Global. Six Challenges. Moving toward a future society in harmony with
        automobiles   and   nature
        https://global.toyota/en/sustainability/esg/challenge2050/ (accessed Jan 12,
        2022).

(12)   Siwal, S. S.; Zhang, Q.; Devi, N.; Thakur, V. K. Carbon-Based Polymer
        Nanocomposite for High-Performance Energy Storage Applications. *Polymers
        (Basel).* **2020**, *12* (3), 1–30.

(13)   Gür, T. M. Review of Electrical Energy Storage Technologies, Materials and
        Systems: Challenges and Prospects for Large-Scale Grid Storage. *Energy
        Environ. Sci.* **2018**, *11* (10), 2696–2767.

(14)   Machrafi, H. *Green Energy and Technology*; 2012.

(15)   Budde-Meiwes, H.; Drillkens, J.; Lunz, B.; Muennix, J.; Rothgang, S.; Kowal, J.;
        Sauer, D. U. A Review of Current Automotive Battery Technology and Future
        Prospects. *Proc. Inst. Mech. Eng. Part D J. Automob. Eng.* **2013**, *227* (5), 761–
        776.

(16)   Kim, T. H.; Park, J. S.; Chang, S. K.; Choi, S.; Ryu, J. H.; Song, H. K. The Current
        Move of Lithium Ion Batteries towards the next Phase. *Adv. Energy Mater.* **2012**,
        2 (7), 860–872.

(17)   Global Battery Alliance. *A Vision for a Sustainable Battery Value Chain in 2030*;
        2019.

(18)   Edström, K.; Dominko, R.; Fichtner, M.; Otuszewski, T.; Perraud, S.; Punckt, C.;
        Tarascon, J.; Vegge, T.; Martin, W. *BATTERY 2030+ Roadmap*; 2020.

(19)   Li, M.; Lu, J.; Chen, Z.; Amine, K. 30 Years of Lithium-Ion Batteries. *Adv. Mater.*
        2018, *30* (33).

(20)   Zeng, X.; Li, M.; Abd El-Hady, D.; Alshitari, W.; Al-Bogami, A. S.; Lu, J.; Amine,
        K. Commercialization of Lithium Battery Technologies for Electric Vehicles. *Adv.
        Energy Mater.* **2019**, *9* (27), 1–25.

(21)   NobelPrize.org.   The   Nobel   Prize   in   Chemistry   2019
        https://www.nobelprize.org/prizes/chemistry/2019/summary/ (accessed Feb 26,
        2020).

(22)   Titirici, M. M. Sustainable Batteries—Quo Vadis? *Adv. Energy Mater.* **2021**,

2003700, 1–11.

(23) DRC: Alarming Research Shows Long Lasting Harm from Cobalt Mine Abuses. *Amnesty International*. 2020.

(24) Ue, M.; Uosaki, K. Recent Progress in Liquid Electrolytes for Lithium Metal Batteries. *Curr. Opin. Electrochem.* **2019**, *17*, 106–113.

(25) Tan, P.; Kong, W.; Shao, Z.; Liu, M.; Ni, M. Advances in Modeling and Simulation of Li–Air Batteries. *Prog. Energy Combust. Sci.* **2017**, *62*, 155–189.

(26) Alvarez Tirado, M.; Castro, L.; Guzmán-González, G.; Porcarelli, L.; Mecerreyes, D. Single- Versus Dual-Ion UV-Cross-Linked Gel Polymer Electrolytes for Li-O2 Batteries. *ACS Appl. Energy Mater.* **2021**, *4*, 295–302.

(27) European Association for Storage of Energy. *Metal-Air Battery*; 2009.

(28) Kwak, W.-J.; Rosy; Sharon, D.; Xia, C.; Kim, H.; Johnson, L. R.; Bruce, P. G.; Nazar, L. F.; Sun, Y.-K.; Frimer, A. A.; Noked, M.; Freunberger, S. A.; Aurbach, D. Lithium–Oxygen Batteries and Related Systems: Potential, Status, and Future. *Chem. Rev.* **2020**, *120* (14), 6626–6683.

(29) Lu, J.; Lau, K. C.; Sun, Y.-K.; Curtiss, L. A.; Amine, K. Review—Understanding and Mitigating Some of the Key Factors That Limit Non-Aqueous Lithium-Air Battery Performance. *J. Electrochem. Soc.* **2015**, *162* (14), A2439–A2446.

(30) Kraytsberg, A.; Ein-eli, Y. Review on Li-Air Batteries — Opportunities , Limitations and Perspective. *J. Power Sources* **2011**, *196*, 886–893.

(31) Olabi, A. G.; Sayed, E. T.; Wilberforce, T.; Jamal, A.; Alami, A. H.; Elsaid, K.; Rahman, S. M. A.; Shah, S. K.; Abdelkareem, M. A. Metal-Air Batteries—a Review. *Energies* **2021**, *14* (21).

(32) Tan, P.; Jiang, H. R.; Zhu, X. B.; An, L.; Jung, C. Y.; Wu, M. C.; Shi, L.; Shyy, W.; Zhao, T. S. Advances and Challenges in Lithium-Air Batteries. *Appl. Energy* **2017**, *204*, 780–806.

(33) Ohara Corporation website https://www.oharacorp.com/lic-gc.html (accessed Dec 15, 2021).

(34) Kwabi, D. G.; Ortiz-Vitoriano, N.; Freunberger, S. A.; Chen, Y.; Imanishi, N.; Bruce, P. G.; Shao-Horn, Y. Materials Challenges in Rechargeable Lithium-Air Batteries. *MRS Bull.* **2014**, *39* (5), 443–452.

(35) Li, F.; Chen, J. Mechanistic Evolution of Aprotic Lithium-Oxygen Batteries. *Adv. Energy Mater.* **2017**, *7* (24), 1–12.

(36) Abraham, K. M.; Jiang, Z. A Polymer Electrolyte − Based Rechargeable Lithium / Oxygen Battery TECHNICAL PAPERS ELECTROCHEMICAL SCIENCE AND TECHNOLOGY A Polymer Electrolyte-Based Rechargeable Lithium / Oxygen Battery. *J. Electrochem. Soc.* **1996**, *143* (1), 1–5.

(37) Wang, Y.; Lai, N. C.; Lu, Y. R.; Zhou, Y.; Dong, C. L.; Lu, Y. C. A Solvent-Controlled Oxidation Mechanism of Li2O2 in Lithium-Oxygen Batteries. *Joule* **2018**, *2* (11), 2364–2380.

(38) Grande, L.; Paillard, E.; Hassoun, J.; Park, J. B.; Lee, Y. J.; Sun, Y. K.; Passerini, S.; Scrosati, B. The Lithium/Air Battery: Still an Emerging System or a Practical Reality? *Adv. Mater.* **2015**, *27* (5), 784–800.

(39) Wang, D.; Mu, X.; He, P.; Zhou, H. Materials for Advanced Li-O2 Batteries: Explorations, Challenges and Prospects. *Mater. Today* **2019**, *26* (June), 87–99.

(40) Guo, H.; Luo, W.; Chen, J.; Chou, S.; Liu, H.; Wang, J. Review of Electrolytes in Nonaqueous Lithium–Oxygen Batteries. *Adv. Sustain. Syst.* **2018**, *2* (8–9).

(41) Sun, C. Recent Advances in Lithium-Air Batteries. *Adv. Mater. Lett.* **2018**, *9* (5), 336–344.

(42) Li, B.; Liu, Y.; Zhang, X.; He, P.; Zhou, H. Hybrid Polymer Electrolyte for Li–O 2 Batteries. *Green Energy Environ.* **2019**, *4* (1), 3–19.

(43) Nasybulin, E.; Xu, W.; Engelhard, M. H.; Nie, Z.; Burton, S. D.; Cosimbescu, L.; Gross, M. E.; Zhang, J. G. Effects of Electrolyte Salts on the Performance of Li-O2 Batteries. *J. Phys. Chem. C* **2013**, *117* (6), 2635–2645.

(44) Wu, S.; Tang, J.; Li, F.; Liu, X.; Zhou, H. Low Charge Overpotentials in Lithium-Oxygen Batteries Based on Tetraglyme Electrolytes with a Limited Amount of Water. *Chem. Commun.* **2015**, *51* (94), 16860–16863.

(45) Zhao, Q.; Zhang, Y.; Sun, G.; Cong, L.; Sun, L.; Xie, H.; Liu, J. Binary Mixtures of Highly Concentrated Tetraglyme and Hydrofluoroether as a Stable and Nonflammable Electrolyte for Li-O2 Batteries. *ACS Appl. Mater. Interfaces* **2018**, *10* (31), 26312–26319.

(46) Chamaani, A.; Safa, M.; Chawla, N.; El-Zahab, B. Composite Gel Polymer Electrolyte for Improved Cyclability in Lithium-Oxygen Batteries. *ACS Appl. Mater. Interfaces* **2017**, *9* (39), 33819–33826.

(47) Liu, K.; Wang, Z.; Shi, L.; Jungsuttiwong, S.; Yuan, S. Ionic Liquids for High Performance Lithium Metal Batteries. *J. Energy Chem.* **2020**, *59*, 320–333.

(48) Stettner, T.; Balducci, A. Protic Ionic Liquids in Energy Storage Devices: Past, Present and Future Perspective. *Energy Storage Mater.* **2021**, *40* (April), 402–414.

(49) Long, L.; Wang, S.; Xiao, M.; Meng, Y. Polymer Electrolytes for Lithium Polymer Batteries. *J. Mater. Chem. A* **2016**, *4* (26), 10038–10039.

(50) Knipping, E.; Aucher, C.; Guirado, G.; Aubouy, L. Room Temperature Ionic Liquids: Versus Organic Solvents as Lithium-Oxygen Battery Electrolytes. *New J. Chem.* **2018**, *42* (6), 4693–4699.

(51) Yang, Q.; Zhang, Z.; Sun, X. G.; Hu, Y. S.; Xing, H.; Dai, S. Ionic Liquids and

Derived Materials for Lithium and Sodium Batteries. *Chem. Soc. Rev.* **2018**, *47* (6), 2020–2064.

(52) Nakamoto, H.; Suzuki, Y.; Shiotsuki, T.; Mizuno, F.; Higashi, S.; Takechi, K.; Asaoka, T.; Nishikoori, H.; Iba, H. Ether-Functionalized Ionic Liquid Electrolytes for Lithium-Air Batteries. *J. Power Sources* **2013**, *243*, 19–23.

(53) Rüther, T.; Bhatt, A. I.; Best, A. S.; Harris, K. R.; Hollenkamp, A. F. Electrolytes for Lithium (Sodium) Batteries Based on Ionic Liquids: Highlighting the Key Role Played by the Anion. *Batter. Supercaps* **2020**, *3* (9), 793–827.

(54) Younesi, R.; Veith, G. M.; Johansson, P.; Edström, K.; Vegge, T. Lithium Salts for Advanced Lithium Batteries: Li-Metal, Li-O2, and Li-S. *Energy Environ. Sci.* **2015**, *8* (7), 1905–1922.

(55) Liu, X.; Shen, X.; Li, H.; Li, P.; Luo, L.; Fan, H.; Feng, X.; Chen, W.; Ai, X.; Yang, H.; Cao, Y. Ethylene Carbonate-Free Propylene Carbonate-Based Electrolytes with Excellent Electrochemical Compatibility for Li-Ion Batteries through Engineering Electrolyte Solvation Structure. *Adv. Energy Mater.* **2021**, *11* (19), 2003905.

(56) Mauger; Julien; Paolella; Armand; Zaghib. Building Better Batteries in the Solid State: A Review. *Materials (Basel).* **2019**, *12* (23), 3892.

(57) Bachman, J. C.; Muy, S.; Grimaud, A.; Chang, H. H.; Pour, N.; Lux, S. F.; Paschos, O.; Maglia, F.; Lupart, S.; Lamp, P.; Giordano, L.; Shao-Horn, Y. Inorganic Solid-State Electrolytes for Lithium Batteries: Mechanisms and Properties Governing Ion Conduction. *Chem. Rev.* **2016**, *116* (1), 140–162.

(58) Cao, C.; Li, Z. Bin; Wang, X. L.; Zhao, X. B.; Han, W. Q. Recent Advances in Inorganic Solid Electrolytes for Lithium Batteries. *Front. Energy Res.* **2014**, *2* (JUN), 1–10.

(59) Yi, J.; Guo, S.; He, P.; Zhou, H. Status and Prospects of Polymer Electrolytes for Solid-State Li–O 2 (Air) Batteries. *Energy Environ. Sci.* **2017**, *10* (4), 860–884.

(60) Mecerreyes, D.; Porcarelli, L.; Casado, N. Innovative Polymers for Next-Generation Batteries. *Macromol. Chem. Phys.* **2020**, *1900490*, 1–7.

(61) Armand, M. The History of Polymer Electrolytes. *Solid State Ionics* **1994**, *69* (3), 309–319.

(62) Elia, G. A.; Hassoun, J. A Polymer Lithium-Oxygen Battery. *Nat. Publ. Gr.* **2015**, *5*, 5:12307.

(63) Zou, X.; Lu, Q.; Zhong, Y.; Liao, K.; Zhou, W.; Shao, Z. Flexible, Flame-Resistant, and Dendrite-Impermeable Gel-Polymer Electrolyte for Li–O2/Air Batteries Workable Under Hurdle Conditions. *Small* **2018**, *14* (34), 1–10.

(64) Voropaeva, D. Y.; Novikova, S. A.; Yaroslavtsev, A. B. Polymer Electrolytes for Metal-Ion Batteries. *Russ. Chem. Rev* **2020**, *89* (10), 1132–1155.

(65) Zhou, D.; Shanmukaraj, D.; Tkacheva, A.; Armand, M.; Wang, G. Polymer Electrolytes for Lithium-Based Batteries: Advances and Prospects. *Chem* **2019**, *5* (9), 2326–2352.

(66) Ren, W.; Ding, C.; Fu, X.; Huang, Y. Advanced Gel Polymer Electrolytes for Safe and Durable Lithium Metal Batteries: Challenges, Strategies, and Perspectives. *Energy Storage Mater.* **2021**, *34* (October 2020), 515–535.

(67) Kim, Y. B.; Kim, I. T.; Song, M. J.; Shin, M. W. Synthesis of a Polyacrylonitrile/Tetrachloro-1,4-Benzoquinone Gel Polymer Electrolyte for High-Performance Li-Air Batteries. *J. Memb. Sci.* **2018**, *563* (March), 835–842.

(68) Pan, J.; Li, H.; Sun, H.; Zhang, Y.; Wang, L.; Liao, M.; Sun, X.; Peng, H. A Lithium–Air Battery Stably Working at High Temperature with High Rate Performance. *Small* **2018**, *14* (6), 1–6.

(69) Ren, M.; Zhang, J.; Zhang, C.; Stanford, M. G.; Chyan, Y.; Yao, Y.; Tour, J. M. Quasi-Solid-State Li-O2 Batteries with Laser-Induced Graphene Cathode Catalysts. *ACS Appl. Energy Mater.* **2020**, *3*, 1702–1709.

(70) Yang, T.; Shu, C.; Zheng, R.; Li, M.; Hou, Z.; Hei, P.; Zhang, Q.; Mei, D.; Long, J. Dendrite-Free Solid-State Li-O2 Batteries Enabled by Organic-Inorganic Interaction Reinforced Gel Polymer Electrolyte. *ACS Sustain. Chem. Eng.* **2019**, *7* (20), 17362–17371.

(71) Zhao, C.; Liang, J.; Zhao, Y.; Luo, J.; Sun, Q.; Liu, Y.; Lin, X.; Yang, X.; Huang, H.; Zhang, L.; Zhao, S.; Lu, S.; Sun, X. Engineering a "Nanonet"-Reinforced Polymer Electrolyte for Long-Life Li-O2 Batteries. *J. Mater. Chem. A* **2019**, *7* (43), 24947–24952.

(72) Balaish, M.; Leskes, M.; Ein-Eli, Y. Investigation of Rechargeable Poly(Ethylene Oxide)-Based Solid Lithium-Oxygen Batteries. *ACS Appl. Energy Mater.* **2018**, *1* (7), 3048–3056.

(73) Yu, W.; Xue, C.; Hu, B.; Xu, B.; Li, L.; Nan, C. W. Oxygen- and Dendrite-Resistant Ultra-Dry Polymer Electrolytes for Solid-State Li–O2 Batteries. *Energy Storage Mater.* **2020**, *27* (October 2019), 244–251.

(74) Baskoro, F.; Wong, H. Q.; Yen, H. J. Strategic Structural Design of a Gel Polymer Electrolyte toward a High Efficiency Lithium-Ion Battery. *ACS Appl. Energy Mater.* **2019**, *2* (6), 3937–3971.

(75) Phan, T. N. T.; Ferrand, A.; Ho, H. T.; Liénafa, L.; Rollet, M.; Maria, S.; Bouchet, R.; Gigmes, D. Vinyl Monomers Bearing a Sulfonyl(Trifluoromethane Sulfonyl) Imide Group: Synthesis and Polymerization Using Nitroxide-Mediated Polymerization. *Polym. Chem.* **2016**, *7* (45), 6901–6910.

(76) Meabe, L.; Goujon, N.; Li, C.; Armand, M.; Forsyth, M. Single-Ion Conducting Poly (Ethylene Oxide Carbonate) as Solid Polymer Electrolyte for Lithium Batteries. *Batter. Supercaps* **2020**, *3*, 68–75.

(77) Porcarelli, L.; Shaplov, A. S.; Bella, F.; Nair, J. R.; Mecerreyes, D.; Gerbaldi, C.

Single-Ion Conducting Polymer Electrolytes for Lithium Metal Polymer Batteries That Operate at Ambient Temperature. *ACS Energy Lett.* **2016**, *1* (4), 678–682.

(78) Sutton, P.; Airoldi, M.; Porcarelli, L.; Martínez, J. L. O.; Mugemana, C.; Bruns, N.; Mecerreyes, D.; Steiner, U.; Gunkel, I. Tuning the Properties of a UV Polymerized , Cross   Linked Solid Polymer Electrolyte for Lithium Batteries. *Polymers (Basel).* **2020**, *12*, 595.

(79) Zhang, H.; Li, C.; Piszcz, M.; Coya, E.; Rojo, T.; Rodriguez-Martinez, L. M.; Armand, M.; Zhou, Z. Single Lithium-Ion Conducting Solid Polymer Electrolytes: Advances and Perspectives. *Chem. Soc. Rev.* **2017**, *46* (3), 797–815.

(80) Deng, K.; Zeng, Q.; Wang, D.; Liu, Z.; Qiu, Z.; Zhang, Y.; Xiao, M.; Meng, Y. Single-Ion Conducting Gel Polymer Electrolytes: Design, Preparation and Application. *J. Mater. Chem. A* **2020**, *8* (4), 1557–1577.

(81) Bouchet, R.; Maria, S.; Meziane, R.; Aboulaich, A.; Lienafa, L.; Bonnet, J.; Phan, T. N. T.; Bertin, D.; Gigmes, D.; Devaux, D.; Denoyel, R.; Armand, M. Single-Ion BAB Triblock Copolymers as Highly Efficient Electrolytes for Lithium-Metal Batteries. *Nat. Mater.* **2013**, *12* (5), 1–6.

(82) Villaluenga, I.; Inceoglu, S.; Jiang, X.; Chen, X. C.; Chintapalli, M.; Wang, D. R.; Devaux, D.; Balsara, N. P. Nanostructured Single-Ion-Conducting Hybrid Electrolytes Based on Salty Nanoparticles and Block Copolymers. *Macromolecules* **2017**, *50* (5), 1998–2005.

(83) Forsyth, M.; Porcarelli, L.; Wang, X.; Goujon, N.; Mecerreyes, D. Innovative Electrolytes Based on Ionic Liquids and Polymers for Next-Generation Solid-State Batteries. *Acc. Chem. Res.* **2019**, *52* (3), 686–694.

(84) Wu, C.; Liao, C.; Li, T.; Shi, Y.; Luo, J.; Li, L.; Yang, J. A Polymer Lithium-Oxygen Battery Based on Semi-Polymeric Conducting Ionomers as the Polymer Electrolyte. *J. Mater. Chem. A* **2016**, *4* (39), 15189–15196.

(85) Shi, Y.; Wu, C.; Li, L.; Yang, J. A Lithiated Perfluorinated Sulfonic Acid Polymer Electrolyte for Lithium-Oxygen Batteries. *J. Electrochem. Soc.* **2017**, *164* (9), A2031–A2037.

(86) Tomé, L. C.; Porcarelli, L.; Bara, J. E.; Forsyth, M.; Mecerreyes, D. Emerging Iongel Materials towards Applications in Energy and Bioelectronics. *Mater. Horizons* **2021**, Advance Article.

(87) Amanchukwu, C. V; Chang, H.-H.; Gauthier, M.; Feng, S.; Batcho, T. P.; Hammond, P. T. One-Electron Mechanism in a Gel−Polymer Electrolyte Li−O 2 Battery. *Chem. Mater.* **2016**, *28*, 7167–7177.

(88) Zhao, H.; Liu, X.; Chi, Z.; Chen, S.; Li, S.; Guo, Z.; Wang, L. Designing a New-Type PMMA Based Gel Polymer Electrolyte Incorporating Ionic Liquid for Lithium Oxygen Batteries with Ru-Based Binder-Free Cathode. *Appl. Surf. Sci.* **2021**, *565*, 150612.

(89) Jung, K. N.; Lee, J. I.; Jung, J. H.; Shin, K. H.; Lee, J. W. A Quasi-Solid-State

Rechargeable Lithium-Oxygen Battery Based on a Gel Polymer Electrolyte with an Ionic Liquid. *Chem. Commun.* **2014**, *50* (41), 5458–5461.

(90) Gao, K. N.; Wang, H. R.; He, M. H.; Li, Y. Q.; Cui, Z. H.; Mao, Y.; Zhang, T. Interfacial Integration and Roll Forming of Quasi-Solid-State Li–O2 Battery through Solidification and Gelation of Ionic Liquid. *J. Power Sources* **2020**, *463* (December 2019), 228179.

Chapter 2

Designing single-ion gel polymer electrolytes by photopolymerization suitable for Li-O₂ batteries

2.1 Introduction

As seen in Chapter 1, the electrolyte plays an essential role on Li-O₂ batteries and aprotic liquid electrolyte cells, also called "non-aqueous", are the most popular due to their highest theoretical capacity[1]. Amongst the most common aprotic solvents, tetraethylene glycol dimethyl ether (TEGDME) is the most used due its low volatility, wide electrochemical window (beyond 4.5 V versus Li^0/Li^+), good solubility of metal alkali salts and relatively low cost [2–6]. However, its liquid nature prompts some drawbacks related to safety issues such as the potential leaking of the toxic and flammable organic electrolyte in the cell [7].

Beyond conventional liquid electrolytes, the so-called gel polymer electrolytes (GPEs) could be a plausible solution to tackle these challenges. In GPEs, a solvent (often named plasticizer) is trapped within the polymer network. This configuration usually shows intermediate ionic conductivity values at room temperature (~10^{-3} to 10^{-4} S·cm^{-1}) [8], much higher than pure solid polymer electrolytes (10^{-5}-10^{-6} S·cm^{-1}) [9]. Nevertheless, one of the main limitations of these GPEs is associated with their low lithium transference number (t_{Li^+}) values, as a consequence of the dual-ion motion of lithium salts used in the electrolytes [10].

Ahead of salt-based GPE electrolytes (combination of a lithium salt, polymer matrix and plasticizer), single ion conducting polymer electrolytes (SIPEs) have drawn great attention due to their good performance when lithium metal is used as negative electrode [11–16]. Although lithium single ion conductors are very popular in lithium metal batteries with different inorganic cathode materials, to the best of our knowledge, they have not been investigated yet in Li-O₂ applications. Only a single-ion GPE based on lithiated perfluorinated sulfonic ionomer (i.e. Nafion™) swollen in DMSO, named as

PFSA-Li, has been considered by Yang et al.[17,18]. The PFSA-Li soft membrane showed an ionic conductivity of 6.4·10⁻⁴ S·cm⁻¹ at room temperature (RT) and a promising cycling stability at 1 A·g⁻¹ during 55 cycles. Performance on symmetrical cells was limited to 60 hours at 0.25 mA·cm⁻² and overpotentials <0.1 V vs Li⁰/Li⁺ were reported.

In this chapter, we will show that lithium single-ion conducting gel polymer electrolytes (SIGPE) prepared from polymerizable lithium salts such as lithium 1-[3-(methacryloyloxy)-propylsulfonyl]-1-(trifluoromethylsulfonyl)imide (LiMTFSI) [19], can report lithium transference number close to unity.

On the other hand, the use of boron-based molecules, either as additives or primary salts, has become popular in electrolyte development [20]. For example, Jimin Shim et al.[21], developed a series of semi-interpenetrated polymeric networks (IPNs) containing PVDF and boron-based tri-methacrylate cross-linkers with different lengths of their ethylene oxide (EO) chains, which exhibited excellent ability as anion-trapping groups when combined with liquid electrolytes based on LiTFSI salt and organic carbonates, obtaining t_{Li^+} values ranging from 0.4 to 0.8. These values were associated to the length of the EO chains [22], which determined the amount of adsorbed liquid electrolyte [23].

In general, anionic centers based on sp³-coordinated boron atoms reside tetra-coordinated with oxygen atoms forming rigid polymeric frameworks, which lowers ionic conductivity [24–26]. To improve it, I. Gonzalez et al.[27] employed both partial crosslinking and tuning of electron-withdrawing substituent groups attached to the BO₄ groups. Electrochemical impedance spectroscopy (EIS) results and theoretical calculations revealed that the electron-withdrawing substituents are insufficient to significantly improve the ionic conductivity, due to the limited mobility of the polymer chains at room temperature [28–30]. Hence, substituents that improve this chain mobility are desirable for achieving higher conductivities in polymers containing this type of borate group [31].

Overall, efforts in this chapter were dedicated on designing single-ion gel polymer electrolytes (SIGPEs) by photopolymerization based on state-of-the-art materials and new lithium conductor methacrylic monomers. Hence, the chapter is divided in two main parts.

The aim of the first part of this chapter is to compare, for the first time, single-ion and dual-ion conducting GPEs that use TEGDME as plasticizer, and to evaluate their performance in Li-O$_2$ cells. For this purpose, a new electrochemical methodology based on dynamic discharge was assessed as a new way to evaluate the polarization effect during Li-O$_2$ discharge.

On the second half of the chapter, single-ion gel polymer electrolytes (SIGPEs) were prepared by UV-photopolymerization based on three new borate lithium methacrylate monomers [32], poly(ethylene glycol) dimethacrylate (PEGDM) and tetraethylene glycol dimethyl ether (tetraglyme, G4) as plasticizer. A deep analysis on the effect of the substituents in the boron atom of the different monomers and the impact of G4 glyme plasticizer content on the ionic conductivity and lithium transference number were analyzed. Overall, we aimed to reduce the amount of TEGDME plasticizer used in a gel formulation by incorporating ether-based chains in a single-ion conducting polymer matrix based in boron chemistry.

First Part

Single versus dual ion UV-crosslinked gel polymer electrolytes based on State-of-the-Art materials and methods for Li-O$_2$ batteries

2.2 Preparation of gel polymer electrolytes (GPEs)

Single-ion GPEs were prepared by UV-co-polymerization of poly(ethylene glycol) dimethacrylate (PEGDM) and lithium 1-[3-(methacryloyloxy)-propylsulfonyl]-1-(trifluoromethylsulfonyl)imide (LiMTFSI) in the presence of TEGDME as a plasticizer and using 2-Hydroxy-2-methylpropiophene (DAROCUR) as a radical photoinitiator. Dual ion GPEs were elaborated in a similar manner, in which PEGDM was UV-polymerised in the presence of a liquid electrolyte composed by lithium bis(trifluoromethanesulfonyl)imide (LiTFSI) dissolved in TEGDME (Scheme 2.1). In both cases, self-standing, flexible and visually transparent membranes could be obtained until a plasticizer content of 80%wt. approximately. Samples with concentrations of TEGDME higher than >80 %wt. were too soft and difficult to handle.
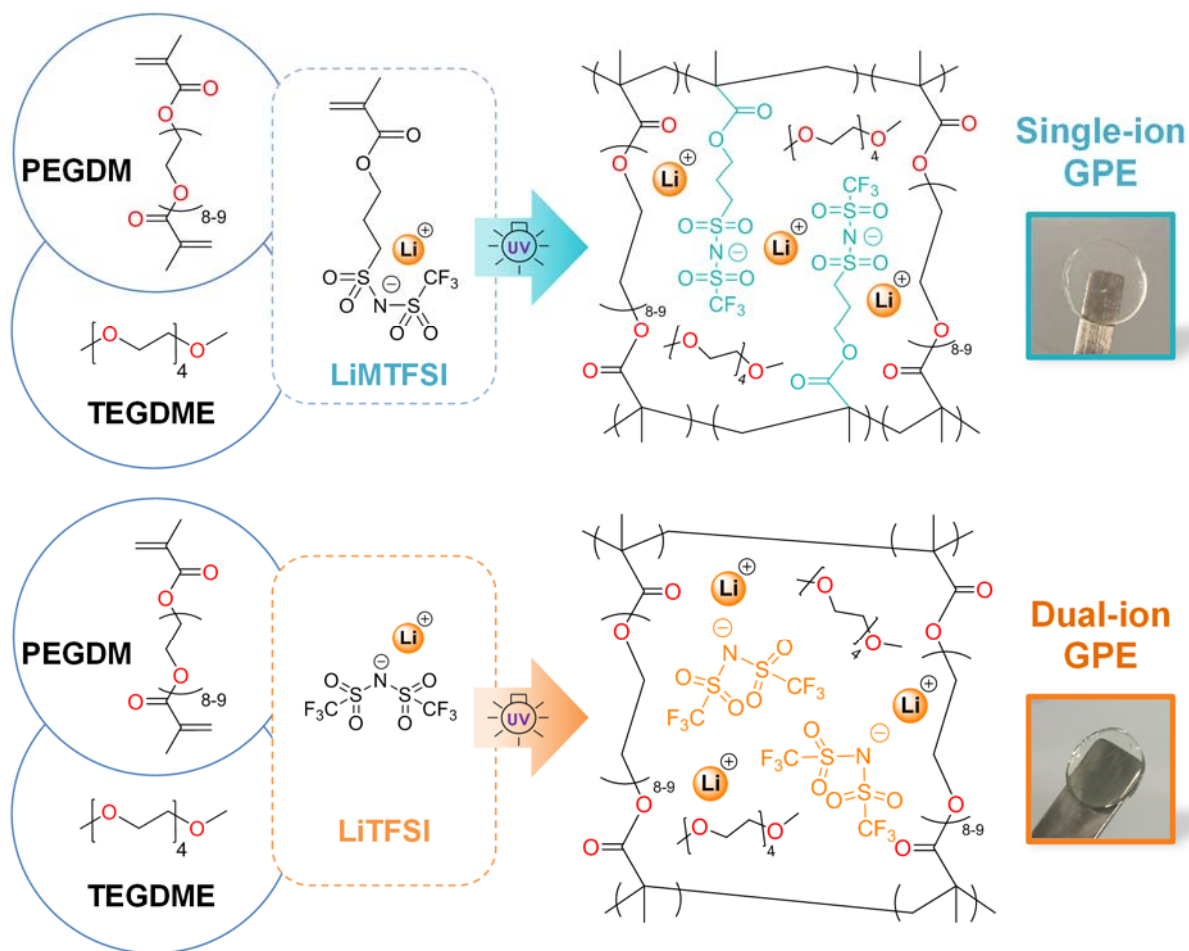
Scheme 2.1. Schematic representation of the preparation of both a) Single ion and b) Dual ion gel polymer electrolytes (GPEs) by UV–photopolymerization.

According to the Fourier Transform Infrared Spectroscopy (FTIR) spectra, monomer conversions higher than ≥95% were reached by the disappearance of the 1635 cm^{-1} band, which is associated to the carbon double bond of methacrylates [33] (Figure 2.1).
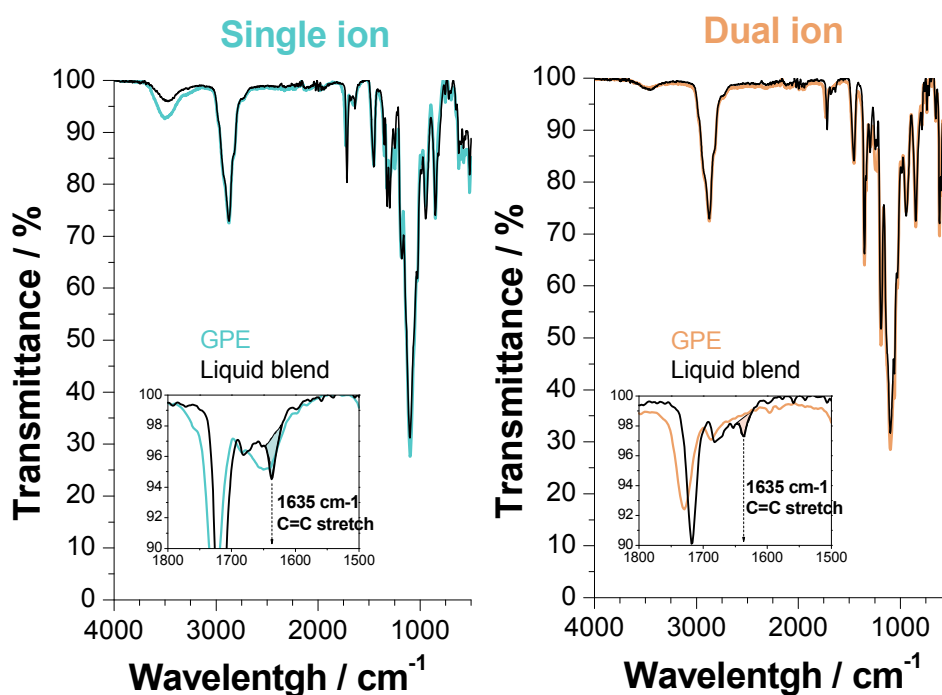
Figure 2. 1. FTIR spectra of the single and dual ion membranes before (liquid blend) and after curing (GPE). The 1635 cm^{-1} band, which is associated to the carbon double bond of methacrylate functionalities[33], disappeared from the cured GPEs´ spectra.

2.3 Gel polymer electrolytes optimization and characterization

2.3.1 Optimization based on ionic conductivity.

To down-select the best single-ion GPE formulations, the ionic conductivity (σ) of GPEs with different compositions was compared at 25 °C (battery operating temperature). For the design of the single ion GPEs, the concentration of the LiMTFSI monomer in the formulation was varied from 10 to 30 %wt., keeping fixed the cross-linker concentration at 10 %wt. As shown in Figure 2.2b, the inclusion of higher concentrations of single-ion lithium monomer did not imply a higher σ. In fact, higher concentrations of the lithium monomer led to higher weight ratios of the polymer matrix and, therefore, less plasticizer in the GPE; thus, limiting the movement of ions. Therefore, a tradeoff between plasticizer and polymer ratio needs to be found. In this case, the sample with composition of 20 %wt. LiMTFSI : 70% wt. TEGDME : 10 %wt. PEGDM, showed the highest conductivity value of 1.64·10^{-4} S·cm^{-1} at RT and was selected for further testing. From now on, this formulation is named as "**Single-ion GPE**". As indicated before, a dual-ion conductive GPE membrane was designed

incorporating the same molar ratio of lithium for comparison. Hence, **"Dual-ion GPE"** with a composition of 90 %wt. (0.84M LiTFSI in TEGDME) : 10 %wt. PEGDM . Figure 2.2c shows the ionic conductivity of these two membranes measured at different temperatures using Electrochemical Impedance Spectroscopy (EIS). The σ of the equivalent liquid electrolyte (0.84M LiTFSI in TEGDME) was also assessed for reference. The Dual-ion GPE achieved a conductivity of $1.44 \cdot 10^{-3}$ S·cm^{-1} at 25°C, showing a value very close to the equivalent liquid electrolyte ($2.88 \cdot 10^{-3}$ S·cm^{-1}). As expected, the ionic conductivity of the Single-ion GPE was lower than the Dual-ion one. This can be explained by the slightly higher content of plasticizer of the dual-ion system and the participation of both highly mobile [TFSI$^-$] and [Li$^+$] ions in the conductivity values.
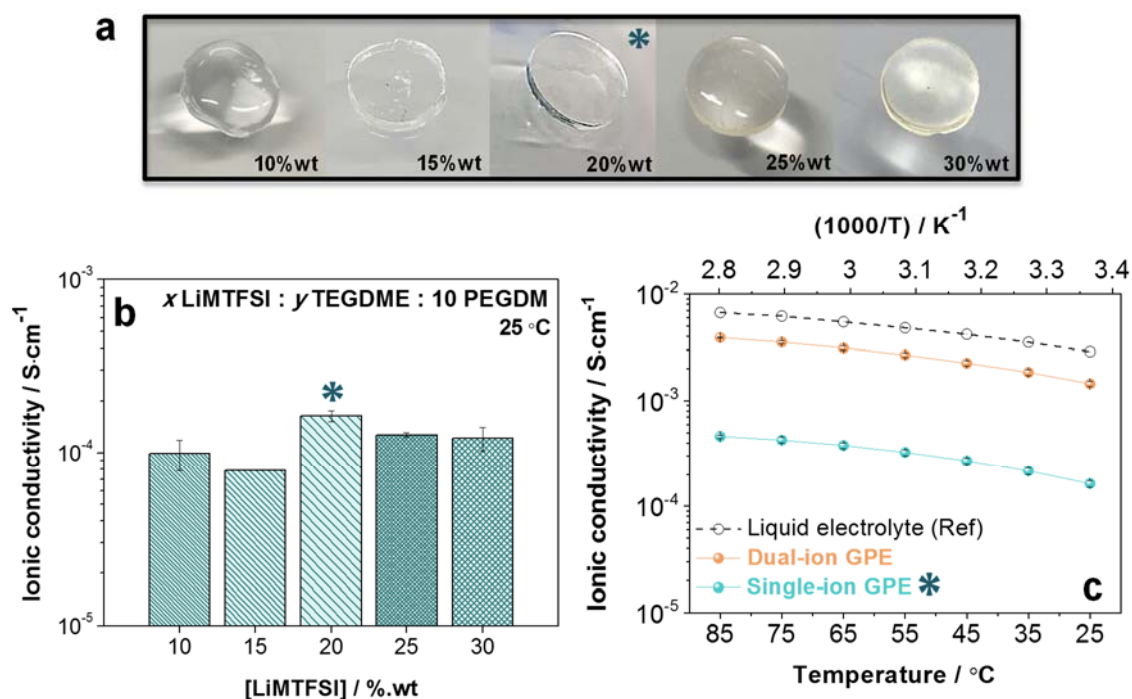
Figure 2. 2. a) Pictures of the single ion membranes containing increasing amount of lithium conductive monomer (LiMTFSI) in wt%., b) Ionic conductivity values of single ion conducting GPEs having 10, 15, 20, 25 and 30 %wt. of LiMTFSI monomer in their formulation at 25°C and, c) Ionic conductivity vs temperature of selected Single ion (*) and Dual ion GPE compared to the analogue liquid electrolyte.

Actually, the proportion of the conductivity that is carried by the lithium cations can be quantified [34] by the calculation of the so-called lithium transference number (t_{Li^+}). The method proposed by Evans-Vincent-Bruce [34,35] was used to measure the t_{Li^+} of

both Single-ion and Dual-ion GPEs. Results of EIS and polarizations tests at 25°C are shown in Figure 2.3.
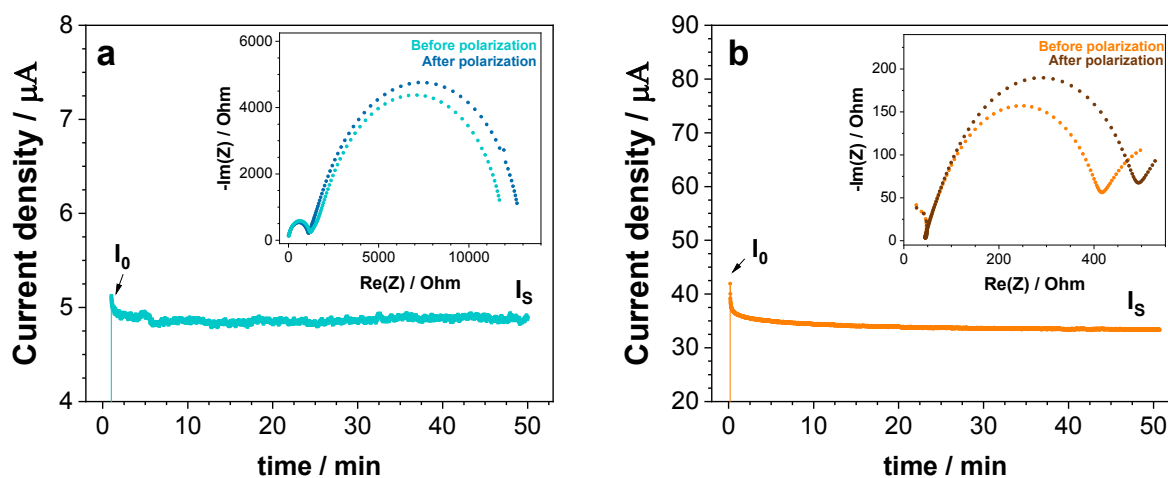
Figure 2. 3. Chronoamperometry and EIS spectra before and after polarization obtained in lithium symmetrical cells for: a) Single ion GPE and b) Dual ion GPE.

The transference number value of the Single-ion GPE was found to be 0.83 ± 0.01; while the Dual ion GPE reached 0.57 ± 0.02. In single ion GPEs, the plasticizer (e.g. TEGDME) can form solvated complexes with the lithium ions, allowing their free movement and achieving t_{Li^+} close to unity [13,18]. For dual ion GPE electrolytes, t_{Li^+} values are usually lower (around 0.5-0.6) [36,37] due to the high mobility of the sulphonamide anion compared to the bulky solvated lithium shell [38]. Overall, the optimized UV-crosslinked GPEs showed excellent ionic conductivity values and lithium transference numbers comparable to literature.

2.3.2 Thermal and mechanical characterization

These characterization techniques were applied to the Dual ion GPE and three different single-ion membranes having increasing concentrations of LiMTFSI conducting monomer (10, 20 and 30 %wt.). The thermal stability was assessed by thermal gravimetrical analysis (TGA) under inert atmosphere (N_2), as shown in Figure 2.4a. In all cases, the samples exhibited a two-step degradation process and curves were slightly shifted at different temperatures, depending on the composition. The initial degradation, between 150 – 200 ºC, was attributed to the initial loss of TEGDME.

This loss was more significant in the samples with larger amount of plasticizer (10 : 80 : 10 and Dual ion GPE, with 80 and 90 %wt. ratio of liquid electrolyte, respectively), achieving loses of up to 60% of their weight at 200 ºC. The second degradation, initiated at around 250 ºC, was greatly attributed to the degradation of the polymeric matrix [13]. Therefore, the TGA curves of the single ion GPEs with higher concentrations of polymer were shifted to the right (higher temperatures). In this second range, the final evaporation of the remaining TEGDME was also considered due to its low volatility (bp 275 ºC). The presence of the LiTFSI salt in dual ion GPE slightly shifted this second step to higher temperatures.
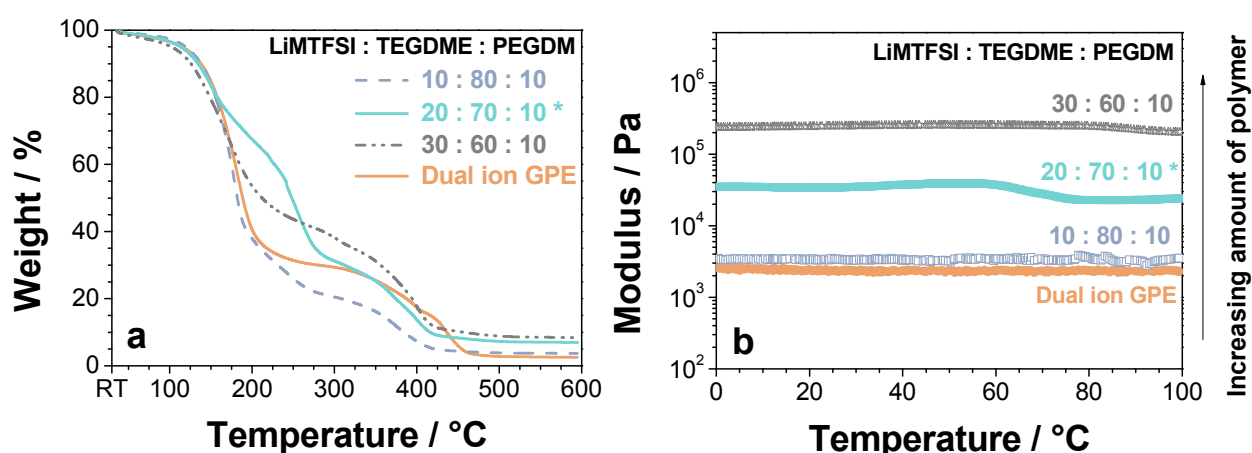
Figure 2. 4. a) TGA analysis under nitrogen atmosphere at 10 ºC/min and b) DMTA analysis at compression from 0 to 100 ºC of GPEs with different weight ratio compositions (%wt. LiMTFSI : %wt. TEGDME : %wt. PEGDM) .

Dynamic mechanical thermal analysis (DMTA) was also assessed, Figure 2.4b. As expected, the storage modulus of the samples increased with the polymer concentration achieving a maximum of $2.53 \cdot 10^5$ Pa for the 30 : 60 : 10 membrane. Thus, it can be concluded that this GPE was stiffer but also more brittle (high cross-linking). The modulus of the Single ion GPE* was one order of magnitude higher than the Dual ion GPE ($3.45 \cdot 10^4$ and $2.24 \cdot 10^3$ Pa, respectively) remaining steady from 0 to 100 ºC. Hence, their thermal and mechanical stability makes them interesting materials for battery applications in temperature ranges bellow 100 ºC.

2.4 Lithium symmetrical cells

Symmetrical lithium cells were assembled to evaluate the electrochemical behavior of the solid electrolytes against lithium metal. First, samples were exposed to ± 0.01, ± 0.1, ± 0.2, ± 0.5, ± 0.8, ± 1 and ± 2 mA·cm^{-2} current rates for two hours/cycle. Three cycles were completed at each rate. Once the highest current was applied (± 2 mA·cm^{-2}), the whole process was applied again for a second loop, starting from the lowest current and for a total of 84 hours (Figure 2.5a).
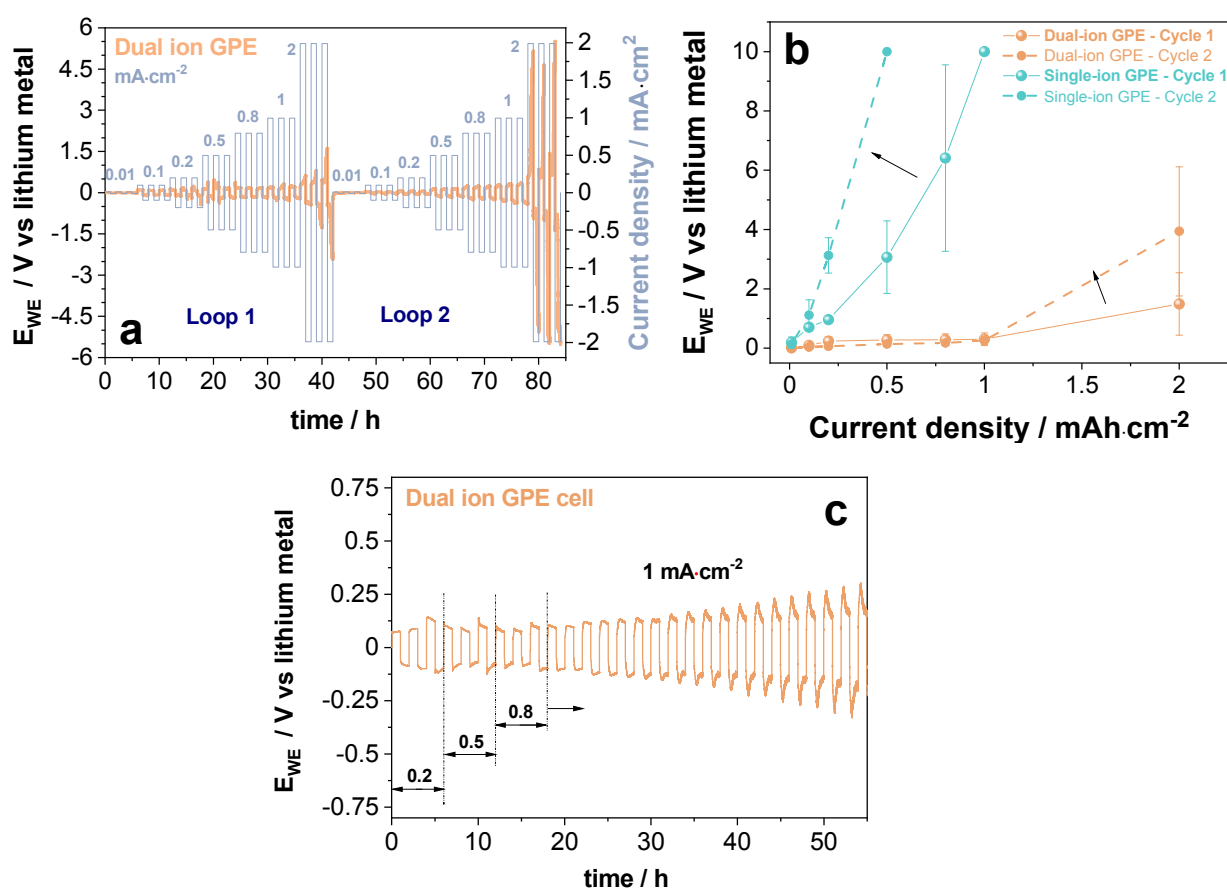
Figure 2. 5. a) Ramp test at increasing current densities from 0.01 to 2 mA·cm^{-2}. Potential against time data for Li | Dual ion GPE | Li cell (raw data); b) Absolute potential against current density; and c) Lithium plating/striping cycles on Dual ion GPE.

As shown on Figure 2.5b), during the first loop, the Dual ion GPE showed much lower overpotentials than the Single ion GPE, exceptionally being 0.3 V vs Li^0/Li$^+$ at 1 mA·cm^{-2} and 1.5 V vs Li^0/Li$^+$ at 2 mA·cm^{-2}. On the other hand, the overpotentials achieved on the second cycle increased significantly in the case of the Single ion GPE

(~3 times the initial value at 0.2 or 0.5 mA·cm^{-2}). This tendency remarkably differed on the Dual ion GPE, in which the overpotential remained steady at 0.3 V vs Li^0/Li$^+$ when current of 1 mA·cm^{-2} was applied. Due to this promising behavior, the Dual ion GPE was then further exposed to lithium plating/striping longer cycling with a cut-off potential of 0.5 V and half-cycle time of one hour (Figure 2.5c). This cell was able to cycle for 40 hours at high current (1 mAh·cm^{-2}) keeping an overpotential below 0.2 V vs Li^0/Li$^+$. Furthermore, this overpotential remained below 0.4 V after 55 hours of cycling.

Hence, the Dual ion GPE, which had a highest ionic conductivity value, showed much better performance in lithium symmetrical cells. This result was initially surprising as single ion electrolytes are expected to show lower overpotentials during lithium plating/stripping. However, it is consistent with a study from Lee J.T. research group [39], in which they compared a single and dual ion electrolyte in lithium symmetrical cells. One of their conclusions was that their single ion electrolyte behaved better than the dual ion only at lower currents. At higher currents, their dual ion sample exceeded the single ion. They attributed this behaviour via the higher inherent impedance of the single ion system, especially noticeable at higher currents. This could probably explain our results since the current rates we used (up to 2 mA·cm^{-2}) were much higher than the ones usually reported in literature for symmetrical lithium cells (0.1 – 0.5 mA·cm^{-2}) [8,13,37,40]. These results also highlight the high number of results obtained with independent types of electrolytes in literature but the lack of comparison between them, which is an important asset for more efficient optimization methods. In this way, this work shows the importance of this concept.

2.5 Li-O$_2$ cells

2.5.1 Galvanostatic discharge and cycling

To further evaluate and compare the performance of the single and dual ion GPE membranes, they were tested on Swagelok Li-O$_2$ cells. Together with the solid electrolytes GPEs, cells using the equivalent liquid electrolyte (0.84M LiTFSI in TEGDME) were also tested for comparison. These cells were first discharged at a galvanostatic current of –5 μA·cm^{-2} (Figure 2.6a) until the potential reached 2 V at 25 °C. When the negative current was applied, the samples first suddenly experienced

an Ohmic drop (*iR*), reaching quickly a plateau at around 2.72 - 2.78 V, which corresponds to the practical potential of the spontaneous electrochemical reaction $2Li + O_2 + 2e^- \rightarrow Li_2O_2$ (lower than the theoretical one (2.96V vs Li^0/Li^+)) due to overpotentials) [41,42] followed by a sharp decrease to 2.0 V vs. Li^0/Li^+ at the end of the discharging [43].
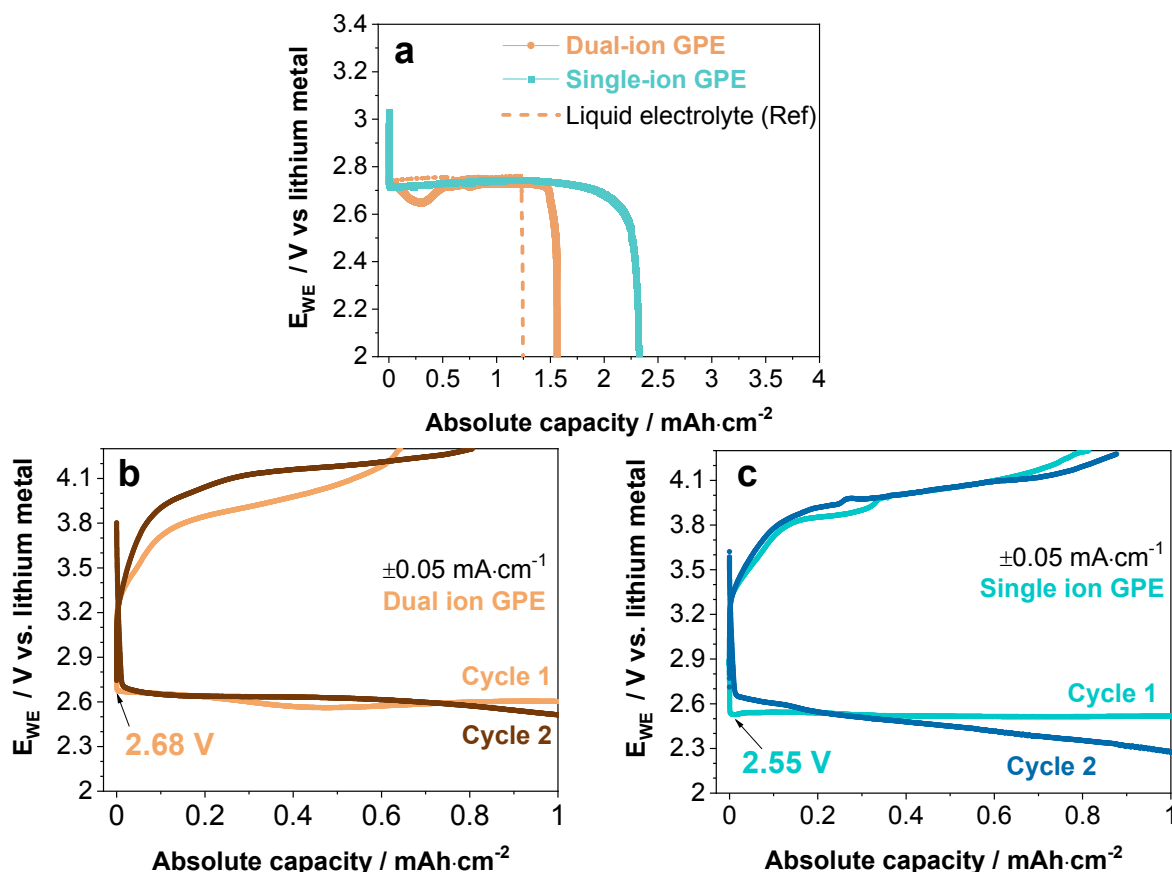
Figure 2. 6. a) Potential against absolute capacity during galvanostatic discharge at -5 $\mu A \cdot cm^{-2}$ and 25 °C. Potential against capacity during galvanostatic cycling at ±50 $\mu A \cdot cm^{-2}$ at 25 °C of b) Dual ion GPE and c) Single ion GPE. Discharge/charge steps restricted to 1 $mAh \cdot cm^{-2}$, unless limiting potential was achieved (4.3 V for charge and 2 V for discharge).

As shown in Figure 2.6, the Single ion GPE achieved the highest absolute capacity for this first discharge, being 1.5 times higher than the Dual ion GPE (2.38 and 1.56 $mAh \cdot cm^{-2}$, respectively). Most likely, this is due to the solely mobility of Li^+ ions in the Single ion membrane, which allows a more homogeneous and ordered mass transfer of lithium ions to the positive electrode, especially whenlow current densities are applied (i.e. –5 $\mu A \cdot cm^{-2}$). Similar conclusions were achieved in other studies done on lithium metal batteries [39]. Interestingly, the GPE solid electrolytes achieved much

higher capacity than the liquid equivalent cell (1.7 and 1.25 times higher for the Single ion and Dual ion cells, respectively). Considering an average carbon loading of 0.72 mg·cm^{-2} in the positive electrode, the relative capacity was as high as 3,306 mAh·g^{-1} for the Single ion GPE cell and 2,190 mAh·g^{-1} for Dual ion GPE cell. In order to provide insights into the rechargeability of the developed electrolytes, discharge/charge cycles at ±50 µA·cm^{-2} for both Single ion and Dual ion Li-O$_2$ cells are carried out with a restricted capacity of 1 mAh·cm^{-2} as shown in Figure 2.6b-c. Different onset potentials for the oxygen reduction reaction (ORR) on the discharge process was observed: 2.68 V and 2.55 V vs Li^0/Li$^+$ for cells using Dual ion and Single ion GPEs, respectively; indicating the higher suitability to higher currents of the Dual ion system.

2.5.2 Dynamic discharge

Cells were then discharged following a dynamic approach, in which increasing negative currents were applied to the sample (Figure 2.7). Each rate was applied for 15 minutes and immediately increased and re-applied for another 15 minutes until the potential of the cell faded below 2 V (Loop x1). OCV was then applied. Interestingly, the potential of the cell increased back to equilibrium values during OCV (Figure 2.7a), indicating that only a part of the discharge capacity was used. After sufficient time and when $dE_{WE} / dt \sim 0$ ($E1_{eq}$, $E2_{eq}$, etc.), the cell was dynamically discharged again (named as Loop x2). The potential increased back again to equilibrium and the cell was discharged again (Loop x3). This innovative process was repeated (e.g. up to 52 loops for Single-ion GPE cells) until the equilibrium potential of the cell at OCV achieved 2 V vs Li^0/Li$^+$, allowing a gradual but complete discharge of the cell (full cell capacity use). The potentials at equilibrium after a single dynamic discharge (E_{eq} in Figure 2.7a), were proportional to the polarization effect of all the Li cations accumulated at the positive electrode that were unable to react with the oxo- radicals due to the short times applied at each rate (15 minutes), the increasing current densities (diffusional limitation at higher rates) and/or the inability to find a free active site on the carbon electrode (i.e. pseudo-capacitive contribution of the battery). During OCV, these unreacted ions re-arranged and, consequently, the potential first suddenly increased to a value proportional to the Ohmic drop (iR) and then, it slowly increased

(ions diffusion phenomena due to concentration gradients after applying current) until equilibrium, i.e. $dE_{WE} / dt \approx 0$.
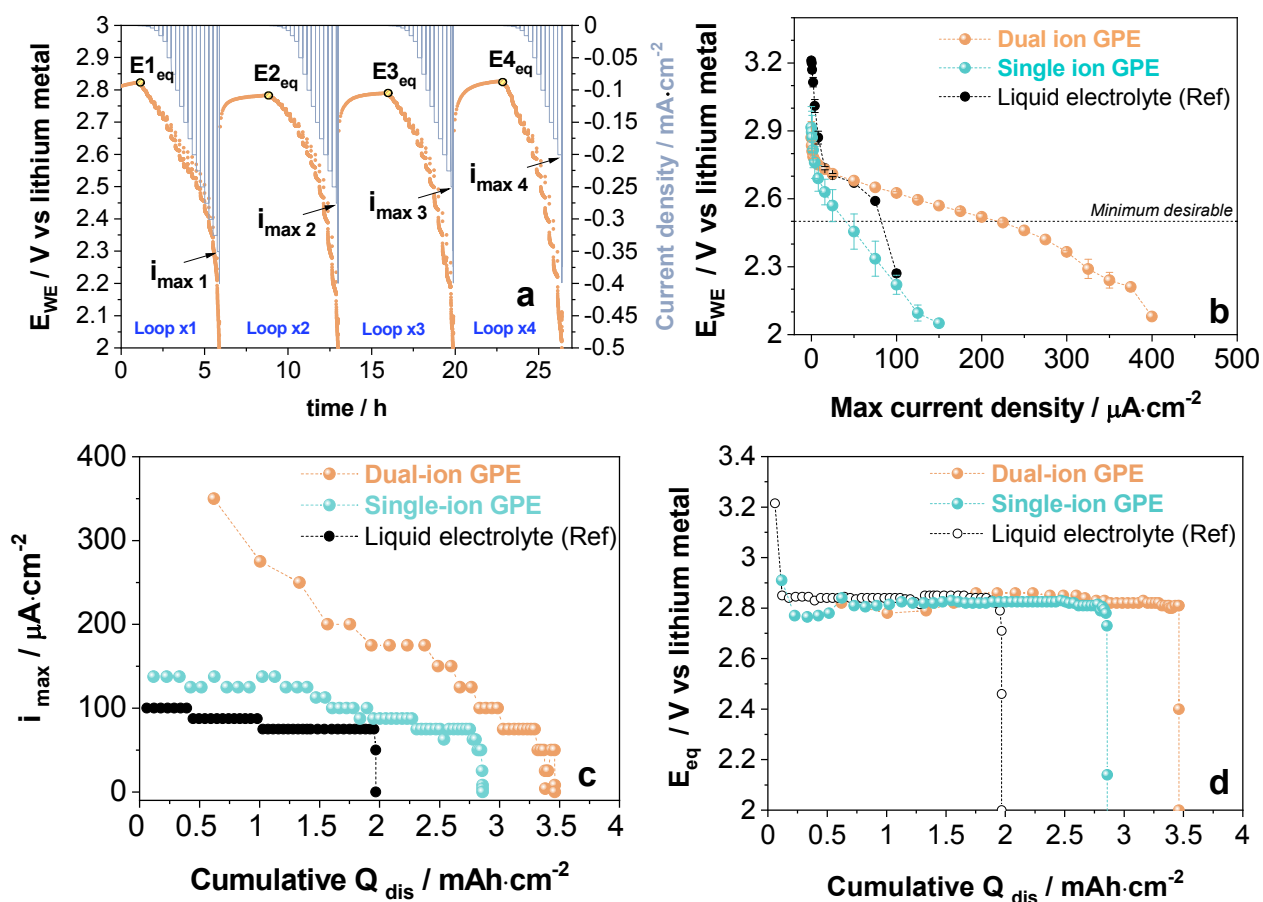
Figure 2. 7. a) Potential against time during the first fourth loops of an innovative dynamic discharge of Li-O$_2$ cells using Dual ion GPE as a solid electrolyte (raw data); b) Average potentials reached at each current density during the first loop on dynamic discharge: c) Maximum current densities stood by the electrolytes during dynamic discharge; and d) Equilibrium polarization potentials against cumulative capacity during dynamic discharge.

Relevant information can be extracted from the raw data of the multiple dynamic discharge (Figure 2.7a). In each loop, the cell is able to withstand a determined maximum current density (i$_{max}$). This information is plotted in Figure 2.7b (single loop, Loop x1) and Figure 2.7c (multiple loops). In general, the cells showed low variations on the maximum currents achieved across discharge (~flat curve), observing that cells using polymeric electrolytes showed superior values than cells using liquid counterpart electrolytes. However, the Dual-ion GPE cell exhibited remarkable high current densities, with a maximum of 350 µA·cm^{-2} and it was still above 175 µA·cm^{-2} when the cumulative capacity was already as high as 2.4 mAh·cm^{-2}. This higher

performance against high currents is in accordance with the results obtained on the symmetrical lithium cells. Furthermore, the equilibrium polarization potentials (E_{eq}) of the cells were plotted against their cumulative capacity (Figure 2.7d). The shape of the curves strongly reminded to the galvanostatic discharge curves, which is in accordance with the above explanation (gradual discharge of the cell). The highest cumulative capacity corresponded with the cell using the Dual-ion GPE (3.46 mAh·cm^{-2} or 4824 mAh·g^{-1}), followed by the one with the Single-ion GPE (2.86 mAh·cm^{-2} or 3984 mAh·g^{-1}) and the one with equivalent liquid electrolyte (1.97 mAh·cm^{-2}). Figuratively, these results seem to be in contradiction with the galvanostatic discharge ones, in which the Single-ion GPE cells had the highest discharge capacities. However, as these equilibrium potentials were proportional to the polarization effect, it would be accurate to expect higher cumulative capacities for cells with the Dual ion system than the Single ion one; in one hand due to the higher amount of mobile ions (Li$^+$ and TFSI$^-$) and, on the other hand, due to the higher maximum currents that the Dual ion GPE was able to withstand, and therefore, higher cumulative capacities could be achieved. Similar effect was also observed in other studies [39], and it could be related to the intrinsic impedance of the Single ion GPE, which was higher than the one of the Dual ion GPE. According the Ohmic law and the Nernst-Planck equation[44], the mass transfer limitation (impedance) is therefore more pronounced when higher currents are applied. On the other hand, this polarization effect seemed to be higher on the polymeric electrolytes than the liquid ones. This could be due to the theoretical higher diffusion of ions (better mobility) in the liquid electrolyte and a better electrolyte | electrode interface.

Second Part

Design of boron-based single-ion gel polymer electrolytes for lithium batteries by photopolymerization

2.6 Preparation of boron-based single-ion gel polymer electrolytes (SIGPEs)

2.6.1 Synthesis of lithium borate methacrylic monomers (SIM-xx)

Three anionic methacrylic monomers based on highly delocalized asymmetric borate groups were synthesized as recently reported [32] (Scheme 2.2).
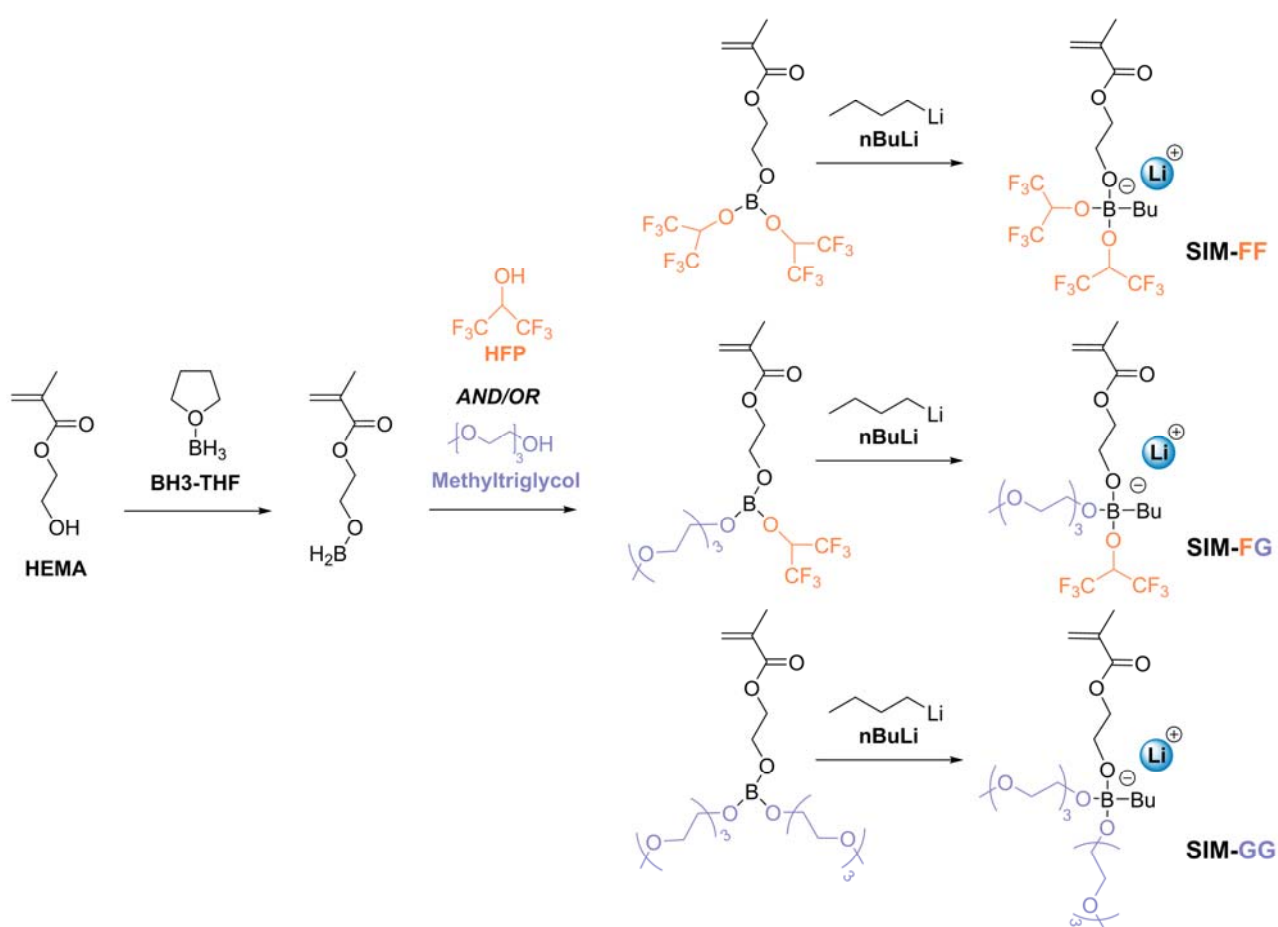
Scheme 2. 2. Synthetic route for the preparation of borate-based single-ion monomers SIM-FF, SIM-FG, and SIM-GG[32].

In the first step, 2-hydroxyethyl methacrylate (HEMA) was covalently bonded to a boron atom (-C-O-B- bond) via the dropwise addition of borane tetrahydrofuran complex (BH₃-THF). In the second step, the desired functionality was added to the

methacrylic-molecule via the addition of triethylene glycol monomethyl ether (methyltriglycol) and/or hexafluoroisopropanol (HFP). Finally, n-butyllithium (n-BuLi) was added to generate the formation of the boron-lithium anionic group. The author would like to thank Dr G. Guzmán-González for the synthesis of these monomers.

Chemical structures of these SIM-xx are composed of an ethoxy-methacrylate group (polymerizable group), a butyl group through a (B-C-) bond (stabilizing agent-decreasing hygroscopicity), and two oxy- (B-OR) substituents, which aimed to modulate the electron-withdrawing ability of borate groups and/or create lithium-ion mobility pathways.

Thus, three custom-made sp^3 boron-based single-ion monomers (SIMs) named as SIM-FF, SIM-FG, and SIM-GG; where *F* or *G* represent the functional substituent groups (F = 1,1,1,1,3,3, 3-hexafluoropropan-2-yl)oxy and/or G = bis((2-(2-(2-(2-methoxy ethoxy)ethoxy) ethyl) boryl)oxy)) were synthesized. The arrangement of these substituents within the polymer network may modulate the electron density of the borate groups (given by the fluorinated functionality, *F*) and/or the promotion of dissociation and solvation of the lithium ions (given by the presence of ethoxy groups in *G*).

2.6.2 Synthesis of single-ion polymer electrolytes (SIPE-xx)

Single-ion Gel Polymer Electrolytes (SIGPEs) were prepared by rapid UV-photopolymerisation process following the success in the first part of this chapter (Scheme 2.3).

Single-ion SIM-FF, SIM-FG, and SIM-GG methacrylic monomers were co-polymerized (independently) with the crosslinker poly(ethylene glycol) dimethacrylate (PEGDM) in the presence of 2-Hydroxy-2-methylpropiophene (DAROCUR) as the radical photoinitiator. In some cases, tetraethylene glycol dimethyl ether (tetraglyme, G4) was added as a plasticizer at different ratios.
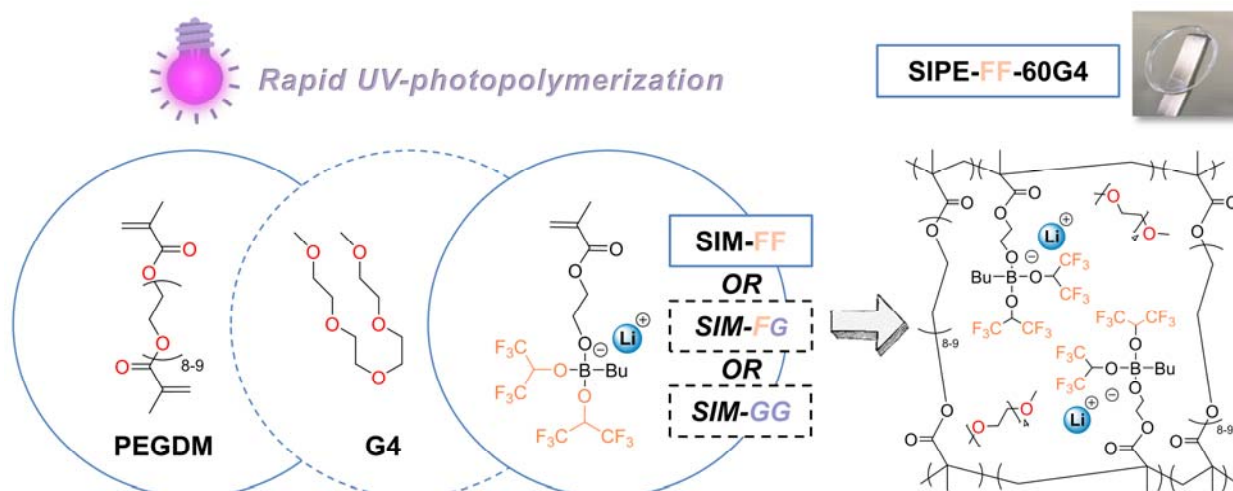
Scheme 2. 3. Lithium single-ion gel polymer electrolyte (SIGPE) synthesis process by UV-photopolymerization. SIPE-FF-60G4 chemical structure is illustrated as an example.

Table 2.1 shows the different formulations of the nine SIGPE electrolytes synthesized in this work. For each of the three monomers, three single ion polymer electrolytes (SIPE) formulations containing increasing amounts of G4 plasticizer were designed and named as SIPE-xx-60G4 (60 %wt. of G4), SIPE-xx-30G4 (30 %wt. of G4), and SIPE-xx (solvent-free solid polymer electrolyte).

Table 2. 1. SIGPE electrolytes compositions in wt%.

Name	SIM-xx[a]	PEGDM [b]	G4 [c]
SIPE-FG-60G4	20	20	60
SIPE-FG-30G4	60	10	30
SIPE-FG	95	5	Solvent free
SIPE-FF-60G4	20	20	60
SIPE-FF-30G4	60	10	30
SIPE-FF	95	5	Solvent free
SIPE-GG-60G4	20	20	60
SIPE-GG-30G4	60	10	30
SIPE-GG	95	5	Solvent free

[a] SIM-FG; SIM-FF or SIM-FG]
[b] Poly(ethylene glycol) dimethacrylate.
[c] Tetraethylene glycol dimethyl ether (tetraglyme, G4).

In all cases, the obtained SIGPEs were self-standing and visually transparent, and monomer conversions were monitored before and after UV-irradiation by Fourier Transform Infrared Spectroscopy (FT-IR). After photopolymerization, the UV-cured gel polymer electrolytes showed high monomer conversions ≥ 95% conversions as seen by the disappearance of the 1635 cm^{-1} band, associated with the stretching of the carbon double bonds of acrylic functionalities [45]. Similarly, to the first part of this chapter, this measurement checked the photopolymerization process and the viability of the proposed synthetic method.

2.7 Characterization of single-ion gel polymer electrolytes (SIGPEs)

Thermal and mechanical testing was undertaken to evaluate the potential use of these membranes as electrolytes in operating battery cells.

2.7.1 Thermal analysis

Two consecutive degradation areas were observed in SIPE-FF-60G4 and SIPE-FF-30G4 samples on the thermal gravimetrical analysis (TGA) curves (Figure 2.8a).

The first degradation was between 100 and 280 °C (associated with the evaporation of the plasticizer and initial decomposition of the weaker bonds of the polymeric network); and the second one, at around 280 °C (associated with the degradation of the polymeric network with stronger bonds).

TGA profiles of the other families of solvent-free solid polymer electrolytes were also completed (Figure 2.8b). SIPE-FG and SIPE-GG also exhibited two polymeric thermal decomposition areas, but with a less pronounced decomposition than the plasticized membranes. Overall, membranes were thermally stable until ~110 °C, well above LIBs operating temperature (e.g. -20 to 60 °C) [46,47].
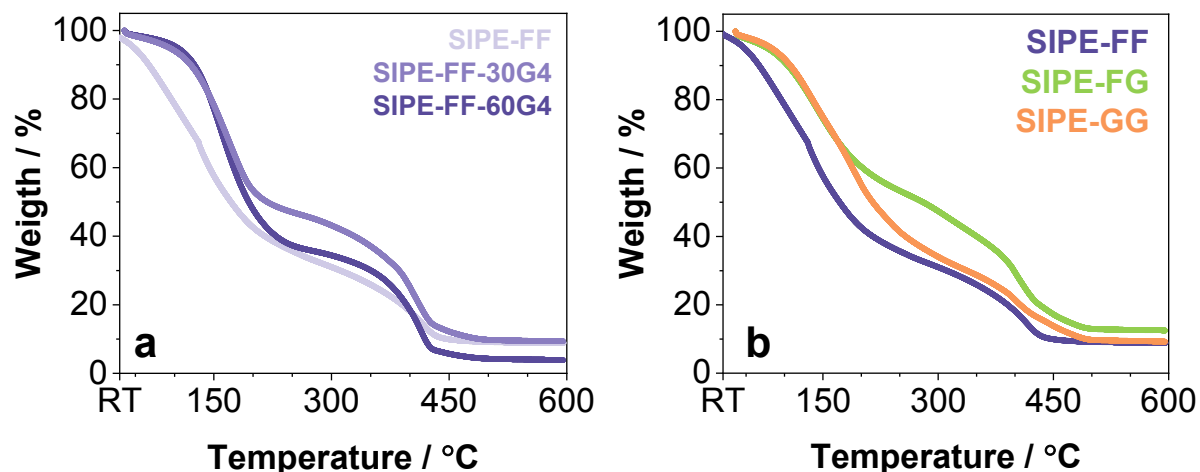
Figure 2. 8. Thermal gravimetrical analysis (TGA) curves of a) SIPE-FF-x family of electrolytes; and b) Solvent-free polymer electrolytes (SIPE-FF, SIPE-FG, and SIPE-GG).

2.7.2 Mechanical analysis

Mechanical stability through dynamic mechanical thermal analysis (DMTA) was also investigated on membranes of the same family containing different amounts of plasticizer (SIPE-GG-xx), Figure 2.9. All electrolyte membranes presented a stable storage modulus from 0 to 100 °C (in between $10^5 - 10^7$ Pa), which increased with lower plasticizer content, having its maximum with the SIPE-GG solvent-free membrane (~$5 \cdot 10^6$ Pa).

Additionally, DMTA measurements at lower temperature range revealed that all membranes were amorphous at RT, having their glass transition temperature (Tg) at -21.0, -37.0, and -33.71 °C for the SIPE-GG, SIPE-GG-30G4, and SIPE-GG-60G4, respectively. This amorphous condition allowed small polymeric segment motions, improving lithium-ion mobility.

Hence, these results make these membranes suitable materials as electrolytes for battery cells from a mechanical perspective, sufficiently strong and flexible to withstand the stresses caused during cells assembly and thickness cells variation during use, without affecting ion transport properties [16].
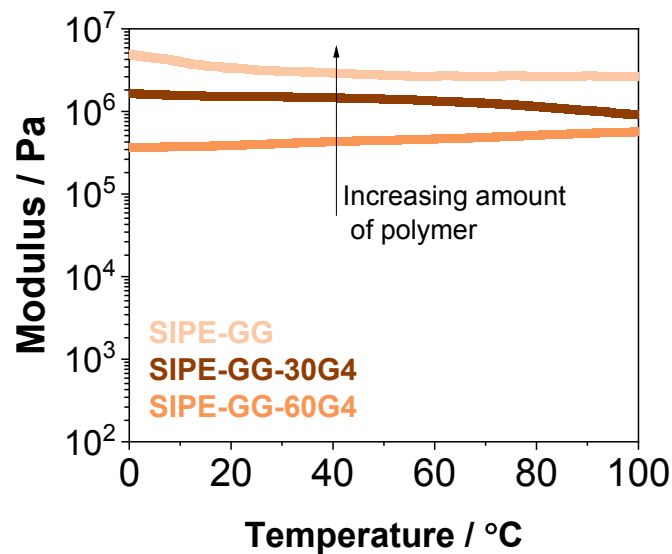
Figure 2. 9. Dynamic mechanical thermal analysis (DMTA) of SIPE-GG-x family membranes at compression from 0 to 100 °C.

2.8 Electrochemical Impedance spectroscopy (EIS) analysis

2.8.1 Ionic conductivity

Ionic conductivities (σ) of the developed SIGPEs were deeply analyzed as a function of the plasticizer content, as well as the impact of the Li$^+$ interaction with the functional moieties of the selected membrane (FF, FG, or GG).
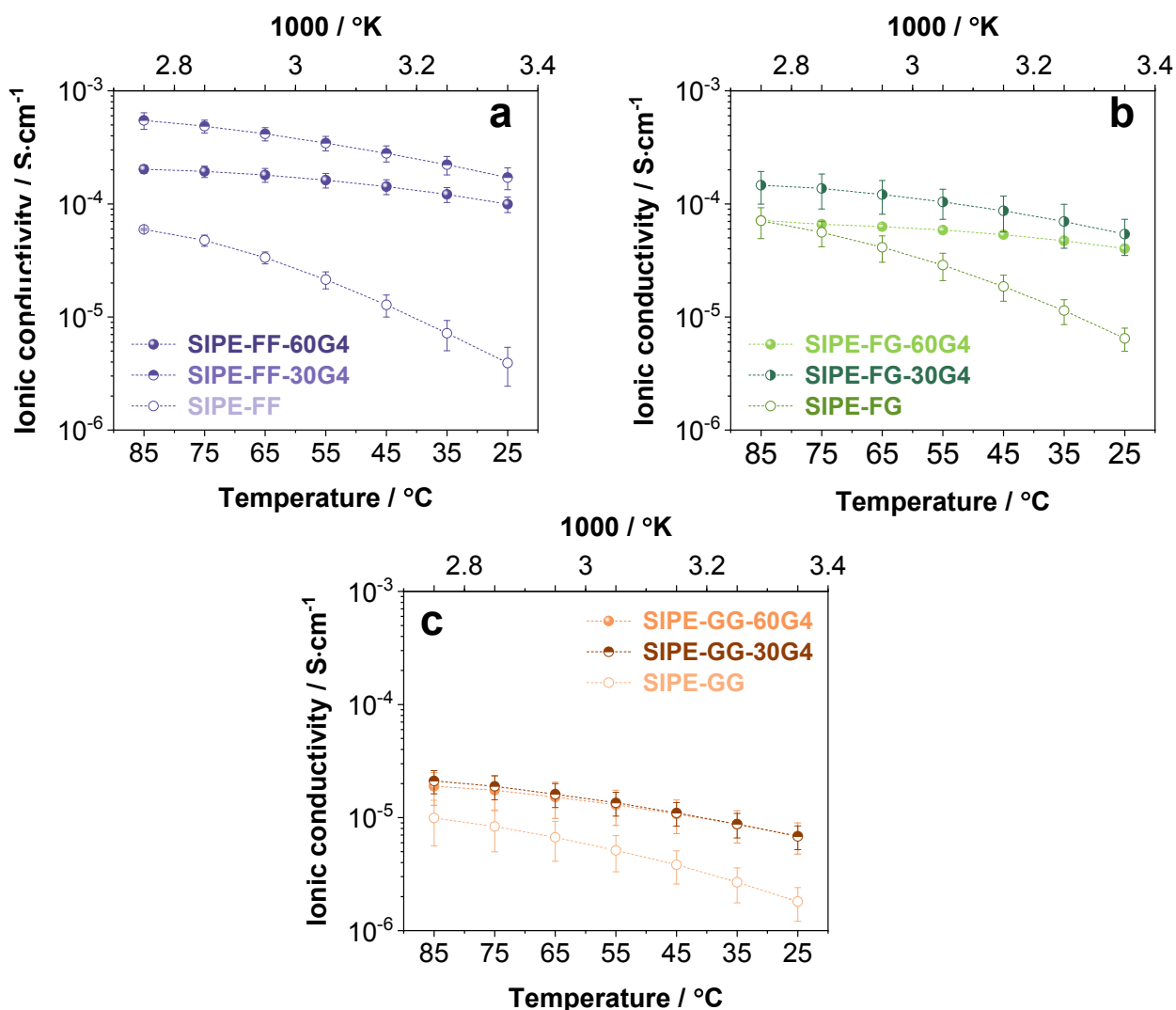
Figure 2. 10. Ionic conductivity values obtained by EIS at different temperatures of a) SIPE-FF-x electrolytes containing increasing amounts of tetraglyme (G4) plasticizer, b) SIPE-FG-x electrolytes family and c) SIPE-GG electrolytes family.

Regarding the plasticizer content, it was common to all membranes that the presence of the plasticizer leads to higher ionic conductivity values (Figure 2.10) compared to solvent-free ones. More particularly, membranes containing 30 %wt. of G4 (SIPE-xx-30G4) had the highest σ values also due to the higher Li$^+$ ratio in the gel polymer electrolyte formulation. The impact of the plasticizer was especially noticeable in the SIPE-FF-xx family (Figure 2.10a), in which there was a difference of 2 orders of magnitude between the ionic conductivity (σ) value at 25 °C of the solvent-free SIPE-FF ($3.92 \cdot 10^{-6}$ S·cm^{-1}) and the SIPE-FF-30G4 ($1.71 \cdot 10^{-4}$ S·cm^{-1}). This difference was partly due to the presence of G4 and partly due to the type of functional group present in the polymeric network. SIGPEs containing borate-fluorinated groups (SIPE-FF-xx),

due to their high electron-withdrawing capability, were expected to weaken the association between the lithium ions and the anionic pendant group, and therefore, ease Li$^+$ mobility from the charged group. In opposition to solvent-free SIPE-FF membranes, the ethoxy groups of the G4 plasticizer present in SIPE-FF-30G4 and SIPE-FF-60G4 provided additional pathways for ion conduction across the electrolyte, hence, enhancing σ and probably explaining the big gap observed between the solvent-free and plasticized membranes.

On the other hand, SIGPEs with borate-ethoxy pendant groups (SIPE-GG-xx), in which the moieties had similar chemical structure to glymes (i.e. G4) were designed to enhance ion mobility through the self-solvating capability of its –C–O– moieties. For this reason, the addition of G4 did not improve significantly the σ of the SIPE-GG-xx family of electrolytes (Figure 2.10c).

Lastly, SIGPEs with asymmetric borate-fluorinated-ethoxy groups (SIPE-FG-xx) were designed to combine both ion delocalization (fluorinated moiety) and ion mobility-pathways capabilities (ethoxy moiety). This effect is observed in the σ of the solvent-free membranes, where SIPE-FG showed the highest value (e.g. $6.47 \cdot 10^{-6}$ S·cm^{-1} at 25 °C) (Figure 2.10b); but it was less significant with the addition of G4 plasticizer.

Furthermore, ionic conductivities increased linearly with temperature and followed Arrhenius-type thermally activated behavior as the following equation (Figure 2.11a) [48,49]:

$$\sigma = \sigma_o \cdot \exp(\frac{-E_a}{kT})$$

, where σ_o is the pre-exponential factor, E_a is the activation energy, and k is the Boltzmann constant.

The effect of the borate-pendant group in the ion transport mechanism was also detected in the SIPEs activation energies (Figure 2.11b). Within the solvent-free membranes, SIPE-FF presented a much higher activation energy than SIPE-FG and SIPE-GG due to the lack of ion mobility-pathways provided by the borate-ethoxy pendant groups. As expected, this energy was significantly reduced by the addition of G4.
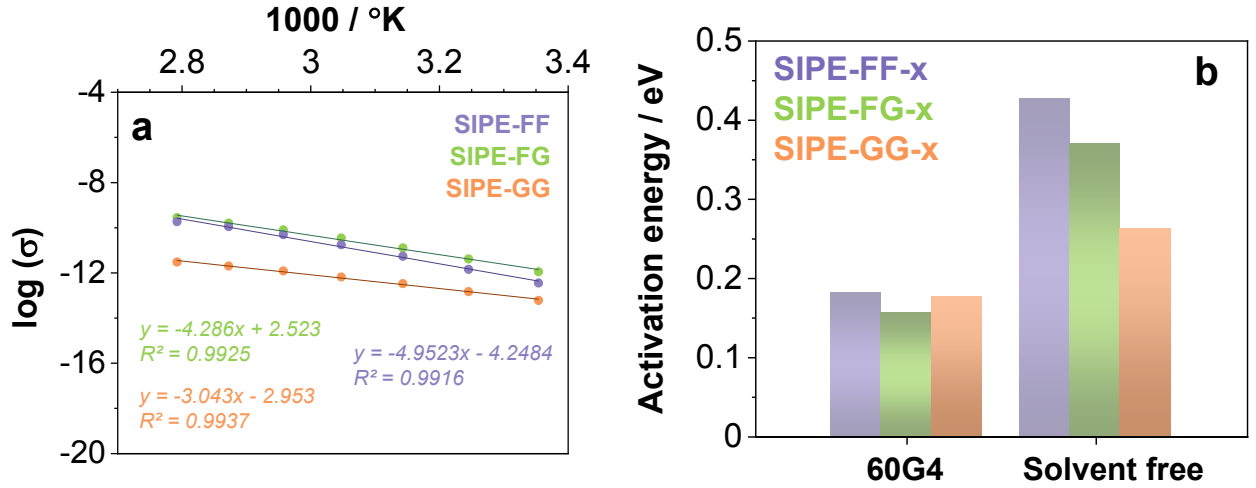
Figure 2. 11. a) Arrhenius fitting plot for SIPE-FF, SIPE-FG, and SIPE-GG electrolytes (solvent-free); and b) Activation energies (eV) calculated following Arrhenius fittings of thermally-activated processes[49].

Overall, the achieved ionic conductivity values in this work are in line with the ones reported in literature [16] for solvent-free single-ion electrolytes ($<10^{-5}$ S·cm^{-1} at 25 °C) and plasticized SIPEs ($< 10^{-3}$ S·cm^{-1} at 25 °C). The SIPE-FF-xx family had the highest ionic conductivity values, but needed the presence of a plasticizer, i.e. G4, to optimize performance. SIPE-FF-30G4, SIPE-FF-60G4, and SIPE-FG-60G4 showed the highest σ values ($1.71\cdot10^{-4}$ S·cm^{-1}, $9.95\cdot10^{-5}$ S·cm^{-1} and $5.4\cdot10^{-5}$ S·cm^{-1} at 25 °C, respectively), making them suitable candidates as solid electrolytes in battery cells from an ion conductive perspective.

2.1.1 Lithium transference number

The lithium transference number (t_{Li^+}) of relevant SIPEs were calculated following the equation proposed by Evans-Vincent-Bruce [34]:

$$t_{Li^+} = \frac{I_s(\Delta V - I_0 \cdot R_0)}{I_0(\Delta V - I_s \cdot R_s)}$$

A DC bias (ΔV, 10 mV) is applied to polarize the SIPEs during a chronoamperometry, I_0 is the initial value of the current upon polarization, I_s is the current reached in the steady-state for the sample after polarization, and R_0 and R_s

are the interfacial resistances before and after the polarization, respectively, obtained by electrochemical impedance spectroscopy (EIS). As an example, Figure 2.12a shows both the response of the current overtime during the ΔV polarization and the correspondent Nyquist plots for the SIPE-FG-60G4 electrolyte at 60 °C.
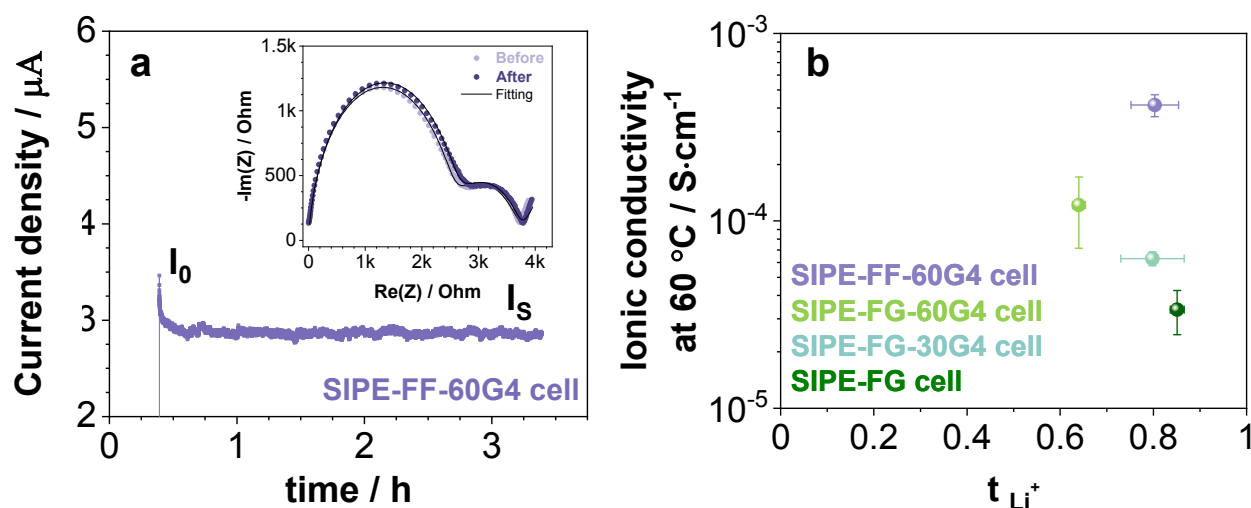
Figure 2. 12. a) Example of chronoamperometry plot for the lithium transference number calculation. Inlet: Nyquist impedance plots before and after polarization, including fitting curves by equivalent circuits; and b) Ionic conductivities at 60°C against lithium transference number of SIPE-FG-x family of electrolytes containing different amounts of G4 plasticizer.

The t_{Li^+} of the solvent-free SIPE-FG electrolyte was found to be 0.85. Solvent-free single-ion conducting polymer electrolytes are close to unity due to the anchoring of the anion group to the polymeric network, thus lowering the accumulation of anions at the electrolyte/negative electrode interface and depressing polarization and resistances due to ion concentration gradients [15,16]. However, these unique transport properties can be slightly affected in plasticized SIPEs, in which there is a partial movement of the anionic groups and polar groups of the polymeric matrix contributing to the solvation of lithium complexes. These partial movements are more significant with increasing lengths of the linking chains between the anionic groups [25,26] and/or the amount/type of solvent incorporated in the polymeric matrices [22]. This behavior was observed in Figure 2.12b, in which t_{Li^+} decreased with higher plasticizer content (0.65 for SIPE-FG-60G4). This might be explained by the formation of lithium-ion solvation complexes with the long G4 glyme plasticizer and the mobile cations, where the negative charge is more delocalized and the Li$^+$ cations disassociate easier. In

accordance, the SIPE-FG-30G4 cell, with intermediate-plasticizer containing electrolyte, had a midway result (0.79) between the solvent-free cell (SIPE-FG) and the high-plasticizer content cell (SIPE-FG-60G4).

For comparison, the t_{Li^+} of the SIPE-FF-60G4 cell was also evaluated giving a value of 0.80. Similarly to the ionic conductivity scenario, this result was a balance of transport properties provided by the borate-fluorinated groups (Li⁺ delocalization) and the presence of the plasticizer (Li⁺ conduction pathways).

2.9 Lithium cells analysis

2.9.1 Stability window

The reversible lithium plating and stripping on/from cupper electrodes of Li⁰/ SIPE-FG-xx family/ Cu cells (Figure 2.13) were investigated by cyclic voltammetry (CV) at 60 °C. As observed, the improvement of the wettability of the electrode surface, generated by increasing amounts of plasticizer, resulted in better interfacial transport during the platting-stripping tests.
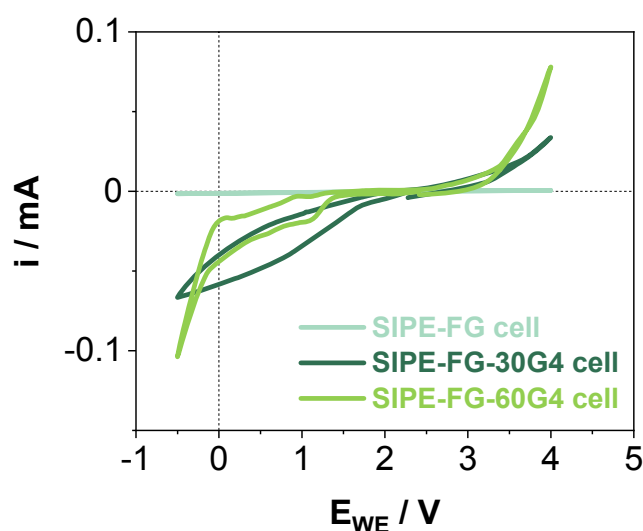
Figure 2. 13. Voltammograms on Li/Electrolyte/Cu cells of SIPE-FG-x electrolytes family.

To evaluate this further, the chemical stability window of SIPE-FF-60G4 and SIPE-FG-60G4 (Figure 2.14) were also investigated. The cathodic scans on Li/ Electrolyte/

Cu cells, showed a couple of reversible redox peaks, stronger on the SIPE-FF-60G4 cells (-0.5 V and 0.17 V vs Li^0/Li^+).
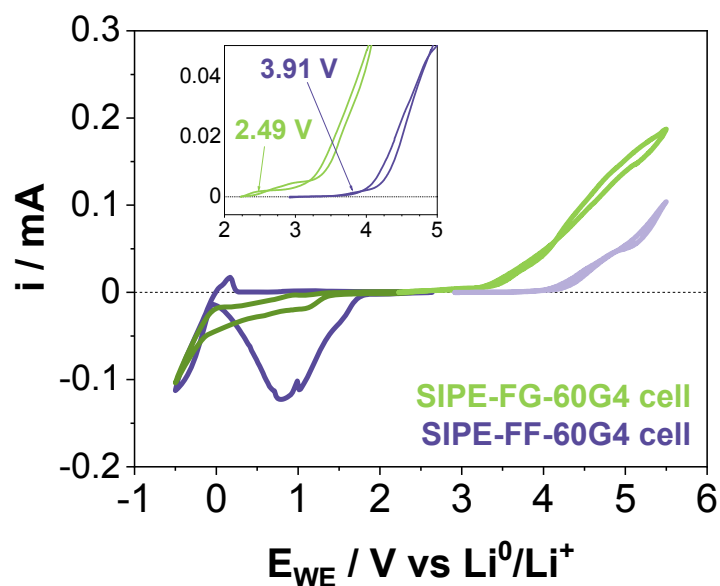
Figure 2. 14. Voltammograms of SIPE-FG-60G4 and SIPE-FF-60G4 electrolytes at 60 °C and a scan rate of 0.2 mV·s^{-1}. Scans were undertaken in Li^0/Cu^0 (from OCV to -0.5 V) and Li^0/Stainless steel (from OCV to 5.5 V) cells.

Figure 2.15 shows the first 5 cycles of the cell containing SIPE-FF-60G4electrolyte during the cathodic scan. There was a very clear irreversible peak at 0.79 V vs Li^0/Li^+ during the first cycle and 1.42 V vs Li^0/Li^+ on the second one. These peaks disappeared in the following cycles. We believe this might be a contribution to the formation of the solid electrolyte interphase (SEI) although a deeper analysis (e.g. such as *in situ* micro-FTIR spectroscopy [50] or X-ray photoelectron spectroscopy (XPS) [51]), which is outside the scope of this chapter, would be needed to study this phenomenon further.

During the anodic scans (Li^0/ Electrolyte/Stainless-steel cells), no oxidation currents were observed up to 2.49 V vs Li^0/Li^+ for the SIPE-FG-60G4 cell and 3.91 V vs Li^0/Li^+ for the SIPE-FF-60G4 cell (Figure 2.14).
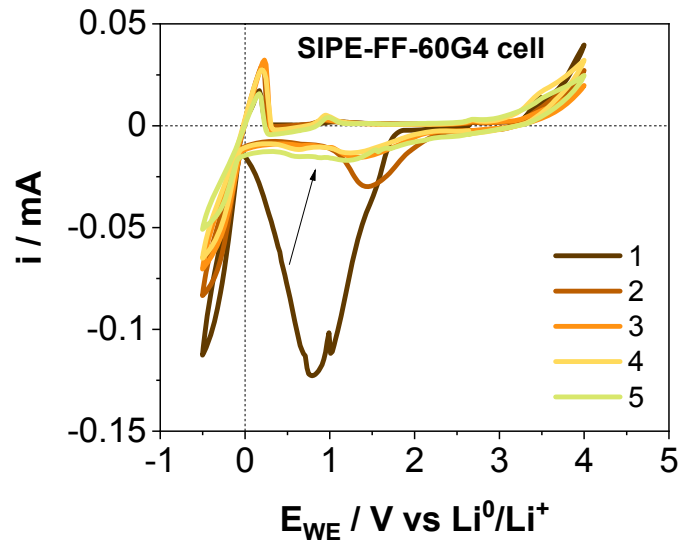
Figure 2. 15. Voltammograms at a scan rate of $0.2 \text{ mV} \cdot \text{s}^{-1}$ of Li/SIPE-FF-60G4/Cu cell.

2.9.2 Lithium symmetrical cells

Lastly, lithium symmetrical cells were assembled to evaluate the polarization potentials at consecutive current rates of ± 0.01, ± 0.1, ± 0.2, and $\pm 0.5 \text{ mA} \cdot \text{cm}^{-2}$ at 60 °C of the most promising SIGPE membranes: SIPE-FF-60G4 and SIPE-FG-60G4, as well as SIPE-GG-60G4 for comparison (Figure 2.16).

For each current density, the cells were cycled three times (2 hours/cycle). According to previous results in this chapter, cells with SIPE-FF-60G4 and SIPE-FG-60G4 electrolytes presented better performance. The critical current density (CCD) for both electrolytes was $\pm 0.2 \text{ mA} \cdot \text{cm}^{-2}$, achieving overpotentials <0.34 V and <1.23 V for SIPE-FF-60G4 and SIPE-FG-60G4, respectively.
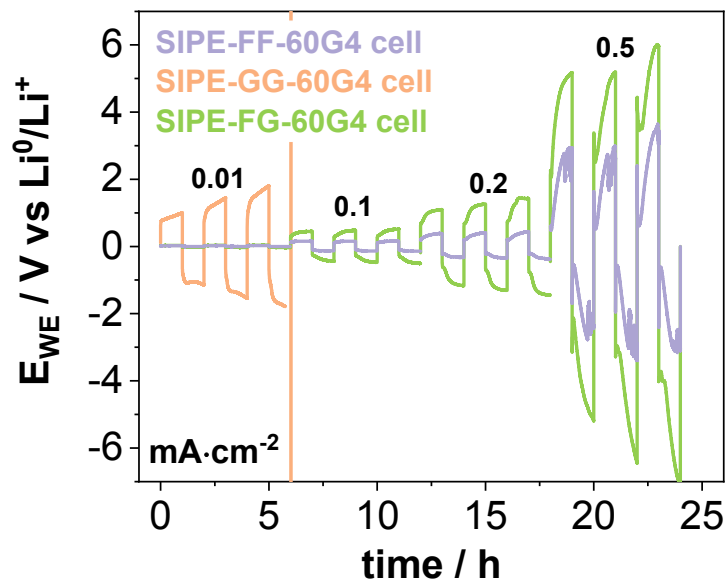
Figure 2. 16. Lithium stripping/platting curves at increasing current densities from 0.01 to 0.5 mA·cm^{-2} in symmetrical lithium cells using SIPE-FF-60G4, SIPE-FG-60G4 and SIPE-GG-60G4 electrolytes.

The same test was undertaken for the rest of the SIPE-FG-xx family electrolytes. As shown in Figure 2.17, CCD was quickly achieved for the solvent-free SIPE-FG cell (±0.01 mA·cm^{-2}, 2.36 V). On the other hand, cell containing SIPE-FG-30G4 electrolyte showed a CCD at (±0.2 mA·cm^{-2}, (1.87 V), concluding that the presence of G4 plasticizer helped to lower the overpotentials when samples are polarized, as seen in literature [52,53].
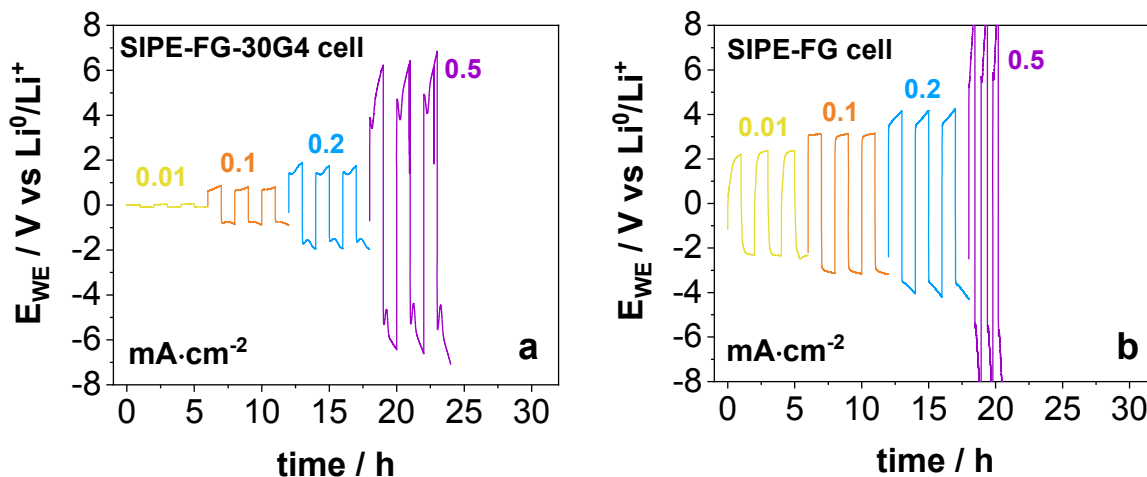
Figure 2. 17. Lithium stripping/platting curves at increasing current densities from 0.01 to 0.5 mA·cm^{-2} in symmetrical lithium cells using: a) SIPE-FG-30G4 and b) SIPE-FG electrolytes.

2.9.3 Long term cycling in lithium symmetrical cells

Furthermore, long-term cycling stability in lithium symmetrical cells of the most promising electrolytes (SIPE-FF-60G4 and SIPE-FG-60G4) were investigated at their CCD (±0.2 mA·cm^{-2}) during 175 hours after a 3 h conditioning at OCV.
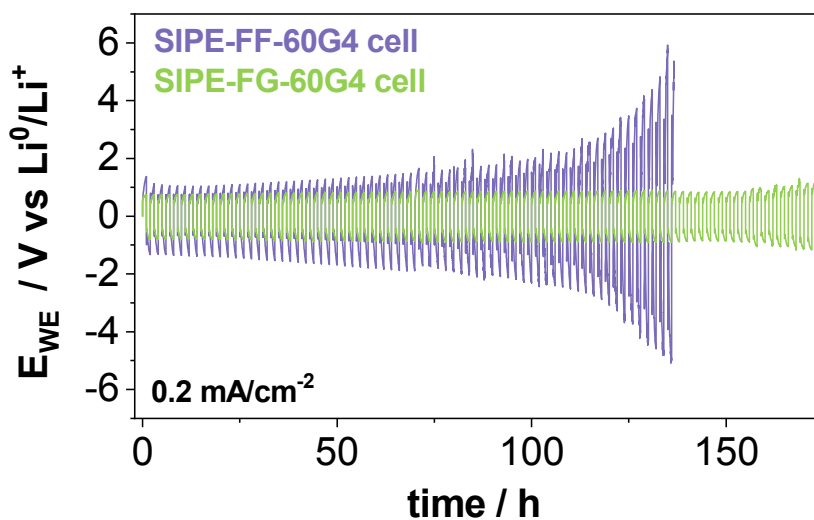
Figure 2. 18. Long cycling of Li/Li cells at 0.2 mA·cm^{-2}.

Figure 2.18 shows that SIPE-FF-60G4 was able to retain overpotentials <1.20 V for around 50 h, following a slow and continued overpotential increase until cell death

occurred after 135 hours. On the other hand, the SIPE-FG-60G4 cell kept the polarization potentials <0.85 V during the whole testing.

2.10 Versatility of the boron chemistry

As demonstrated in this chapter, the sp3 boron chemistry can be very versatile. Amongst the different materials that can be synthetised, lithium molten salts probably represent the most desired ones. If successful, these new set of materials could provide all the advantages sought on an electrolyte, all-in-one type of solution:

- No need of a toxic organic solvent
- Liquidity of the lithium salt that improves lithium ions mobility.

To complete this chapter a new family of tailored-designed lithium molten salts will be evaluated for the first time in lithium metal cells and their initial feasibility in Li-O$_2$ cells assessed. The author would like to thank Dr G. Guzmán-González for the synthesis and provision of these innovative lithium salts.

2.10.1 New lithium molten salts

Five custom-made sp^3 boron-based lithium molten salts (LMSs) named as LMS-xxx (e.g. LMS-AFG); were synthesized. In this nomenclature, and similarly to SIGPEs; *A, F or G* represent the functional substituent groups (A = (ethane-2,1-diyl) diacetate)boryl)oxy), F = 1,1,1,1,3,3, 3-hexafluoropropan-2-yl)oxy, and G = ((2-(2-(2-(2-methoxy ethoxy)ethoxy) ethyl) boryl)oxy)).

In the same way than in the analyzed SIGPEs, the organization of these substituents within the molten salt modulated different functionalities. The electron density of the borate groups was given by the fluorinated functionality (*F)*; the promotion of dissociation and solvation of the lithium ions was given by the ethoxy groups in *G;* and the "ethoxy acetate" group given by *A* could provide a self-solvating effect, similar to polymers with fluorinated substituents[32]. An overview of the structures is given in Figure 2.19.
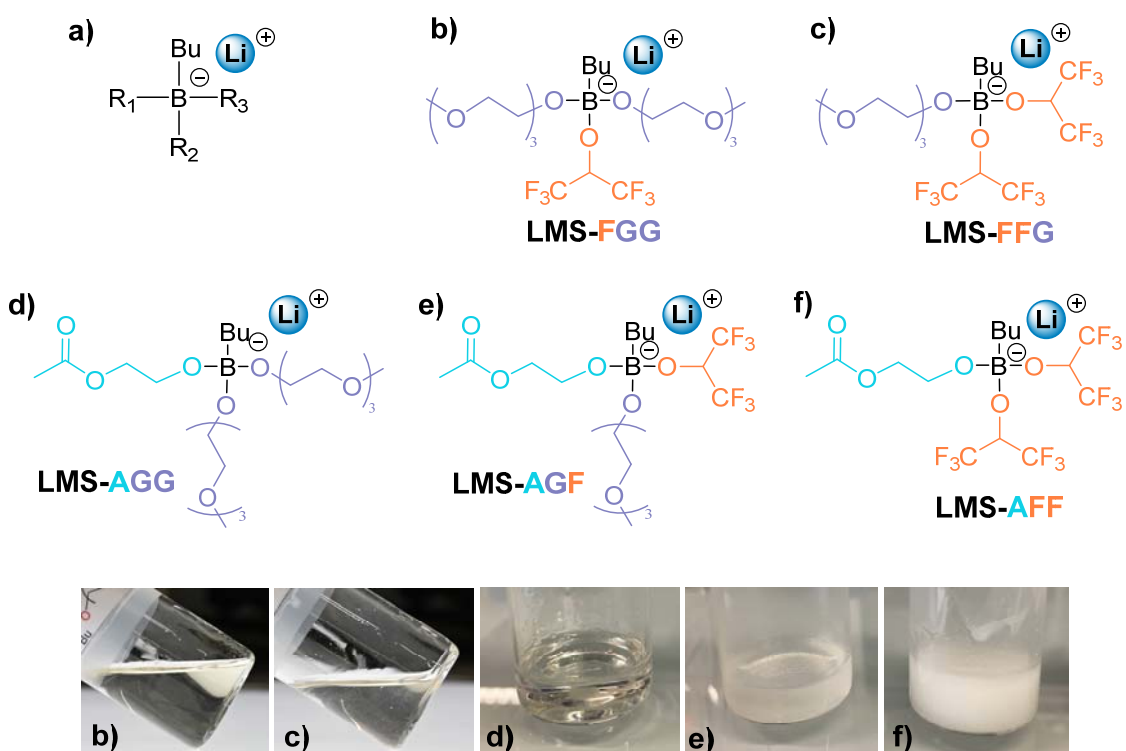
Figure 2. 19. Lithium molten salts structures tailored-designed for this work.

2.10.2 Preparation of gels containing molten salts

Gels containing the selected molten salt (GLMS) were also prepared by UV-photopolymerisation following a similar approach as the one presented previously in this chapter. In this case, a standard liquid electrolyte (LE) is not needed, hence, poly(ethylene glycol) dimethacrylate (PEGDM) was directly mixed with the lithium molten salt at a fixed weight ratio (80 %wt. molten salt : 20 %wt. PEGDM) in the presence of 2-Hydroxy-2-methylpropiophene as the photoinitiator. After UV-irradiating for 5 min on the drop-casted solution self-standing and transparent membranes were obtained for all the salts with the exception of LMS-AFF, in which a phase separation occurred.

2.10.3 Thermal and mechanical characterization of the gels

Preliminary thermal and mechanical testing was undertaken in the GLMS gels. First, thermal gravimetrical analysis (TGA) in the same conditions as previously described

in this chapter was undertaken on three of the gels (Figure 2.20a). The thermograms are very similar to the ones shown on Figure 2.8 using G4-plasticized gels. Two degradation areas related to the degradation of the polymer network (same in both cases, SIGPE and GLMS gels) and the plasticizers/molten salts are observed. Possibly, one of the key differences between these curves is that the thermal stability is lower in the case of the molten salt gels. For instance, GLMS-FGG gel had a T_{onset} of 95.24 °C against the 122.65 °C observed for SIPE-FF-60G4.
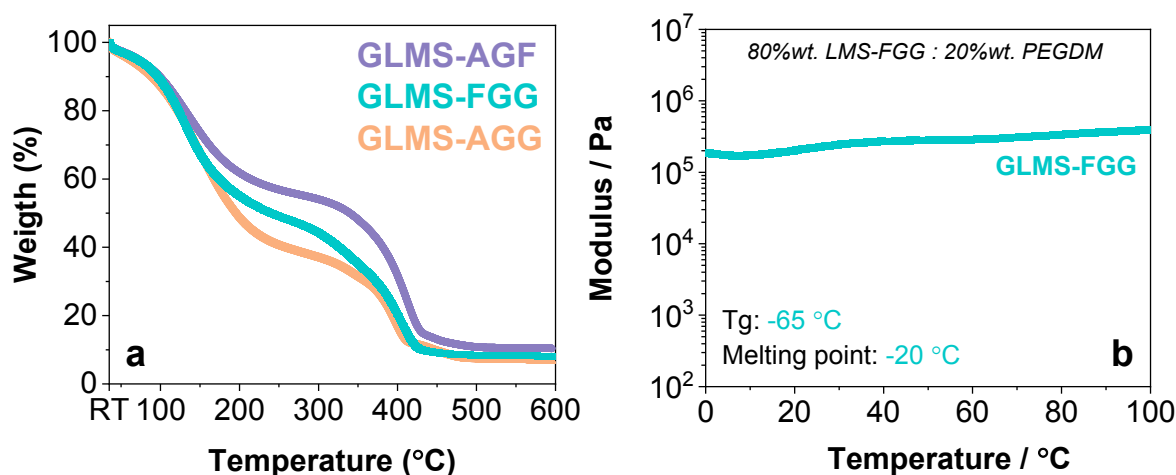
Figure 2. 20. a) Thermal gravimetrical analysis (TGA) curves; and b) Dynamic mechanical thermal analysis (DMTA) of GLMS-FGG membrane from 0 to 100 °C.

A preliminary investigation on the mechanical properties of the GLMS-FGG gel was undertaken via DMTA (Figure 2.20b). In this case, the storage modulus smoothly increased from $2 \cdot 10^6$ Pa (25 °C) to $4 \cdot 10^6$ Pa (100 °C). This phenomenon might be related to the earlier degradation of these gels found on the TGA. Possibly, the degradation was related mostly to the molten salt, leading to a higher polymeric content with increasing temperatures and, therefore, a higher modulus. The Tan δ derivative showed a Tg transition at -65 °C and a melting point at -20 °C.

2.10.4 Ionic conductivity

The ionic conductivity (σ) of the GLMS-AGF, GLMS-FGG and GLMS-AGG gels were analyzed by EIS (Figure 2.21).
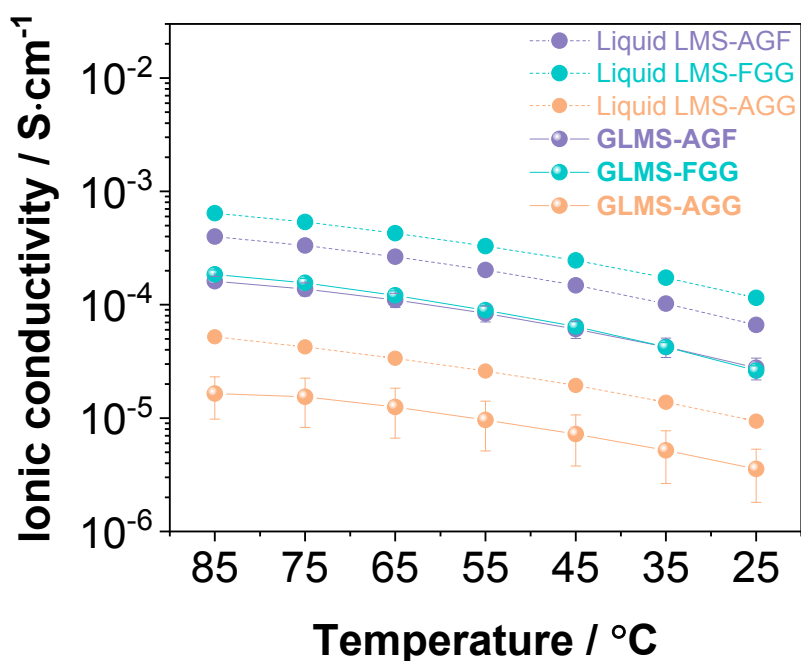
Figure 2. 21. Ionic conductivity values at different temperatures for gel and molten salt cells.

As shown in the plot, GLMS-AGG had the lowest conductivity ($3.55 \cdot 10^{-6}$ S·cm^{-1} at 25 °C), but it was improved by one order of magnitude when the acetate functionality (G) was substituted with a fluorinated one (F). The value of GLMS-FGG increased to $2.62 \cdot 10^{-5}$ S·cm^{-1} at 25 °C. As seen with the SIPE gels, the fluorinated moiety is able to decrease the energy bond of the borate and Li$^+$ and then improve the cation mobility. The acetate and ethoxy groups can provide pathways for ion conduction, but the presence of the fluorinated group seems to be key for disassociating the lithium ion from the borate group. This hypothesis was also confirmed in the GLMS-AGF gel ($2.62 \cdot 10^{-5}$ S·cm^{-1} at 25 °C, same as GLMS-FGG), as the main difference between GLMS-AGF and GLMS-AGG was the addition of the F moiety.

Liquid cells, in which only the molten salt is used as electrolyte, showed the same trend than the gels but with higher values (e.g. Liquid LMS-FGG had a σ value of $1.15 \cdot 10^{-4}$ S·cm^{-1} at 25 °C).
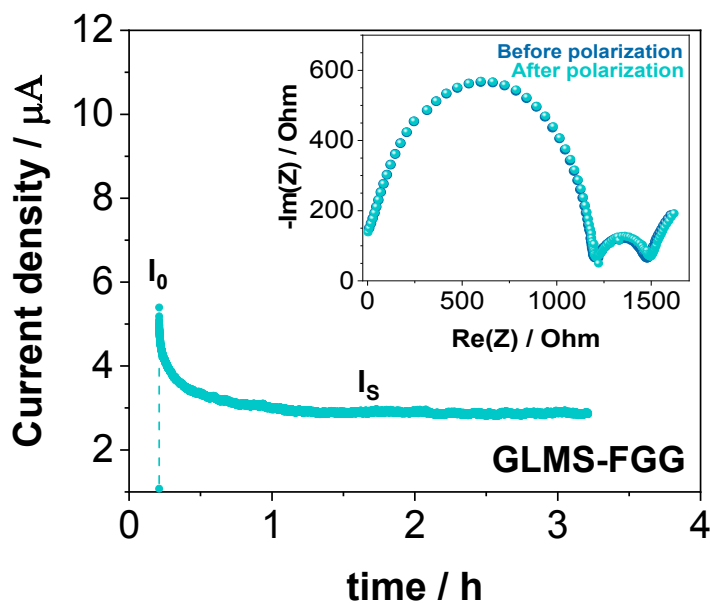
Figure 2. 22. Chronoamperometry plot for the lithium transference number calculation following the Evans-Vincent-Bruce method[34] of GLMS-FGG gel electrolyte. Inlet: Nyquist impedance plots before and after polarization.

On the other hand, the lithium transference number (t_{Li^+}) was calculated for the GLMS-FGG gel (Figure 2.22), and it was 0.49. As seen previously in this chapter, this value is closer to organic solvent based gels (i.e. 0.57 for the Dual ion GPE reported earlier) than iongel based cells (room temperature molten salts) (i.e. $0.14 - 0.25$ values for iongels that are reported in the forthcoming Chapter 4). This finding is very positive, as it indicates the potential of these lithium molten salts as electrolytes, directly comparable with the organic-based electrolytes.

2.10.5 Initial trials on lithium metal cells

First, the stability against upper potentials of GLMS-FGG gel against lithium is shown in Figure 2.23. During this anodic scans (Li^0/ Electrolyte/Stainless-steel cells), no oxidation currents were observed up to 3.51 V vs Li^0/Li^+.
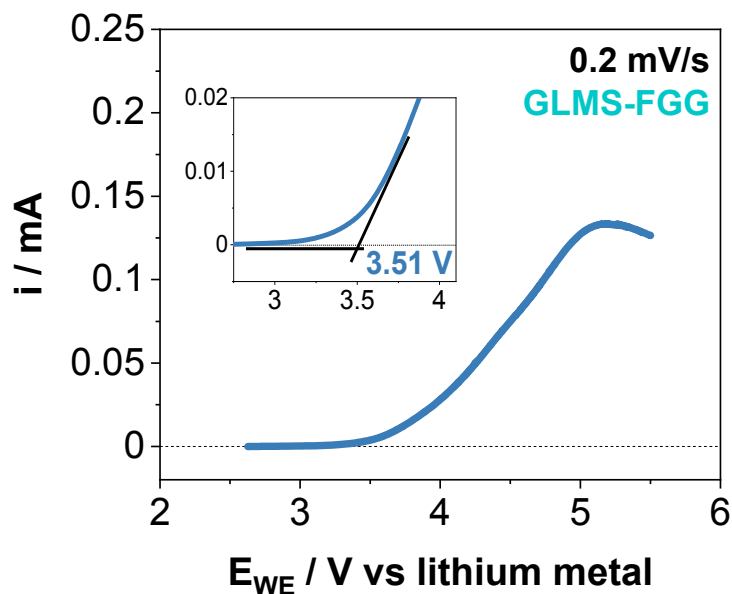
Figure 2. 23. Voltammetry of Li^0/Stainless steel cells (from OCV to 5.5 V) using GLMS-FGG gel as electrolyte at a scan rate of 0.2 mV·s^{-1} .

Lithium symmetrical cells were also assembled to evaluate the polarization potentials of the gels, from ±0.01, ±0.1, ±0.2 to ±0.5 mA·cm^{-2} at 25 °C and 60 °C. All gels were evaluated but only results on GLMS-FGG and GLMS-FFG cells are shown (Figure 2.24). The rest of the gels presented very high polarizations even at low current perturbations.

Regarding temperature, both gels had very similar polarizations at 25 and 60 °C. This shows initial suitability of these gels to be used at room temperature (feature not usual in room temperature ionic liquids). The critical current density (CCD) at 60 °C was ±0.2 mA·cm^{-2} for cell using GLMS-FGG (~1.1 V) and ±0.1 mA·cm^{-2} for the one using GLMS-FFG (~1.6 V). These values were similar to the ones achieved on the boron-based SIPEs cells analyzed earlier in this chapter.
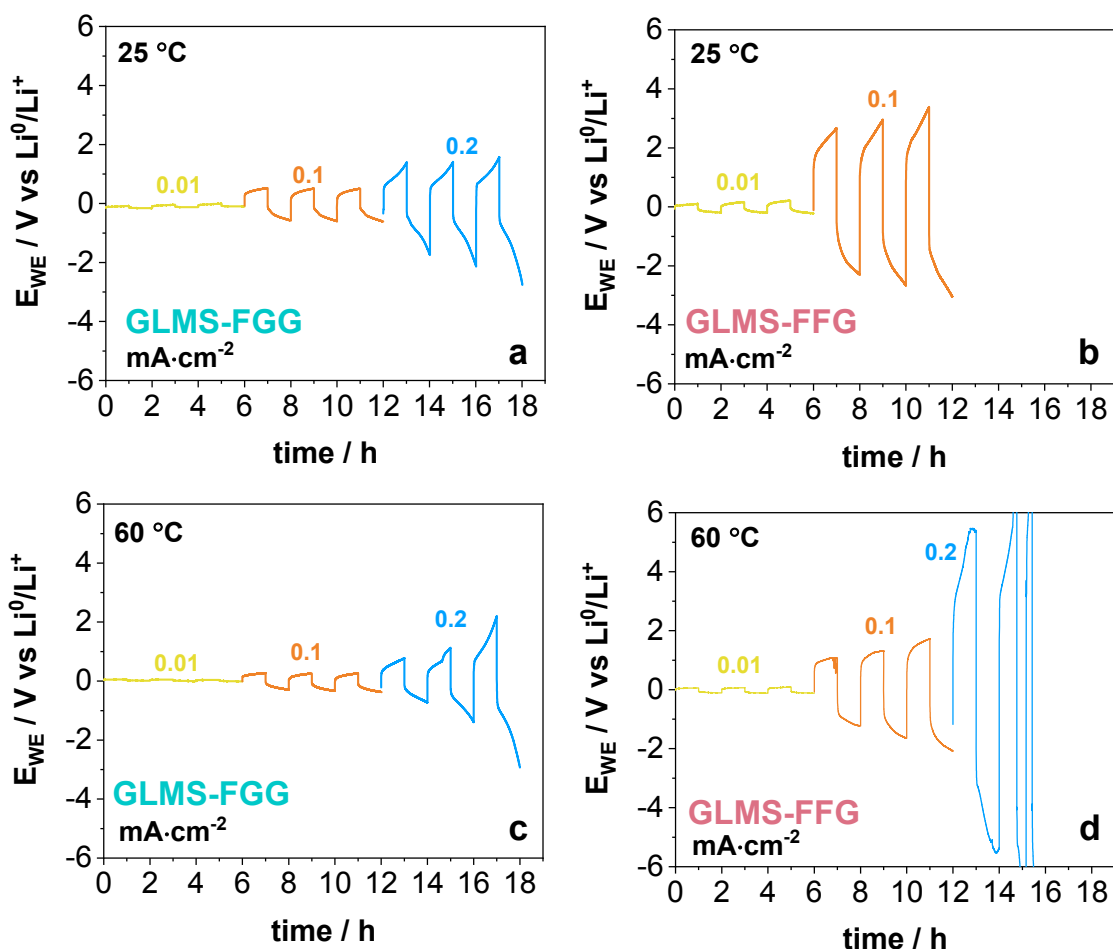
Figure 2. 24. Lithium stripping/platting curves at increasing current densities from 0.01 to 0.2 mA·cm^{-2} in symmetrical lithium cells at 25 °C and 60 °C.

Due to the lower polarization potentials observed for GLMS-FGG samples, these cells were also evaluated from a longer-term cycling stability at ±0.2 mA·cm^{-2} at 25 °C and 60 °C (Figure 2.25). Initially, similar overpotentials were expected for both temperatures; however, a fast increase of the potential was observed when cycled at RT leading to a quick death. At 60 °C, Li/Li cells were able to cycle for 57 hours with overpotentials <1 V.
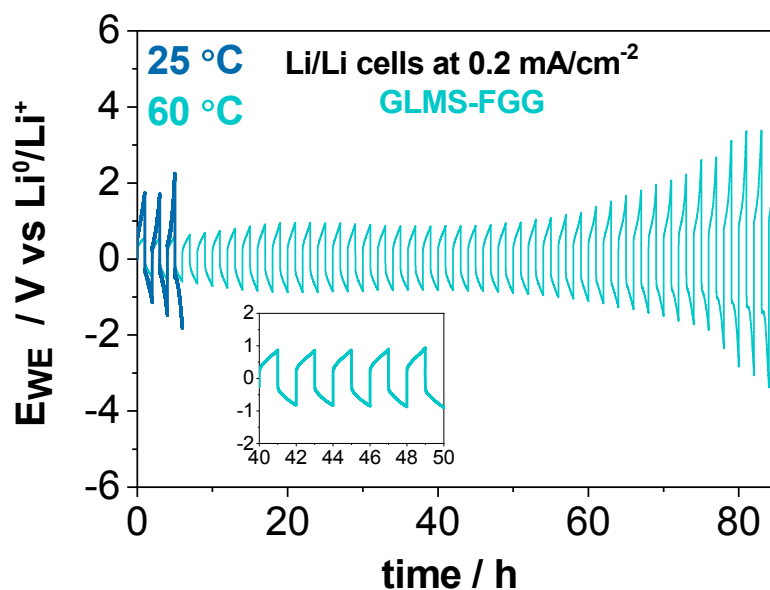
Figure 2. 25. Long cycling of GLMS-FGG gel electrolyte in lithium symmetrical cells at 0.2 mA·cm^{-2} and two temperatures.

2.11 Conclusions

In conclusion, in this chapter different families of single ion gel polymer electrolytes have been proposed as suitable materials for Li-O$_2$ batteries.

On the first part of this chapter, single ion gel polymer electrolytes based on TEGDME and LiMTFSI lithium conductive monomer have been compared for the first time with its dual ion GPE counterparts as solid electrolytes for Li-O$_2$ batteries. These two new families of electrolytes were prepared in a simple manner by fast UV-photopolymerization. Gel polymer electrolytes showed a powerful combination of high ionic conductivity (1.64·10^{-4} S·cm^{-1} for single ion GPE and < 1.44·10^{-3} S·cm^{-1} for dual ion GPE at 25°C) mechanical strength (3.45·10^4 Pa for single ion GPE and > 2.24·10^3 Pa for dual ion GPE) and good thermal stability (T$_{onset}$ 150 °C, for both electrolytes). These properties make both GPEs feasible alternatives to liquid electrolytes for Li-O$_2$ cells.

The work presented in this first part of the chapter directly compares key features of two GPE systems by common characterization techniques and a new method to evaluate polarization effect during discharge in Li-O$_2$ cells. The Dual ion GPE showed a superior behaviour against high rates, even after long cycling in lithium symmetrical

cells. On the other side, Single ion GPE showed excellent performance and higher capacities than the dual ion GPE in Li-O_2 cells. Interestingly, both solid GPEs behaved as good as, or in a superior manner, than the liquid electrolyte counterpart, settling a step forward to solid and safer Li-O_2 systems.

These results might indicate the challenges associated in the design of all-in-one electrolyte solutions and therefore, the importance of a rational design stimulated by feasible objectives. The design strategy proposed in this chapter will be used as a baseline for optimization in the forthcoming chapters.

On the second part of this chapter, a new family of lithium single-ion polymer electrolytes (SIGPEs) based on tailored designed borate-based lithium conducting monomers were designed by UV-photopolymerization. Three functional lithium conducting borate monomers, based on fluorinated (SIM-FF), ethoxy (SIM-GG), or a combination of both functionalities (SIM-FG), have been photo-polymerized in the presence of G4 plasticizer. As a result, self-standing and visually transparent gel polymer electrolytes were obtained in a clean and fast way. All membranes presented good thermal and mechanical stability up to 100 °C.

The role of the different substituents in the boron atom on electrochemical properties was analyzed based on Li$^+$ transport characteristics in solvent-free electrolytes. SIPEs with asymmetric borate-fluorinated-ethoxy groups (SIPE-FG-xx) combined both Li$^+$ ion delocalization (fluorinated moiety) and ion mobility-pathways capabilities (ethoxy moiety), which translated on the highest conductivity value of the solvent-free SIPE electrolytes ($6.47 \cdot 10^{-6}$ S·cm^{-1} at 25 °C for SIPE-FG) and t_{Li^+} (0.85).

The addition of plasticizer into the membranes created new pathways for the Li$^+$ transport, which turned into a significant decrease of the activation energy of the ionic conduction process and a massive improvement of the SIPE-FF-30G4 and SIPE-FF-60G4 ionic conductivities at RT ($1.71 \cdot 10^{-4}$ and $9.95 \cdot 10^{-5}$ S·cm^{-1}, respectively). These values were the highest ones achieved in this work. Furthermore, the optimized single-ion gel polymer electrolytes presented a reversible plating/stripping of lithium and the lowest overpotentials on lithium symmetrical cells with a critical current density of ±0.2 mA·cm^{-2}.

In addition, findings in this chapter shows the versatility of boron-based chemistry and a new set of lithium molten salts at RT have been evaluated for lithium metal batteries for the first time.

2.12 Experimental part

2.12.1 Materials

Poly(ethylene glycol) dimethacrylate (PEGDM, Aldrich, Mn 550), tetraethylene glycol dimethyl ether (TEGDME, Aldrich, ≥99%)) and 2-Hydroxy-2-methylpropiophene (DAROCUR, Aldrich, 97%) were dried by adding activated 4Å molecular sieves (Aldrich, 4-8 mesh) and allowed 5 days for drying effect. Additionally, PEGDM was dried under vacuum for 24 hours and TEGDME was additionally dried at 55 °C under vacuum overnight. Water content was measured by Coulometric Karl Fischer (Table 2.2).

Table 2. 2. Water content by Coulometric Karl-Fischer of initial materials before and after applying a drying method. Theoretical water content of GPEs.

Water content (ppm)	As received	Dry	*Drying Efficiency*
PEGDM	1441.6 ± 29.9	17.9 ± 4.6	*99%*
TEGDME	94.7 ± 1.4	4.6 ± 1.8	*95%*
LiTFSI in TEDGME[a]	110	16	*86%*
LiTFSI	850	80	*91%*
Dual ion GPE[b]	353.9	30.1	*92%*
Single ion GPE[b,c]	255.3	61.6	*76%*

[a] Dilution factor = 20
[b] Theoretical GPE water content calculated as WaterGPE = WaterPEGDM · %wt PEGDM + WaterTEGDME · %wt TEGDME + WaterLiTFSI or LiMTFSI · %wt LiTFSI or LiMTFSI
[c] Assuming LiMTFSIWater at 250ppm in all cases

Lithium 1-[3-(methacryloyloxy)-propylsulfonyl]-1-(trifluoromethylsulfonyl)imide (LiMTFSI) was synthetized as described elsewhere[54] and dried under vacuum for 24 hours. Lithium bis(trifluoromethanesulfonyl)imide (LiTFSI, TCI, >98.0%) was dried under vacuum at 100°C for 24 hours.

All material preparation and cells assemblies were carried out inside an argon filled glovebox with levels of H_2O < 0.01 ppm and O_2 < 0.01ppm.

Liquid electrolytes. 0.84M LiTFSI in TEGDME mixture was stirred for at least 2 hours at RT before use.

Gel polymer electrolytes based on sulfonamide functional groups. A mixture of 0.84M of LiMTFSI in TEGDME was stirred for at least 2 hours before being mixed with PEGDM at different weight ratios and stirred for another hour. DAROCUR was added at this step at 3% w/w of the monomers. Then, the solution was drop-casted on a silicon mould (Φ 11.28 mm circular voids) and irradiated with a UV-LED lamp (300 – 400 nm, with peak at 385 nm. Lightningcure® V3, Hamamatsu) for 6 minutes at a distance of 9 cm. Self-standing and visually transparent Single-ion GPEs were then obtained. Dual ion GPEs were obtained in the same manner but using the liquid electrolyte mixture described above.

SIGPE electrolytes based on boron chemistry. SIGPE liquid blend mixtures were prepared by mixing the selected SIM-xx monomer with PEGDM and G4 at the ratios described in Table 2.1. The mixture was stirred for at least 2 hours at RT. DAROCUR photoinitiator was then added at 3% w/w of the monomers and mixtures were drop-casted on a silicon mold (Φ 11.28 mm) and irradiated with a UV-LED lamp for 5 minutes (300 – 400 nm, 385 nm peak. Lightningcure® V3).

GLMS-xxx electrolytes based on boron chemistry. Gels using lithium molten salts were prepared by mixing the selected LMS with PEGDM at a fix weight ratio of 0.8 LMS : 0.2 PEGDM. The mixture was stirred for at least 2 hours at RT. DAROCUR photoinitiator was then added at 3% w/w of the monomers and mixtures were drop-casted on a silicon mold (Φ 11.28 mm) and irradiated with a UV-LED lamp for 5 minutes (300 – 400 nm, 385 nm peak).

2.12.2 Methods

Fourier transform infrared spectroscopy (FT-IR). Chemical characterization was studied using a FT-IR ATR, Bruker Alpha I Spectrometer. The measuring probe was at RT and under air atmosphere.

Thermal gravimetric analysis (TGA). Thermal degradation was investigated employing a TGA Q 500 (TA instruments). About 10 mg of sample were heated from RT to 600 °C at a heating rate of 10 °C/min under nitrogen flux of 90 mL/min.

Dynamic mechanical thermal analysis (DMTA). Mechanical properties were studied using a Dynamic Mechanical Analyzer, Triton 2000 DMA (Triton Technology) at compression. Circular samples of 1 cm^2 and 2 – 2.5 mm thick were used. Samples were first cooled down to -100 °C with liquid nitrogen and heated till 100 °C at a heating rate of 4 ^{0}C/min and a frequency of 1.0 Hz.

Impedance spectroscopy (EIS). Ionic conductivities were measured by electrochemical impedance spectroscopy (EIS) using an Autolab 302N Potentiostat Galvanostat coupled to a Microcell HC temperature controller. Circular membranes (Φ 11 mm) were used with a thickness of ~500 µm. The membranes were sandwiched between two stainless steel electrodes and sealed in a Microcell under argon atmosphere in a glove box. The measurements were carried out from 85°C to 25°C, dwell of 30 minutes for temperature stabilization and -10 °C step. The frequency range was set from 0.1 MHz to 0.1 Hz and 10 mV amplitude. According to literature[55], the ionic conductivity of solid polymer electrolytes (SPEs), including GPEs, can be calculated following the equation:

$$\sigma = \frac{1}{R_b} \cdot \frac{d}{S}$$

, where σ is the ionic conductivity (S·cm^{-1}), d is the thickness (cm) of the GPE, S is the area (cm^{-2}) of electrodes in contact with the GPE and R_b (Ω) is the bulk resistance of GPE, which can be extracted from the Nyquist plot obtained in EIS.

Lithium transference number. The lithium transference number (t^+_{Li}) were calculated following the method proposed by Evans-Vincent-Bruce[34,35]:

$$t^+_{Li} = \frac{I_s(\Delta V - I_0 \cdot R_0)}{I_0(\Delta V - I_s \cdot R_s)}$$

where *ΔV* is a small DC bias applied to polarize the sample (10 mV) during a chronoamperometry, *I$_0$* is the initial value of the current upon polarization with DC bias, *I$_s$* is the current reached in the steady-state for the sample polarized with DC bias. *R$_0$* and *R$_s$* are the resistances of the solid electrolyte interface (SEI) before and after the

polarization, respectively, measured via EIS and using a 10mV potential excitation amplitude. Measurements were carried out at 25°C (first part of the chapter) and 60°C (second part of the chapter).

2.12.3 Electrodes preparation

Negative electrode. Lithium circular electrodes were punched (Φ 8 mm and 120 µm thick) from a rolled piece of lithium metal purchased from Rockwood Lithium (USA) and carefully rubbed with a plastic spatula to remove any dust/rust. These lithium thin films were then placed and pressed over a circular piece (Φ 11.28 mm and 20 µm thick) of electrodeposited NI000320 nickel (0.02 mm thick, GoodFellow, 99.9%). Beforehand, nickel samples were washed with ethanol in an ultrasounds bath for 1 hour at maximum power and dried under vacuum at 100 °C for 24 hours.

Positive electrode. Positive electrodes were formed by a gas diffusion layer (GDL) coated with a slurry containing 0.6%wt of carbon (Ketjen Black 600, Akzonobel), 1.6%wt of binder (LITHion^{TM} dispersion, Ion Power Inc) and 97.8%wt of anhydrous 2-propanol (IPA, MilliPore Sigma, max. 0.005% H_2O, ≥ 99.9%)). The GDL sheets were punched into circular samples (Φ11.28 mm) and dried under vacuum at 120 °C for 24 hours. The carbon was previously dried at 100 °C under vacuum for 24 hours. The binder and IPA were directly used from the supplier after adding activated 4Å molecular sieves and allowed 5 days for drying effect. The water content, measured by Coulumetric Karl Fischer, decreased from 252 to 218 ppm for the binder; and from 64 to 8 ppm for the IPA after the addition of the zeolites. To make the slurry, all the components were placed in a glass vial and mixed homogeneously using an Ultraturrax IKA T18, at speed 2 for 45 minutes. The slurry was immediately used and 70 µL of the ink was deposited on each circular GDL. These were covered and allowed to dry at RT for 24 hours. The coated GDLs had an average carbon loading of 0.72 mg·cm^{-2}.

2.12.4 Lithium symmetrical cells

The polymer electrolyte (Φ 11.28 mm) was sandwiched between two lithium foils and placed between stainless steel caps. This sandwich was then placed between two electronically isolated stainless steel spacers. This stack was kept vertically aligned through a hollow PEEK cylinder. A set of 3 nuts/bolts/insulator O-rings were used to ensure a good tightening and a good flatness. A Teclock thickness gauge was used to ensure that the thickness of the electrolyte was even all along the electrode | electrolyte contact surface. This stack was then placed in a sealed container to keep the cell under inert atmosphere during testing.
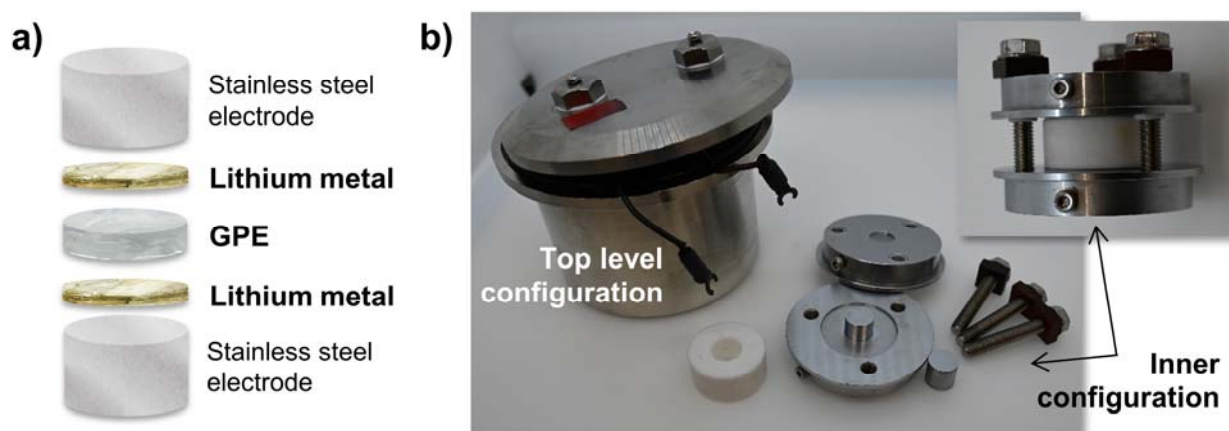
Figure 2. 26. a) Lithium symmetrical cell scheme (inner configuration); and b) Lithium symmetrical cells designed at Toyota Motor Europe (TME).

These symmetrical cells were specifically designed at Toyota Motor Europe (TME), and were prepared inside a glovebox with levels of H_2O < 0.01 ppm and O_2 < 0.01ppm. All parts were rigorously dried at 60 °C under vacuum for 24 hours before introducing them in the glovebox.

2.12.5 Li-O_2 cells

The electrolyte (Φ 11.28 mm) was sandwiched between the negative and positive electrodes. In the case of liquid Li-O_2 cells, two glass fiber sheets previously dried at 150 °C under vacuum for 24 hours (Φ 11.28 mm, Whatman®, GF/A grade) were soaked with the liquid electrolyte mixture (500 µL) and placed between the electrodes. The positive electrode was placed with the coated side facing the electrolyte surface.

This stack was then sandwiched in a stainless steel/PEEK Swagelok cell. The cell was tighten manually and placed vertically inside a sealed plastic container. The argon gas inside the container was then purged and replaced by oxygen gas outside the glovebox (oxygen flow at 0.2 l/min for 30 minutes, Praxair, > 99.5%).
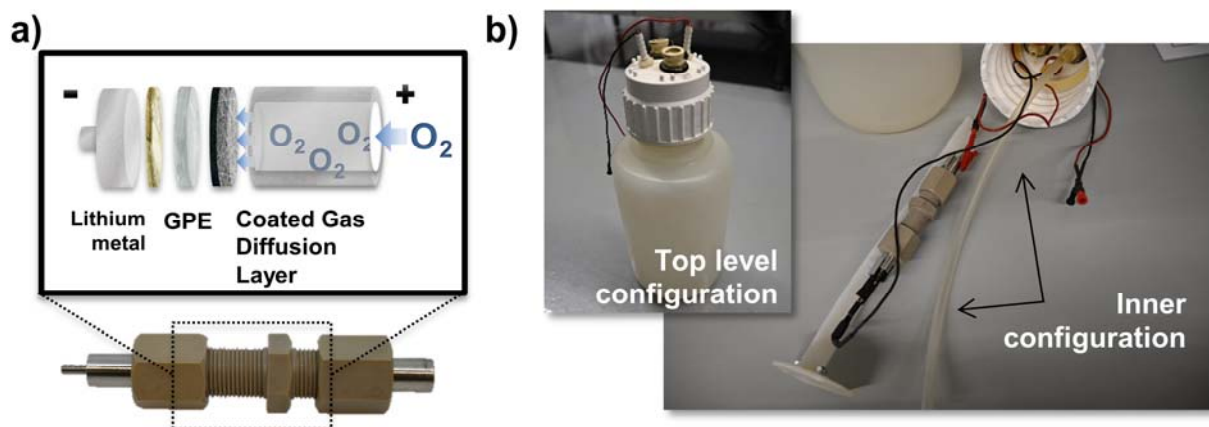
Figure 2. 27. Lithium-O_2 Swagelok cell: a) Inner level scheme; and b) Top level configuration.

Li-O_2 Swagelok cells - specifically designed at TME - were assembled inside a glovebox with levels of H_2O < 0.01 ppm and O_2 < 0.01ppm. All parts were rigorously dried at 60 °C under vacuum for 24 hours before introducing them in the glovebox.

2.13   References

(1)   Tan, P.; Jiang, H. R.; Zhu, X. B.; An, L.; Jung, C. Y.; Wu, M. C.; Shi, L.; Shyy, W.; Zhao, T. S. Advances and Challenges in Lithium-Air Batteries. *Appl. Energy* **2017**, *204*, 780–806.

(2)   Li, B.; Liu, Y.; Zhang, X.; He, P.; Zhou, H. Hybrid Polymer Electrolyte for Li–O 2 Batteries. *Green Energy Environ.* **2019**, *4* (1), 3–19.

(3)   Nasybulin, E.; Xu, W.; Engelhard, M. H.; Nie, Z.; Burton, S. D.; Cosimbescu, L.; Gross, M. E.; Zhang, J. G. Effects of Electrolyte Salts on the Performance of Li-O2 Batteries. *J. Phys. Chem. C* **2013**, *117* (6), 2635–2645.

(4)   Wu, S.; Tang, J.; Li, F.; Liu, X.; Zhou, H. Low Charge Overpotentials in Lithium-Oxygen Batteries Based on Tetraglyme Electrolytes with a Limited Amount of Water. *Chem. Commun.* **2015**, *51* (94), 16860–16863.

(5)   Zhao, Q.; Zhang, Y.; Sun, G.; Cong, L.; Sun, L.; Xie, H.; Liu, J. Binary Mixtures of Highly Concentrated Tetraglyme and Hydrofluoroether as a Stable and Nonflammable Electrolyte for Li-O2 Batteries. *ACS Appl. Mater. Interfaces* **2018**, *10* (31), 26312–26319.

(6)   Chamaani, A.; Safa, M.; Chawla, N.; El-Zahab, B. Composite Gel Polymer Electrolyte for Improved Cyclability in Lithium-Oxygen Batteries. *ACS Appl. Mater. Interfaces* **2017**, *9* (39), 33819–33826.

(7)   Mauger; Julien; Paolella; Armand; Zaghib. Building Better Batteries in the Solid State: A Review. *Materials (Basel).* **2019**, *12* (23), 3892.

(8)   Zou, X.; Lu, Q.; Zhong, Y.; Liao, K.; Zhou, W.; Shao, Z. Flexible, Flame-Resistant, and Dendrite-Impermeable Gel-Polymer Electrolyte for Li–O2/Air Batteries Workable Under Hurdle Conditions. *Small* **2018**, *14* (34), 1–10.

(9)   Elia, G. A.; Hassoun, J. A Polymer Lithium-Oxygen Battery. *Nat. Publ. Gr.* **2015**, *5*, 5:12307.

(10)   Baskoro, F.; Wong, H. Q.; Yen, H. J. Strategic Structural Design of a Gel Polymer Electrolyte toward a High Efficiency Lithium-Ion Battery. *ACS Appl. Energy Mater.* **2019**, *2* (6), 3937–3971.

(11)   Phan, T. N. T.; Ferrand, A.; Ho, H. T.; Liénafa, L.; Rollet, M.; Maria, S.; Bouchet, R.; Gigmes, D. Vinyl Monomers Bearing a Sulfonyl(Trifluoromethane Sulfonyl) Imide Group: Synthesis and Polymerization Using Nitroxide-Mediated Polymerization. *Polym. Chem.* **2016**, *7* (45), 6901–6910.

(12)   Meabe, L.; Goujon, N.; Li, C.; Armand, M.; Forsyth, M. Single-Ion Conducting Poly (Ethylene Oxide Carbonate) as Solid Polymer Electrolyte for Lithium Batteries. *Batter. Supercaps* **2020**, *3*, 68–75.

(13)   Porcarelli, L.; Shaplov, A. S.; Bella, F.; Nair, J. R.; Mecerreyes, D.; Gerbaldi, C. Single-Ion Conducting Polymer Electrolytes for Lithium Metal Polymer Batteries That Operate at Ambient Temperature. *ACS Energy Lett.* **2016**, *1* (4), 678–682.

(14)   Sutton, P.; Airoldi, M.; Porcarelli, L.; Martínez, J. L. O.; Mugemana, C.; Bruns, N.; Mecerreyes, D.; Steiner, U.; Gunkel, I. Tuning the Properties of a UV Polymerized , Cross   Linked Solid Polymer Electrolyte for Lithium Batteries. *Polymers (Basel).* **2020**, *12*, 595.

(15)   Zhang, H.; Li, C.; Piszcz, M.; Coya, E.; Rojo, T.; Rodriguez-Martinez, L. M.; Armand, M.; Zhou, Z. Single Lithium-Ion Conducting Solid Polymer Electrolytes: Advances and Perspectives. *Chem. Soc. Rev.* **2017**, *46* (3), 797–815.

(16)   Deng, K.; Zeng, Q.; Wang, D.; Liu, Z.; Qiu, Z.; Zhang, Y.; Xiao, M.; Meng, Y. Single-Ion Conducting Gel Polymer Electrolytes: Design, Preparation and Application. *J. Mater. Chem. A* **2020**, *8* (4), 1557–1577.

(17)   Wu, C.; Liao, C.; Li, T.; Shi, Y.; Luo, J.; Li, L.; Yang, J. A Polymer Lithium-Oxygen Battery Based on Semi-Polymeric Conducting Ionomers as the Polymer Electrolyte. *J. Mater. Chem. A* **2016**, *4* (39), 15189–15196.

(18)   Shi, Y.; Wu, C.; Li, L.; Yang, J. A Lithiated Perfluorinated Sulfonic Acid Polymer

Electrolyte for Lithium-Oxygen Batteries. *J. Electrochem. Soc.* **2017**, *164* (9), A2031–A2037.

(19) Alvarez Tirado, M.; Castro, L.; Guzmán-González, G.; Porcarelli, L.; Mecerreyes, D. Single- Versus Dual-Ion UV-Cross-Linked Gel Polymer Electrolytes for Li-O2 Batteries. *ACS Appl. Energy Mater.* **2021**, *4*, 295–302.

(20) Hernández, G.; Mindemark, J.; Naylor, A. J.; Chien, Y. C.; Brandell, D.; Edstrom, K. Elimination of Fluorination: The Influence of Fluorine-Free Electrolytes on the Performance of LiNi1/3Mn1/3Co1/3O2/Silicon-Graphite Li-Ion Battery Cells. *ACS Sustain. Chem. Eng.* **2020**, *8* (27), 10041–10052.

(21) Shim, J.; Lee, J. S.; Lee, J. H.; Kim, H. J.; Lee, J.-C. Gel Polymer Electrolytes Containing Anion-Trapping Boron Moieties for Lithium-Ion Battery Applications. *ACS Appl. Mater. Interfaces* **2016**, *8* (41), 27740–27752.

(22) Hosseinioun, A.; Nürnberg, P.; Schönhoff, M.; Diddens, D.; Paillard, E. Improved Lithium Ion Dynamics in Crosslinked PMMA Gel Polymer Electrolyte. *RSC Adv.* **2019**, *9* (47), 27574–27582.

(23) Bin, M. A.; Susan, H.; Kaneko, T.; Noda, A.; Watanabe, M. Ion Gels Prepared by in Situ Radical Polymerization of Vinyl Monomers in an Ionic Liquid and Their Characterization as Polymer Electrolytes. *J. Am. Chem. Soc* **2005**, *127*, 4976–4983.

(24) Zhu, M.; Wu, J.; Wang, Y.; Song, M.; Long, L.; Siyal, S. H.; Yang, X.; Sui, G. Recent Advances in Gel Polymer Electrolyte for High-Performance Lithium Batteries. *J. Energy Chem.* **2019**, *37*, 126–142.

(25) Deng, K.; Wang, S.; Ren, S.; Han, D.; Xiao, M.; Meng, Y. Network Type Sp3 Boron-Based Single-Ion Conducting Polymer Electrolytes for Lithium Ion Batteries. *J. Power Sources* **2017**, *360*, 98–105.

(26) Guzmán-González, G.; Ávila-Paredes, H. J.; Rivera, E.; González, I. Electrochemical Characterization of Single Lithium-Ion Conducting Polymer Electrolytes Based on Sp3 Boron and Poly(Ethylene Glycol) Bridges. *ACS Appl. Mater. Interfaces* **2018**, *10* (36), 30247–30256.

(27) Guzmán-González, G.; Ramos-Sánchez, G.; Camacho-Forero, L. E.; González, I. Charge Delocalization on BO 4- Centers to Improve Conductivity on Single Lithium Ion Conducting Polymer Electrolytes: A Computational/Experimental Approach. *J. Phys. Chem. C* **2019**, *123* (29), 17686–17694.

(28) Van Humbeck, J. F.; Aubrey, M. L.; Alsbaiee, A.; Ameloot, R.; Coates, G. W.; Dichtel, W. R.; Long, J. R. Tetraarylborate Polymer Networks as Single-Ion Conducting Solid Electrolytes. *Chem. Sci.* **2015**, *6* (10), 5499–5505.

(29) Zhang, Y.; Pan, M.; Liu, X.; Li, C.; Dong, J.; Sun, Y.; Zeng, D.; Yang, Z.; Cheng, H. Overcoming the Ambient-Temperature Operation Limitation in Lithium-Ion Batteries by Using a Single-Ion Polymer Electrolyte Fabricated by Controllable Molecular Design. *Energy Technol.* **2018**, *6* (2), 289–295.

(30) Zhang, Y.; Cai, W.; Rohan, R.; Pan, M.; Liu, Y.; Liu, X.; Li, C.; Sun, Y.; Cheng,

H. Toward Ambient Temperature Operation with All-Solid-State Lithium Metal Batteries with a Sp3 Boron-Based Solid Single Ion Conducting Polymer Electrolyte. *J. Power Sources* **2016**, *306*, 152–161.

(31) Dai, K.; Zheng, Y.; Wei, W. Organoboron-Containing Polymer Electrolytes for High-Performance Lithium Batteries. *Adv. Funct. Mater.* **2021**, *31* (13), 2008632.

(32) Guzmán-González, G.; Vauthier, S.; Alvarez-Tirado, M.; Cotte, S.; Castro, L.; Guéguen, A.; Casado, N.; Mecerreyes, D. Single ion Lithium Conducting Polymers with High Ionic Conductivity Based on Borate Pendant Groups. *Angew. Chemie Int. Ed.* **2021**, *e202114024*.

(33) Nyquist, R. A.; Fiedler, S.; Streck, R. Infrared Study of Vinyl Acetate , Methyl Acrylate and Methyl Methacrylate in Various Solvents. *Vib. Spectrosc.* **1994**, *6*, 285–291.

(34) Zugmann, S.; Fleischmann, M.; Amereller, M.; Gschwind, R. M.; Wiemhöfer, H. D.; Gores, H. J. Measurement of Transference Numbers for Lithium Ion Electrolytes via Four Different Methods, a Comparative Study. *Electrochim. Acta* **2011**, *56* (11), 3926–3933.

(35) Evans, J.; Vincent, C. A.; Bruce, P. G. Electrochemical Measurement of Transference Numbers in Polymer Electrolytes. *Polymer (Guildf).* **1987**, *28* (13), 2324–2328.

(36) Lv, Y.; Li, Z.; Yu, Y.; Yin, J.; Song, K.; Yang, B.; Yuan, L.; Hu, X. Copper/Cobalt-Doped LaMnO3 Perovskite Oxide as a Bifunctional Catalyst for Rechargeable Li-O2 Batteries. *J. Alloys Compd.* **2019**, *801*, 19–26.

(37) Yang, T.; Shu, C.; Zheng, R.; Hu, A.; Hou, Z.; Li, M.; Ran, Z.; Hei, P.; Long, J. Excellent Electrolyte-Electrode Interface Stability Enabled by Inhibition of Anion Mobility in Hybrid Gel Polymer Electrolyte Based Li-O2 Batteries. *J. Memb. Sci.* **2020**, *604* (October 2019), 118051.

(38) Fong, K. D.; Self, J.; Diederichsen, K. M.; Wood, B. M.; McCloskey, B. D.; Persson, K. A. Ion Transport and the True Transference Number in Nonaqueous Polyelectrolyte Solutions for Lithium Ion Batteries. *ACS Cent. Sci.* **2019**, *5* (7), 1250–1260.

(39) Rohan, R.; Kuo, T. C.; Chen, M. W.; Lee, J. T. Nanofiber Single-Ion Conducting Electrolytes: An Approach for High-Performance Lithium Batteries at Ambient Temperature. *ChemElectroChem* **2017**, *4* (9), 2178–2183.

(40) Yang, T.; Shu, C.; Zheng, R.; Li, M.; Hou, Z.; Hei, P.; Zhang, Q.; Mei, D.; Long, J. Dendrite-Free Solid-State Li-O2 Batteries Enabled by Organic-Inorganic Interaction Reinforced Gel Polymer Electrolyte. *ACS Sustain. Chem. Eng.* **2019**, *7* (20), 17362–17371.

(41) Grande, L.; Paillard, E.; Hassoun, J.; Park, J. B.; Lee, Y. J.; Sun, Y. K.; Passerini, S.; Scrosati, B. The Lithium/Air Battery: Still an Emerging System or a Practical Reality? *Adv. Mater.* **2015**, *27* (5), 784–800.

(42) Girishkumar, G.; McCloskey, B.; Luntz, A. C.; Swanson, S.; Wilcke, W. Lithium-

Air Battery: Promise and Challenges. *J. Phys. Chem. Lett.* **2010**, *1* (14), 2193–2203.

(43) Wang, Y.; Lai, N. C.; Lu, Y. R.; Zhou, Y.; Dong, C. L.; Lu, Y. C. A Solvent-Controlled Oxidation Mechanism of Li2O2 in Lithium-Oxygen Batteries. *Joule* **2018**, *2* (11), 2364–2380.

(44) Bard, Allen J.; Faulkner, L. R. . *ELECTROCHEMICAL METHODS - Fundamentals and Applications*, Second edi.; Harris, D. E. S., Ed.; JOHN WILEY & SONS, INC.: Austin, 2001; Vol. 2.

(45) Vijayakumar, V.; Anothumakkool, B.; Kurungot, S.; Winter, M.; Nair, J. R. In Situ Polymerization Process: An Essential Design Tool for Lithium Polymer Batteries. *Energy Environ. Sci.* **2021**, *14*, 2708–2788.

(46) Wang, J.; Zheng, Q.; Fang, M.; Ko, S.; Yamada, Y.; Yamada, A. Concentrated Electrolytes Widen the Operating Temperature Range of Lithium   Ion Batteries. *Adv. Sci.* **2021**, *2101646*, 2101646.

(47) Ma, S.; Jiang, M.; Tao, P.; Song, C.; Wu, J.; Wang, J.; Deng, T.; Shang, W. Temperature Effect and Thermal Impact in Lithium-Ion Batteries: A Review. *Prog. Nat. Sci. Mater. Int.* **2018**, *28* (6), 653–666.

(48) Aziz, S. B.; Woo, T. J.; Kadir, M. F. Z.; Ahmed, H. M. A Conceptual Review on Polymer Electrolytes and Ion Transport Models. *J. Sci. Adv. Mater. Devices* **2018**, *3* (1), 1–17.

(49) Singh, V. K.; Shalu; Balo, L.; Gupta, H.; Singh, S. K.; Singh, R. K. Solid Polymer Electrolytes Based on Li+/Ionic Liquid for Lithium Secondary Batteries. *J. Solid State Electrochem.* **2017**, *21* (6), 1713–1723.

(50) Cheng, X. B.; Zhang, R.; Zhao, C. Z.; Wei, F.; Zhang, J. G.; Zhang, Q. A Review of Solid Electrolyte Interphases on Lithium Metal Anode. *Adv. Sci.* **2015**, *3* (3), 1–20.

(51) Huang, K.; Bi, S.; Kurt, B.; Xu, C.; Wu, L.; Li, Z.; Feng, G.; Zhang, X. Regulation of SEI Formation by Anion Receptors to Achieve Ultra Stable Lithium Metal Batteries. *Angew. Chemie Int. Ed.* **2021**, *60* (35), 19232–19240.

(52) Lai, J.; Xing, Y.; Chen, N.; Li, L.; Wu, F.; Chen, R. Electrolytes for Rechargeable Lithium–Air Batteries. *Angew. Chemie - Int. Ed.* **2020**, *59* (8), 2974–2997.

(53) Choudhury, S.; Tu, Z.; Nijamudheen, A.; Zachman, M. J.; Stalin, S.; Deng, Y.; Zhao, Q.; Vu, D.; Kourkoutis, L. F.; Mendoza-Cortes, J. L.; Archer, L. A. Stabilizing Polymer Electrolytes in High-Voltage Lithium Batteries. *Nat. Commun.* **2019**, *10* (1), 1–11.

(54) Chem, P.; Shaplov, A. S.; Vlasov, P. S.; Armand, M.; Lozinskaya, E. I.; Ponkratov, D. O.; Malyshkina, I. A.; Vidal, F.; Okatova, O. V; Pavlov, G. M.; Wandrey, C.; Godovikov, I. A.; Vygodskii, Y. S. Design and Synthesis of New Anionic "' Polymeric Ionic Liquids '" with High Charge Delocalization. *Polym. Chem.* **2011**, *2* (11), 2609–2618.

(55) Qian, X.; Gu, N.; Cheng, Z.; Yang, X.; Wang, E.; Dong, S. Methods to Study the

Ionic Conductivity of Polymeric Electrolytes Using a.c. Impedance Spectroscopy. *J. Solid State Electrochem.* **2001**, *6* (1), 8–15.

El capítulo 3 está sujeto a confidencialidad por la autora

Chapter 4

Designing highly conductive iongel soft solid electrolytes suitable for Li-O₂ batteries

4.1 Introduction

In the previous chapter, 1,2,3 – Trimethoxypropane (TMP) was presented as a greener and low toxicity glyme to be used in an electrolyte for Li-O₂ batteries. Nonetheless, more environmentally friendly materials need to be investigated as glyme alternatives. In this this chapter, a tetra-alkyl ammonium based ionic liquid (IL) will be evaluated as plasticizer to prepare polymer-based iongel soft solid electrolytes.

From a material perspective, many efforts have been put in developing more efficient electrolytes that comply with a broad set of properties such as high ionic conductivity or more environmentally friendly electrolytes [1]. In that sense, ionic liquids (IL) seem a good alternative to conventional flammable organic solvents due to a combination of good transport properties, non-volatility, low toxicity, non-flammability and stability against superoxide radicals [2,3].

The most investigated ionic liquids in Li-O₂ batteries are based on imidazolium- and pyrrolidinium- cations[2,4–7] and fluorine-based anions (i.e. bis(trifluoromethanesulfonyl)imide, TFSI) [8]. Recently, less commonly used tetra-alkyl ammonium based ILs, such as N,N-Diethyl-N-methyl-N-(2-methoxyethyl)ammonium bis(trifluoromethanesulfonyl)imide ([DEME][TFSI]) has shown suitable properties for application in this type of batteries. For instance, Ulissi and co-workers [9,10] showed that [DEME][TFSI] allowed a reversible, low polarization during galvanostatic cycling in Li-O₂ cells.

Similarly to previous chapters, a plausible way to further improve the liquid electrolyte cells is via the development of gel polymer electrolytes. They are also known as iongels, ionic liquid gels or iongels if an IL-based electrolyte is used [11].

Although this approach is quite popular in lithium-ion [12–14], lithium-metal [15–17], sodium-metal [18,19] or other type of batteries [6,20], it has not been largely explored for Li-O$_2$ cells.

Regarding salt concentration in ionic liquid based electrolytes, recent studies have shown that superconcentrated IL electrolytes (>1:1 molar ratio, IL:salt) are able to provide an efficient protection to lithium-metal [21–24] or sodium-metal anodes [25]. Interestingly, effect of salt concentration is deeply studied in IL-based liquid electrolytes for Li-O$_2$ applications [26–28] but it is not largely evaluated when these are use in solid electrolytes. To the best of our knowledge, only one example could be found for iongels at high salt concentrations or all-solid-state sodium cells [18].

Hence, *in the first part of this chapter* a full study to obtain optimized solid polymer electrolytes for Li-O$_2$ batteries based on a low polarization ionic liquid ([DEME][TFSI]) will be presented. Effects of salt concentration on a polymer-based electrolyte will be studied for the first time for Li-O$_2$ applications. By combining promising results of recent works and previous chapters, we present a simple but effective way of preparing iongels suitable for Li-O$_2$ cells that show good mechanical and thermal stability, high ionic conductivity and good battery performance, demonstrating equal or superior properties to the equivalent battery cells using ionic liquid electrolytes.

Actually, as seen later in the chapter, these polymer-based iongel electrolytes exhibit great ionic conductivity values and battery performance results for a gel electrolyte. However, it is possible to explore the enhancement of these properties (or other, such as lithium metal protection) via the modification of the ionic liquid.

In fact, a way to seek higher metal-O$_2$ performance is through the increase of fluorine content within the electrolyte structure, as they have a beneficial effect in the formation of a passivating lithium protection layer[29] and/or a tendency to increase oxygen solubility in the solution (active material in this type of cells)[30] which usually translates in higher capacities. A relatively easy way to increase the fluorinated content in ionic liquid based electrolytes is through the tuning of the anions and/or cations of the ionic liquid [31,32].

Hence, *in the second half of this chapter* we will present a full study to obtain highly conductive iongel electrolytes based on five different ionic liquids designed to improve lithium ion transport. The optimized formulation developed in the first part of

this chapter will be used as a reference for the development of the iongels of the second part. DEME-TFSI cation and anion will be tuned to increase the presence of fluorine moieties with highly delocalized charge. Synergy between IL and salts cations and anions will be explored through the iongel polymer electrolyte properties and performance in Li-O$_2$ battery cells.

First Part

Iongel soft solid electrolytes based on [DEME][TFSI] ionic liquid for low polarization Li-O$_2$ batteries

4.2 Preparation of iongel membranes based on [DEME][TFSI]

Iongels containing a liquid electrolyte (LE) based on [DEME][TFSI] ionic liquid and LiTFSI salt were prepared by UV-photopolymerisation as previously shown for Li-ion and sodium batteries [18,33,34]. As shown in Scheme 4.1, poly(ethylene glycol) dimethacrylate (PEGDM) was directly mixed with the liquid electrolyte at different weight ratios (from 50 to 90 %wt., Table 4.1) in the presence of 2-Hydroxy-2-methylpropiophene as the photoinitiator. After UV-irradiating for <2 min on the drop-casted solution, self-standing and transparent membranes were obtained.

Table 4. 1. Iongel electrolytes compositions in wt%.

Sample	Liquid electrolyte [a]	PEGDM [b]
Iongel-xmol% [a]-50	50	50
Iongel-xmol% [a]-75	75	25
Iongel-xmol% [a]-80	80	20
Iongel-xmol% [a]-85	85	15
Iongel-xmol% [a]-90	90	10

[a] LiTFSI at x = 13, 20, 32 and 52 mol% in [DEME][TFSI]
[b] poly(ethylene glycol) dimethacrylate.

In all cases, the degree of cross-linking was monitored via Fourier Transform Infrared Spectroscopy (FTIR) spectra, and conversions of ≥ 95% were reached. The C=C stretching vibration of the acrylic groups (1640-1635 cm^{-1}) of the PEGDM

dimethacrylate monomer significantly decreased/disappeared after the UV-irradiation, confirming high monomer conversion [35].
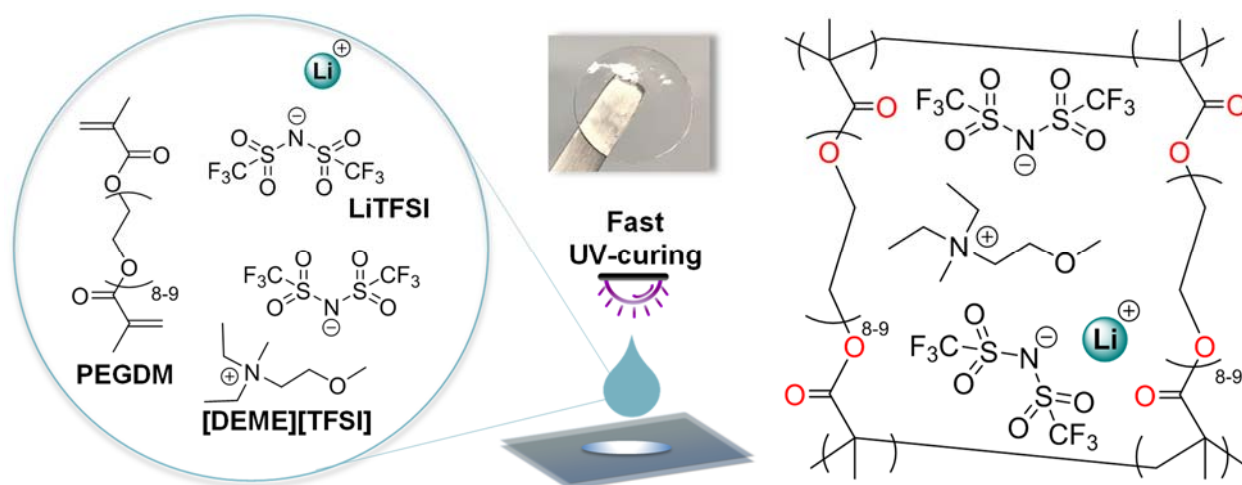
Scheme 4. 1. Schematic representation of the rapid UV-photopolymerisation process undertaken to obtain the cross-linked iongel electrolytes.

4.3 Impact of LiTFSI concentration in the iongels physico-thermal properties

Impact of LiTFSI salt concentration in the physico-thermal properties of the iongels was assessed. Up to four different molar concentrations of salt within the iongel were studied. Thus, iongels including 13 mol%, 20 mol%, 32 mol% and 52 mol% of LiTFSI in [DEME][TFSI] were formulated. Note that, the last ionogel (52 mol%) includes a superconcentrated LE in which the molar ratio of the salt is ≥ to the molar ratio of the ionic liquid .

4.3.1 Impact on the thermal analysis

The thermal stability of these iongels was evaluated through thermal gravimetrical analysis, TGA. Iongels containing up to 90 %wt. of ionic liquid electrolyte ILE were studied. As shown in Figure 4.1a, all membranes did not present any thermal degradation until 315 °C due to the remarkable high thermal stability of [DEME][TFSI] ionic liquid (~325 °C decomposition temperature) [30]. Furthermore, the presence of higher LiTFSI concentrations did not change significantly this thermal stability.
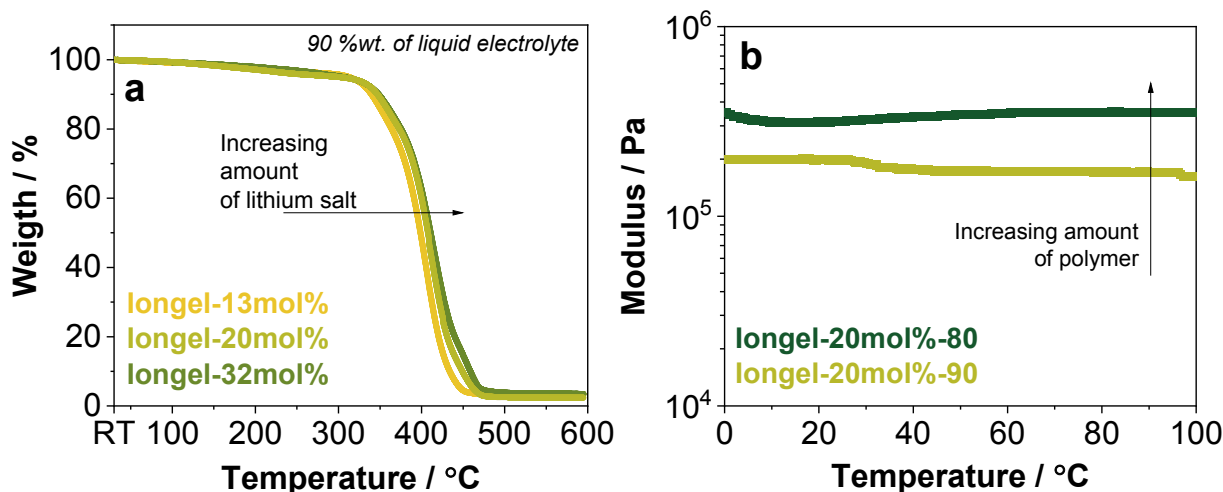
Figure 4. 1. a) TGA analysis under nitrogen atmosphere at 10 °C/min of iongel membranes, and b) DMTA analysis at compression mode from 0 to 100 °C of Iongel-20mol% membranes containing 80 and 90 %wt. of liquid electrolyte.

4.3.2 Impact on the mechanical analysis

Their mechanical strength was evaluated through dynamic mechanical thermal analysis (DMTA), Figure 4.1b. Results showed that the modulus and the membranes are stable from room temperature to high temperature (100 ° C) due to its cross-linked nature.

Larger content of polymer in the formulation provoked an increase of the membrane modulus (e.g. from $2 \cdot 10^5$ Pa to $4 \cdot 10^5$ Pa for Iongel-20mol%-90 and Iongel-20mol%-80, respectively). According to the Tan δ derivative, Tg decreased from -22.6 to -43.2 °C for Iongel-TFSI-80 and Iongel-TFSI-90, respectively. Hence, iongels with higher ILE content showed a lower glass transition value.

Overall, the low Tg of these iongels and their mechanical robustness, even at very high ILE contents, together with their very high thermal stability, make these polymer electrolytes interesting materials for battery testing.

4.4 Iongel optimization via ionic conductivity

To down-select the most promising iongel compositions, their ionic conductivity (σ) at different temperatures was evaluated with Electrochemical Impedance

Spectroscopy (EIS) measurements. As a baseline, [DEME][TFSI] based iongels at different LE weight ratios were assessed at fixed salt concentrations. Then, the most promising formulation (fixed LE:polymer weight rate) was used to evaluate the impact of salt concentration. Accordingly, iongels at increasing LE weight ratios (50, 75, 80, 85 and 90%wt.) were prepared at a fixed molar concentration of 13 mol% of LiTFSI in [DEME][TFSI] (Table 4.1).

As shown in Figure 4.2a, increasing weight ratios of the ILE lead to higher σ values. There was a difference of one order of magnitude between Iongel-13mol%-50 and Iongel-13mol%-90, achieving the last composition a conductivity as high as $1.19 \cdot 10^{-3}$ S·cm⁻¹ at 25 °C, very close to the liquid electrolyte σ value at the same temperature ($1.96 \cdot 10^{-3}$ S·cm⁻¹). Hence, iongels containing 90 %wt. of ILE was the chosen composition for further characterization.
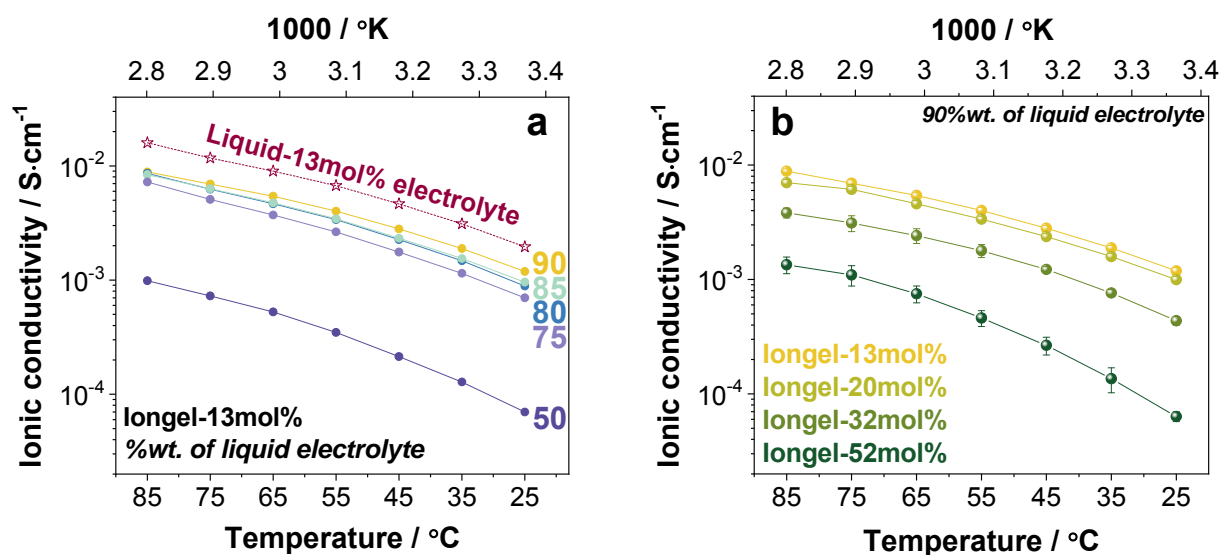
Figure 4. 2. a) Ionic conductivity versus temperature of Liquid-13mol% electrolyte and Iongel-13mol% membranes containing increasing amounts of liquid electrolyte, from 50 to 90 %wt.; and b) Ionic conductivity versus temperature of iongel membranes containing 90 %wt. of liquid electrolyte at increasing LiTFSI molar concentrations, from 13mol% to 52mol%.

Then, iongels at different LiTFSI concentrations were prepared (Figure 4.2b). As only iongels containing 90 %wt. of ILE will be studied from this point, only the molar ratio will be indicated in the nomenclature of the samples for simplicity (i.e. Iongel-52mol%).

As shown in Figure 4.2b, iongels at lower salt concentrations lead to ionic conductivities two orders of magnitude higher than superconcentrated Iongel-52mol% (~1.19·10^{-3} S·cm^{-1} versus 6.35·10^{-5} S·cm^{-1} at 25 °C for Iongel-13mol% and Iongel-52mol%, respectively). In opposition to intuitive results, in which a higher concentration of ions would drove to higher ionic conductivities, the much higher viscosity of the superconcentrated ILE played a dominant role, offering a higher resistance and slower ion transport [2,36].

Overall, iongels with 90 %wt. of ILE and intermediate salt concentrations (13 or 20mol%) showed the highest ionic conductivities, directly comparable to their liquid counterparts while being soft solid materials.
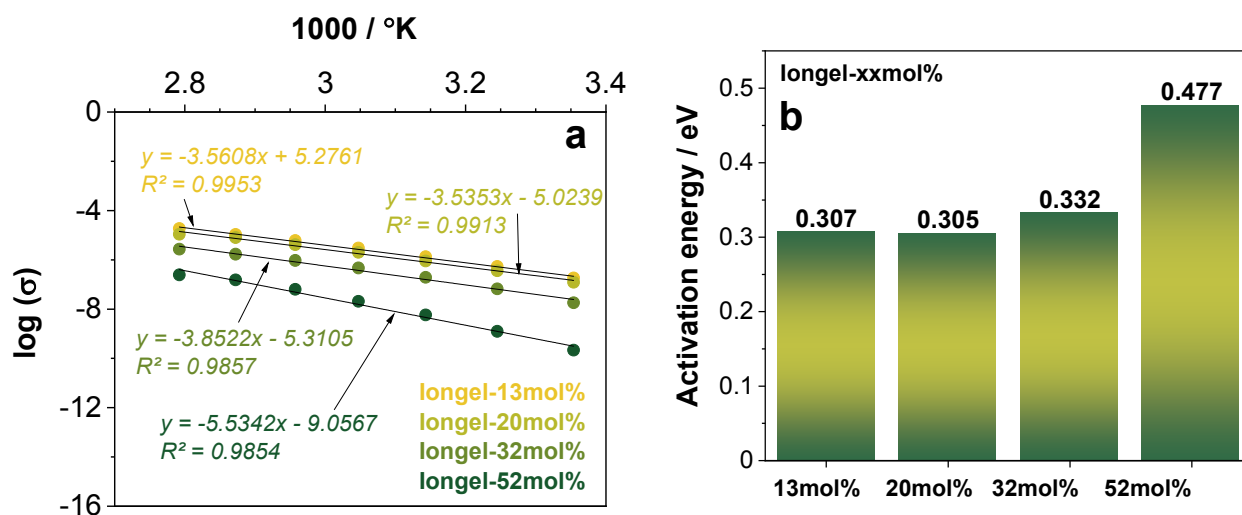
Figure 4. 3. a) Arrhenius fitting plot for the iongels; and b) Activation energies (eV) calculated following Arrhenius fittings of thermally-activated processes [37,38].

Additionally, the pseudo-activation energy values for the ionic conduction process of these iongels were calculated following the Arrhenius-model for thermally activated processes [37] (Figure 4.3a). The calculated pseudo-energy values increased with higher salt concentration and they were 0.31, 0.31, 0.33 and 0.48 eV for Iongel-13mol%, Iongel-20mol%, Iongel-32mol% and Iongel-52mol%, respectively (Figure 4.3b). Hence, more diluted electrolytes (e.g. Iongel-13mol% or Iongel-20mol%) favored the decrease of Ea, facilitating ion transport.
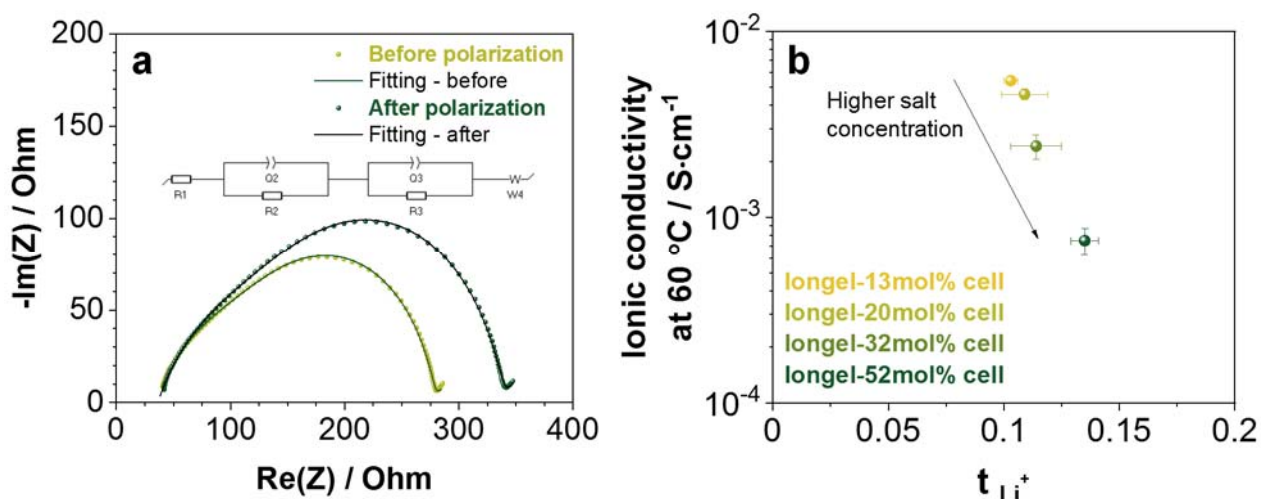
Figure 4. 4. Lithium transference number calculation at 60 °C of the longel-20mol% cell: a) Nyquist plot before and after polarization, as well as their calculated fitting curves using brick-layer model; and b) Ionic conductivities at 60 °C versus lithium transference number.

The fraction of current carried exclusively by the Li⁺ ions, was also evaluated through the calculation of the lithium transference number (t_{Li}^+) on lithium symmetrical cells at 60 °C. As in previous chapters, this was done following the well-known Evans-Vincent-Bruce method [39], where the cell is polarized by a small potential (10mV) during a chronoamperometry and the resistance of the SEI (solid electrolyte interphase) is measured by EIS before and after the excitation (Figure 4.4).

The results showed t_{Li}+ ranging between 0.10 and 0.14 (Figure 4.4b), increasing with LiTFSI molar concentration. This tendency was found in other studies [23,40], in which the t_{Li}+ improved from 0.1 to 0.2 using highly-concentrated ionic liquid electrolytes suggesting different lithium-ion transport mechanisms for high concentrated systems [23]. In lower concentrated ILE the ion pairs formed (Li – [TFSI⁻]₂), do not favour Li transport and lowers t_{Li^+}; however, in higher concentrated electrolytes, t_{Li^+} would be favoured via the Li – O atoms coordination formed between the aggregates [26].

4.5 Lithium symmetrical cells

4.5.1 Stability against lithium metal

To determine the stability of these iongels against lithium metal, stripping/plating cycles at increasing current densities were performed on lithium symmetrical cells at 60°C after 3 h conditioning at OCV. This testing temperature was selected following the optimization work done by other research group with liquid cells using a LE based on [DEME][TFSI] [9]. Current densities were increased from 0.01 to 1 mA·cm⁻², cycled 3 times at each current (1 hour half-cycle). The average potential (in absolute value) achieved at each current rate for each iongel is plotted in Figure 4.5.
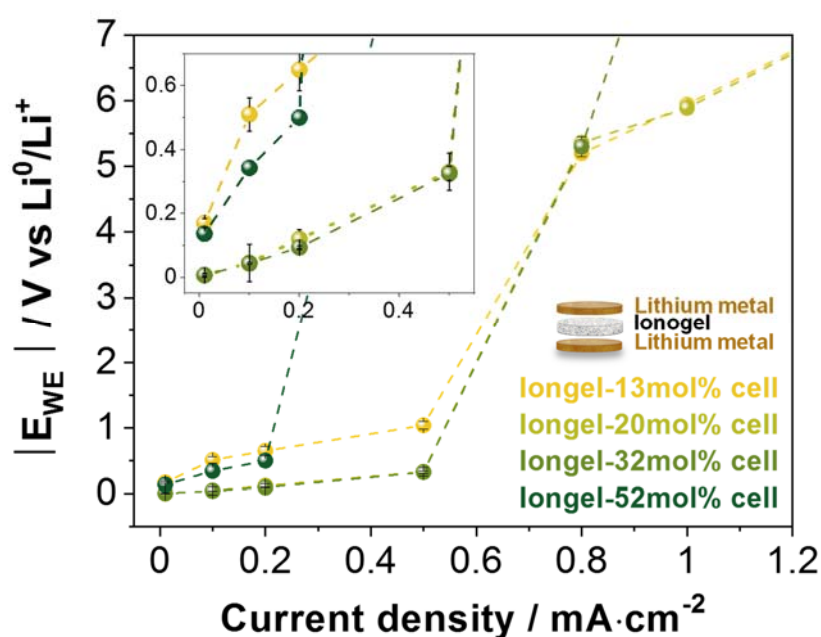
Figure 4. 5. Average potentials achieved in lithium symmetrical cells using different iongels during galvanostatic test with increasing current densities (from 0.01 to 1 mA·cm⁻²).

Cells having lower salt-concentrated iongels led to lower overpotentials, showing a critical current density (CCD, where potential exceeds 1 V) of 0.5 mA·cm⁻² (i.e. Iongel-13mol%, Iongel-20mol% and Iongel-32mol% cells). Unexpectedly, the superconcentrated Iongel-52mol% cell had the lowest CCD (0.2 mA·cm⁻²). Highly-concentrated ILE are usually explored to improve the stability against lithium metal, mitigating dendrites growth and improving stability of the solid electrolyte interface layer (SEI) [23,40]. The limited performance of the superconcentrated Iongel-52mol% electrolyte compared to literature could be related to the use of polymeric structures in our study, which might limit the SEI interfacial structure achieved in pure

superconcentrated liquid electrolytes [25,41], baseline of the good performance of these systems.

4.5.2 Long galvanostatic cycling

Cells with iongel-based electrolytes were further cycled (1h plating, 1h stripping) in galvanostatic mode at 0.5 mA·cm^{-2} (Figure 4.6a). Iongel-13mol% and Iongel-20mol% cells behaved very similarly, with ~0.7 V overpotentials for 27 and 18 hours, respectively. Then, they suffered from a "soft" short-circuit, showed off by voltage drops caused by lithium dendrites growth [42–44]. Cells with higher concentrated Iongel-32mol% had lower overpotential (~0.2 V) for 14 hours, and then showed a sharp polarization increase until cell death.
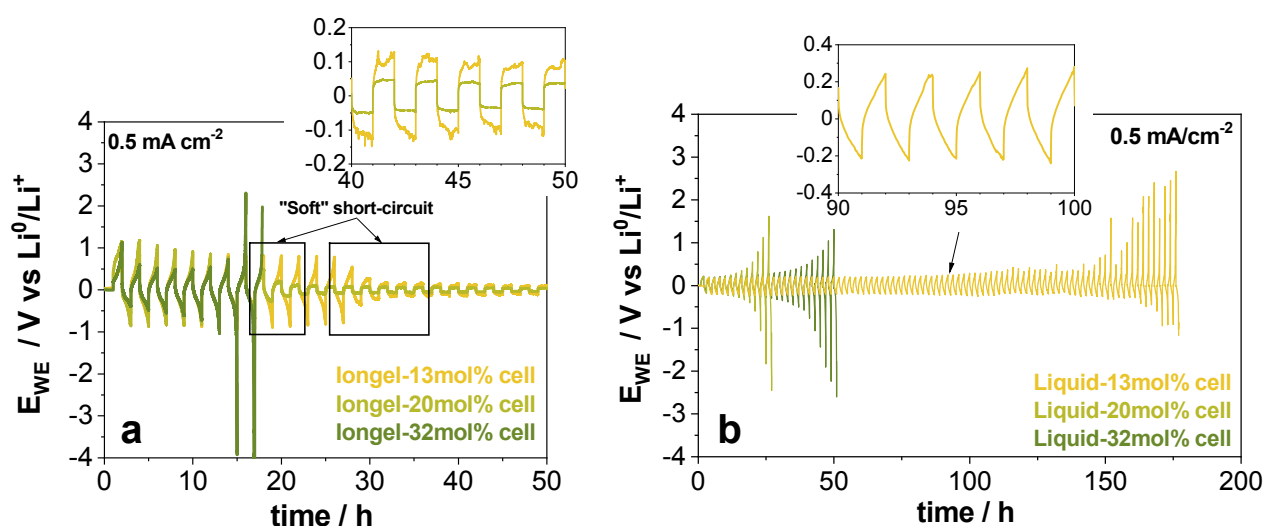
Figure 4. 6. Long cycling on lithium symmetrical cells at 0.5 mA·cm^{-2} and 60 °C with a) Iongel and b) Liquid electrolytes.

Same test was also done on cells with liquid equivalent electrolytes (Figure 4.6b). A constant overpotential of ~0.2 V over cycling was observed. Cell with liquid-20mol% electrolyte was stable for 22 hours, the one with Liquid-32mol% electrolyte for 45 hours and the one with Liquid-13mol% electrolyte, the best out of the liquid electrolytes, for 154 hours; being in accordance with similar reported results on cells with liquid electrolytes [9].

4.6 Li-O₂ cells

4.6.1 Stability windows of iongel electrolytes

Before testing in Li-O₂ cells, the stability window for upper potentials of Li⁰/ Iongels /Stainless steel cells were investigated by cyclic voltammetry at 60 °C and at a scan rate of 0.2 mV·s⁻¹ (Figure 4.7).

No significant differences were observed for Iongel-13mol%, Iongel-20mol% and Iongel-32mol% electrolyte cells, in which no oxidation currents occurred up to 3.72 - 3.78 V. The superconcentrated electrolyte cell (Iongel-52mol%) showed a higher anodic stability, up to 3.98 V, in accordance to other studies on superconcentrated DEME-TFSI liquid electrolytes [21,23].

Following these results, cut-off potentials of 2 and 3.6 V were established for Li-O₂cells cycling.

Figure 4. 7. Voltammograms at a scan rate of 0.2 mV·s⁻¹ of Li⁰/Stainless steel cells with: a) Iongel-13mol% electrolyte, b) Iongel-20mol% electrolyte, c) Iongel-32mol% electrolyte and d) Iongel-52mol% electrolyte. Scans undertaken from OCV to 5.5 V.
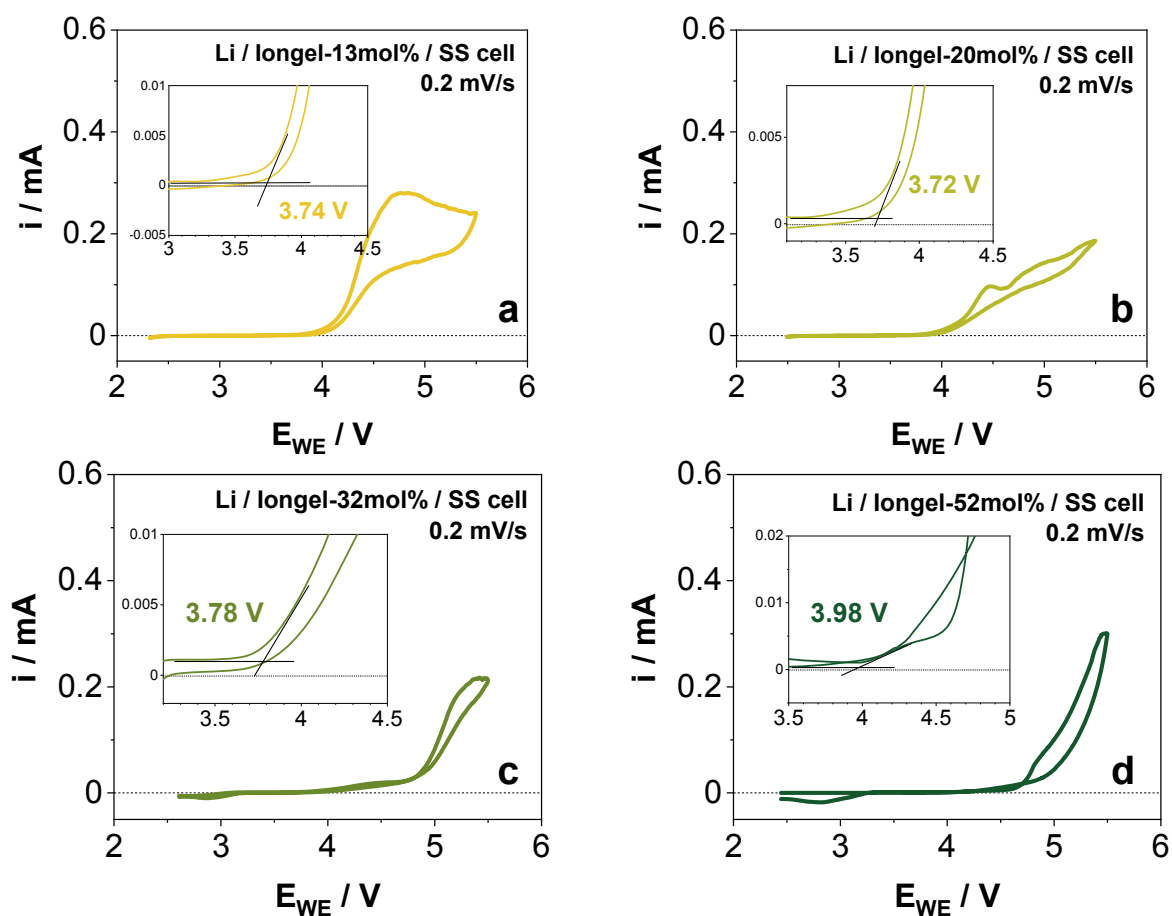
4.6.2 Dynamic discharge (rate test)

Swagelok Li-O$_2$ batteries were prepared and cells were first discharged in dynamic mode at 60 °C to determine the maximum current rate at which the cells can operate (Figure 4.8). Cells were discharged at increasing current densities (from 5 μA·cm^{-2} to 0.28 mA·cm^{-2}) for 15 min/per rate. Steady potentials achieved at each rate are plotted (average of 3 cells per each electrolyte).
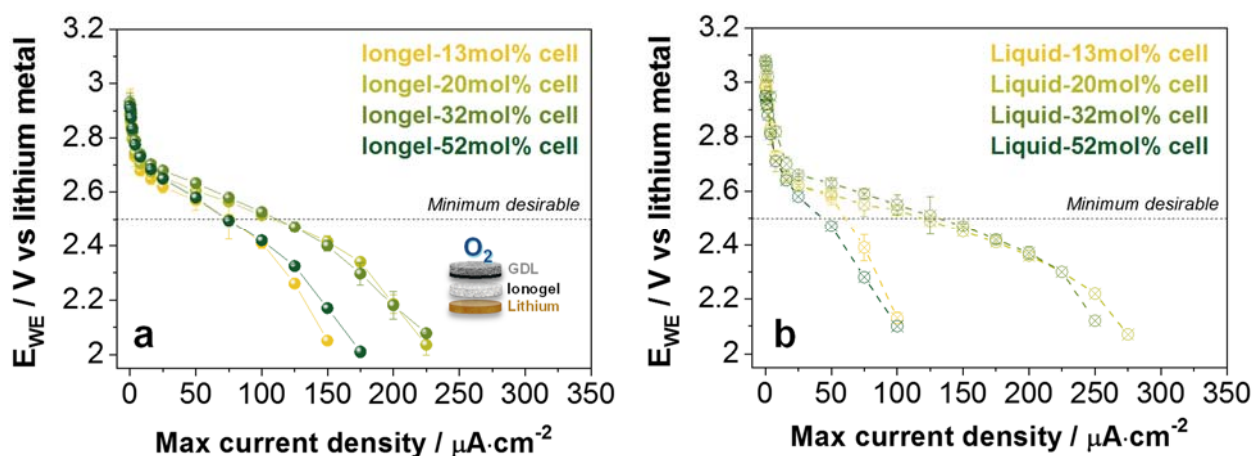
Figure 4. 8. Dynamic discharge of Li-O$_2$ cells at 60 °C (rate test): discharge potential against current density at increasing LE salt concentrations of a) Iongel and b) Liquid electrolytes.

Results on iongel-based cells (Figure 4.8a) showed that electrolytes with intermediate salt-concentration could be cycled at higher current rates (100 μA·cm^{-2} for Iongel-20mol% and Iongel-32mol% cells) than Iongel-13mol% and Iongel-52mol% cells (~75 μA·cm^{-2}). Considering all results, 50 μA·cm^{-2} was selected as current density for further galvanostatic testing, with an average discharge potential of ~ 2.6 V.

Within cells using liquid electrolytes (Figure 4.8b), electrolytes with intermediate salt concentrations showed the highest current values (125 μA·cm^{-2} for Liquid-20mol% and Liquid-32mol%), similarly to iongel-based cells.

This test was also carried out at 25 °C on cells with electrolytes having the lowest salt concentrations (13mol% and 20mol%, both liquid and polymeric electrolytes). In these conditions, 20 μA·cm^{-2} seemed to be the acceptable rate. Those current rates were similar to the ones reported in literature for cells using [DEME][TFSI]-based ILE at room temperature[9].

4.6.3 Dynamic discharge (multiple loops)

As seen in Chapter 2 (Figure 2.7), when a dynamic discharge loop was completed, only a small portion of the cell discharge capacity was used. Subsequently, as soon as the cell was no longer polarized (OCV), the potential tends to reach equilibrium over time until $dE_{WE}/dt \sim 0$ ($E1_{eq}$, $E2_{eq}$, etc.). Once the potential was stable (usually closed to initial cell potential at OCV), cells could be discharged again. This operation (dynamic discharge) could be repeated several times, until no capacity was left and $E_{eq} \leq 2$ V. In every loop, cells were able to discharge until a specific current density, named as i_{max1}, i_{max2}, etc. These two sets of data – e.g. $E1_{eq}$ and i_{max1} - were also used to analyze further the different electrolytes developed in this chapter.

When the equilibrium polarization potentials at OCV ($E1_{eq}$, $E2_{eq}$, etc.) were plotted versus the cumulative discharge capacities of cells, the shape of the curve mimic the one of a galvanostatic discharge (Figure 4.9a). According to the results, cells using iongel with higher salt concentrations lead to higher cumulative capacities (32mol% > 20mol% > 13mol% iongels). This could be explained as the equilibrium potentials are proportional to the amount of mobile ions present in the electrolyte (higher polarization effect for higher ion-concentrated LE). This rule was no longer followed on cells with the superconcentrated electrolyte (Iongel-52mol%), in which the viscosity, kept being the dominant resistance force for ion transport and ion mobility, was then significantly reduced (low polarization).

In addition, cells using liquid-based electrolytes were also tested for comparison (Figure 4.8c). Cells using iongels presented lower polarizations than cells using liquid electrolytes, exhibiting lower cumulative capacities and a difference in equilibrium potentials of 0.1 V (2.7 and 2.8 V for iongel and liquid electrolyte cells, respectively).
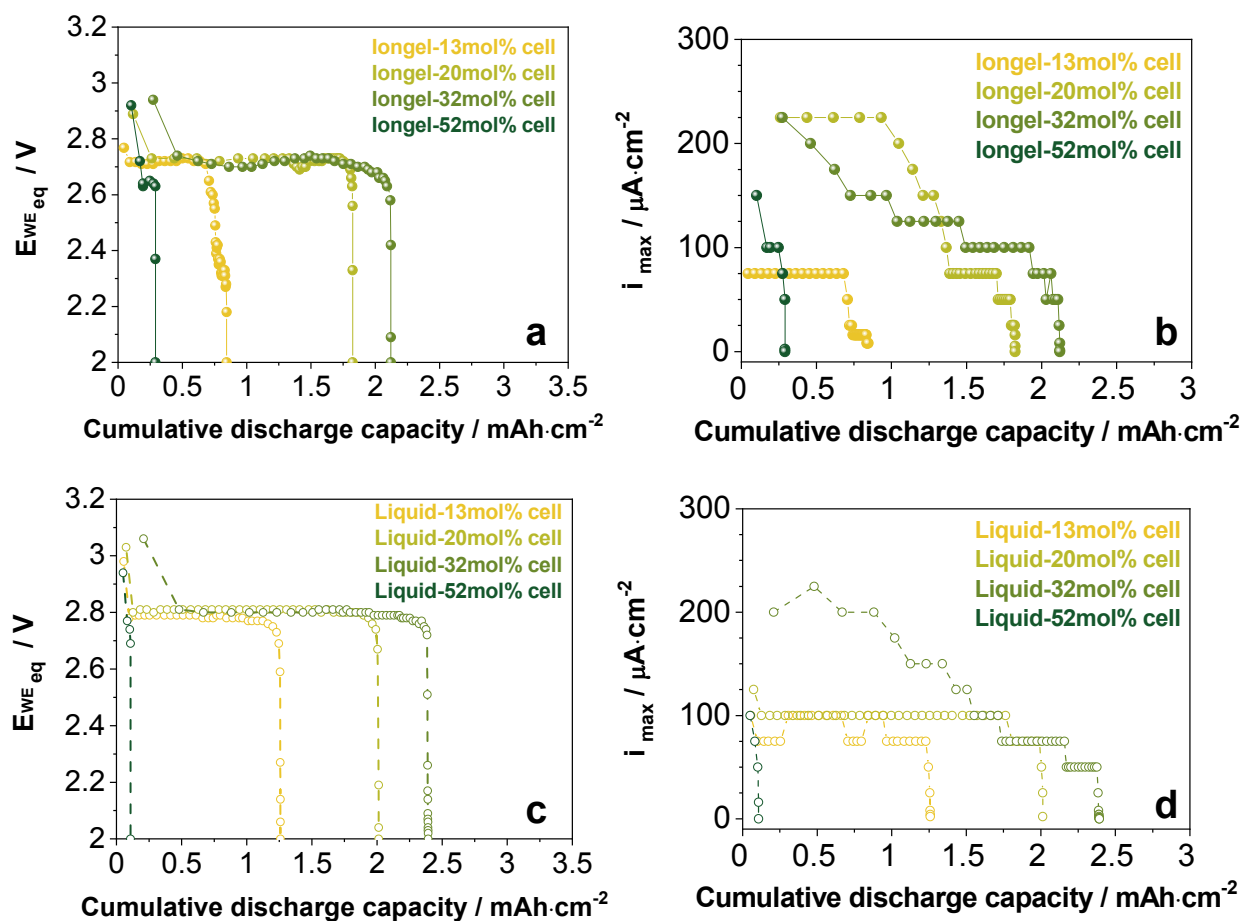
Figure 4. 9. Dynamic discharge curves in Swagelok Li-O_2 cells at 60 °C. Equilibrium polarization potential at OCV ($E1_{eq}$, $E2_{eq}$, etc.) against cumulative discharge capacity achieved after each consecutive loops in cells with a) Iongels and c) Liquid electrolytes. Maximum current densities (i_{max1}, i_{max2}, etc.) achieved at the end of each discharge loop in cells with b) Iongel and d) Liquid electrolytes.

On the other hand, the maximum currents achieved on each loop (i_{max1}, i_{max2}, etc.) also played an important role in the final cumulative discharge capacity. Figure 4.9b shows how these current rates were much higher during discharge of cells using Iongel-20mol% and Iongel-32mol% electrolytes, with maximums of 225 µA·cm⁻² (~ 75 and 150 µA·cm⁻² for Iongel-13mol% and Iongel-52mol%, respectively). Cells with liquid electrolytes also presented a similar trend (Figure 4.9d).

4.6.4 Galvanostatic discharge/charge

Afterwards, Li-O$_2$ iongel cells were fully discharged/charged in galvanostatic mode at the selected rate (50 µA·cm^{-2}), temperature (60 °C), and after 3 h conditioning at OCV. Figure 4.9 shows that the absolute discharge capacity of the cell using Iongel-13mol% electrolyte (3.3 mAh·cm^{-2}) was the highest of the group and three times higher than the cell with superconcentrated Iongel-52mol% electrolyte. However, cell with Iongel-20mol% electrolyte seemed to have the highest Coulombic efficiency (100%, 2.5 mAh·cm^{-2}).

Same test was also done at a higher rate (0.1 mA·cm^{-2}), obtaining lower capacities (~ 0.7 mAh·cm^{-2}, value for all cells with iongel electrolytes) and confirming the results obtained on the dynamic discharge test.
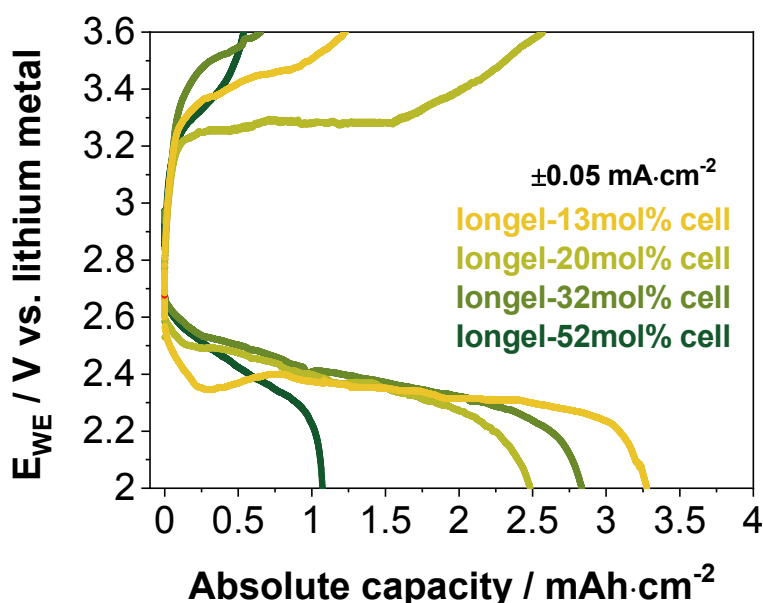
Figure 4. 10. Potential versus absolute capacity obtained for Li-O$_2$ cells with different iongels at ± 0.05 mA·cm^{-2}.

4.6.5 Cycling with limited capacity

Lastly, Li-O$_2$ cells were cycled with limited capacity (0.2 mA·cm^{-2}) at 50 µA·cm^{-2} and 2/3.6 V as cut-off potentials. Figure 4.11a displays the discharge capacity retention of the cells with iongels. Due to their lack of performance on previous tests, cells with superconcentrated iongel were not further tested.

Cells with Iongel-13mol% and Iongel-20mol% electrolytes started to fade after 25 cycles, although the fading of the 20mol% one seemed to be slightly smoother. The cyclability of cells with liquid electrolytes was also undertaken for comparison (Figure 4.11b). Cell with Liquid-13mol% electrolyte presented the best capacity retention, keeping 100% of the discharge capacity for 22 cycles.

Based on these results, we can conclude that cells using iongel-based electrolytes had higher cyclability than cells using liquid electrolyte.
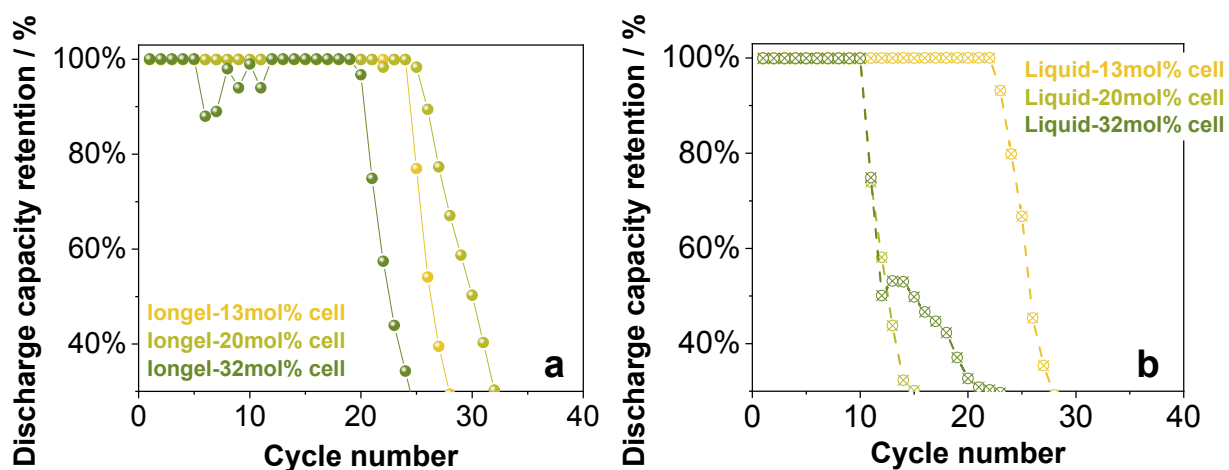
Figure 4. 11. Discharge capacity retention versus cycle number at ± 0.05 mA·cm^{-2} with limited capacity (0.2 mAh·cm^{-2}) of Li-O$_2$ cells using a) Iongel and b) Liquid electrolytes.

Second Part

Influence of anion and cation structure on the design of highly conductive iongel electrolytes suitable for Li-O$_2$ batteries

El capítulo 4 -2ª parte, está sujeto a confidencialidad por la autora

El capítulo 5 está sujeto a confidencialidad por la autora

Chapter 6

Conclusions and discussion

In this thesis, new polymeric materials were developed aiming at improving the actual Li-O$_2$ batteries. The goal of different chapters has been focused in the development of polymer-based solid electrolytes and new polymer binders that are suitable for this type of batteries. In our work we aimed at developing materials and methods combining industrially scalable polymerization processes such as UV-photopolymerization, more secure solid electrolytes based in gel electrolytes or iongels, low toxicity solvents such as green glymes or ionic liquids and new ionic compounds including poly(ionic liquid)s, borate salts and fluorinated anions.

In **Chapter 2**, efforts were dedicated on designing gel polymer electrolytes based on state-of-the-art materials such as TEGDME (popular solvent/plasticizer Li-O$_2$ electrolytes, also called G4) or LiMTFSI (widely recognized lithium ion conductor monomer). Firstly, single ion gel polymer electrolytes were compared for the first time to its dual ion Gel Polymer Electrolytes (GPE) counterparts as solid electrolytes for Li-O$_2$ batteries. The comparison was done via common characterization techniques and a new method to evaluate polarization effect during discharge. Remarkably, both GPEs behaved at least as good as their liquid equivalent systems, stimulating the potential of these gels as electrolytes. Furthermore, these results pointed out the challenges associated in the design of all-in-one electrolyte solutions; which highlighted the importance of rational material designs. The approach proposed in this chapter was used as a baseline for the gels optimization in the forthcoming chapters.

In the second half of this Chapter 2 we tried to reduce the amount of solvent used in a gel formulation by incorporating ether-based chains in a single-ion conducting polymer matrix based in boron chemistry. Three functional lithium borate monomers were tailored designed and combined with G4 as a plasticizer to get Single Ion Gel Polymer Electrolytes (SIGPEs); or they were polymerized alone, so Single Ion Polymer Electrolye (SIPE) could be obtained. The role of two types of substituents (borate-

fluorinated or ethoxy groups) and their combination on the borate group was examined via the polymer electrolyte electrochemical properties. Moreover, findings in this chapter showed the versatility of boron-based chemistry and a new set of lithium molten salts at RT were also evaluated for lithium metal batteries for the first time.

In **Chapter 3**, the use of 1,2,3 – Trimethoxypropane, TMP – a greener and low toxicity glyme derived from bio-sourced glycerol – was investigated for the first time as an alternative solvent/plasticizer to linear glymes. GPEs formulation was improved by an optimized combination of tri-, di- and mono- functional acrylates, making more robust gels. GPEs based on TMP plasticizer showed ionic conductivity values as good as its toxic isomer diglyme-based GPE and they presented ability to dissolve and promote Li^+ ions conduction at room temperature. In lithium symmetrical cells, the use of the gels based on TMP lowered potential polarizations at rates as high as 2 $mA \cdot cm^{-2}$. They also had comparable performance to tetraglyme and diglyme-based gels on $Li-O_2$ cells, where TMP-gels presented the highest absolute capacity. Moreover, and beyond lithium-O_2, this greener solvent could be also used in other battery technologies such as lithium-metal or sodium metal/Na-O_2 rechargeable batteries.

Following the spirit of the third chapter, **Chapter 4** also pursued the use of more environmentally friendly plasticizers. For that, tetra-alkyl ammonium based ionic liquids were evaluated as plasticizers to prepare polymer-based iongel soft solid electrolytes.

Firstly, it was presented a comprehensive optimization study in the development of iongel electrolytes based on a low polarization ionic liquid, DEME-TFSI. Within the optimization process, several polymer/ ionic liquid electrolyte ratios and salt concentrations were studied; including superconcentrated gel electrolytes. This process allowed finding iongels with an ionic conductivity close to the liquid counterpart, exceptional thermal stability and great $Li-O_2$ cycling capability with high Coulombic efficiency. Moreover, findings of this chapter confirmed the capability and performance of the polymeric-based ionic liquid electrolytes, which is directly comparable to the one obtained with liquid electrolytes. The optimized and fast approach was used as the baseline for the second part of this chapter.

Subsequently, the second half of Chapter 4 presented a whole new family of polymeric iongel electrolytes based on tailored-designed ionic liquids, using DEME-TFSI as a baseline. Versatility of the UV-photopolymerization process for preparing iongels containing diverse liquid electrolytes was demonstrated. The hunt of alternative materials allowed reporting one of the highest ionic conductivities observed in literature using iongels as electrolytes and based on DEME-FSI ionic liquid. Moreover, this iongel was also able to slow down dendritic growth more efficiently compared to its liquid counterpart. The addition of fluorinated functional groups within the ionic liquid structure greatly enhanced some of the iongels properties; but it was concluded that alternative strategies had to be employed to optimize further the performance at the positive electrode of Li-O$_2$ cells.

Last but not least, in ***Chapter 5*** a whole family of a tunable and functional poly(diallyldimethylammonium)-based poly(ionic liquid) (PIL) was evaluated for the first time as polymer binders for air electrodes in Li-O$_2$ cells. Thus, PIL polymers were tweaked through the tuning of the PIL anion. Up to four air cathodes using PIL binders were evaluated in four types of electrolyte (two liquid and two polymer-based). Despite the electrolyte used, the PIL-based electrodes were able to clearly and effectively enhanced the capacity and cycling capability of the cells analyzed when compared to the well-known lithiated Nafion^{TM}, commonly used as binder. Moreover, and beyond lithium-O$_2$, this new family of binders could be explored in other battery technologies.

Final thoughts

Before concluding this chapter, the results obtained in the individual chapters have been compared from different angles. Overall, different class of polymer electrolytes have been proposed, including GPEs, SIGPEs and SIPEs. According to literature, they got different set of properties that make them attractive from a design point of view, such as ionic conductivity or lithium ion transference number (t_{Li}^+). Actually, it is usually recognized (from a theoretical point of view) that single ion polymer conductors offer an enhanced protection to lithium metal as well as lower overpotentials during full cell cycling due to their higher t_{Li}^+ values. Both are desirable features in Li-O$_2$ batteries, as

presented on Chapter 1. Hence, a discussion on this matter considering the results obtained in this work is presented below.
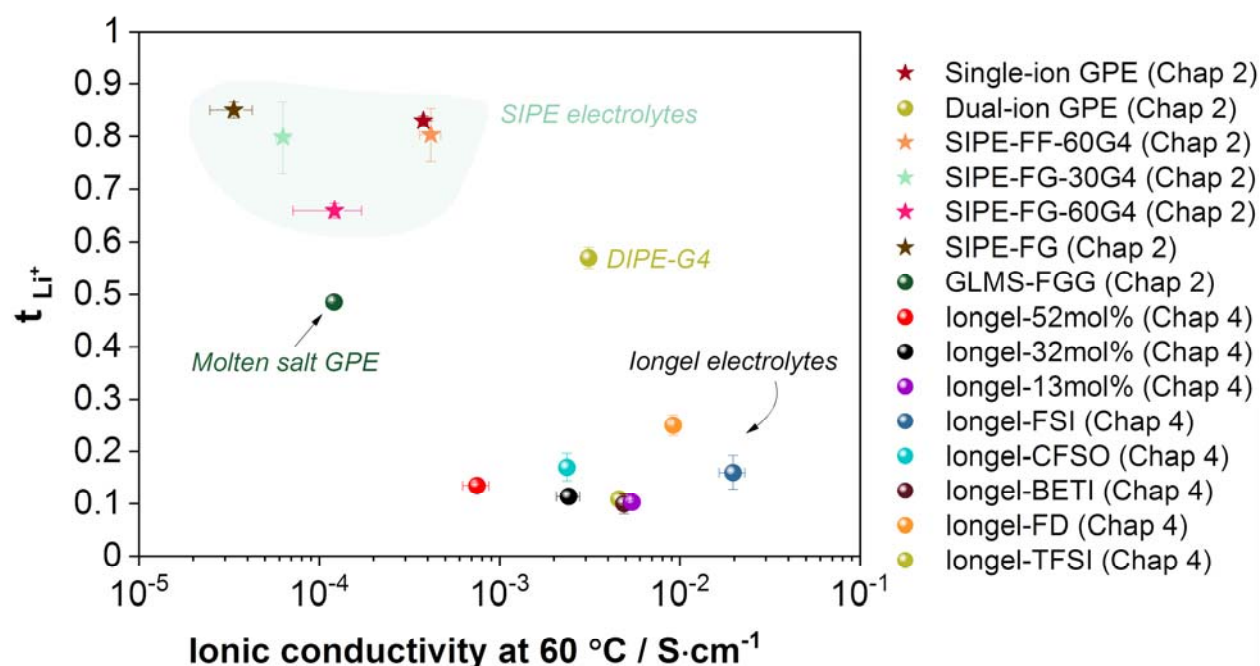
Figure 6. 1. Lithium transference number versus ionic conductivity.

First, lithium transference numbers versus ionic conductivities were plotted. Unfortunately, we did not have t_{Li}^+ data for all the polymer electrolytes developed in the manuscript (such as the ones in Chapter 3), but Figure 6.1 summarizes a good part of them. Looking at the plot, two clouds of data points can be noted, one belonging to single ion conductors (plotted as *stars*), and the other to dual ion conductors (plotted as *spheres*). Overall, systems either have higher t_{Li}^+ and lower conductivities (SIPE); or vice versa (dual ion). But, does this mean that the absolute ionic conductivity number carried by the lithium ions are much higher in single ion than dual ions?

Actually, we can easily quantify this absolute amount by multiplying the ionic conductivity of the electrolyte by its t_{Li}^+ number, which eventually is a proportional percentage. Equivalent results to Figure 6.1 are plotted in Figure 6.2.
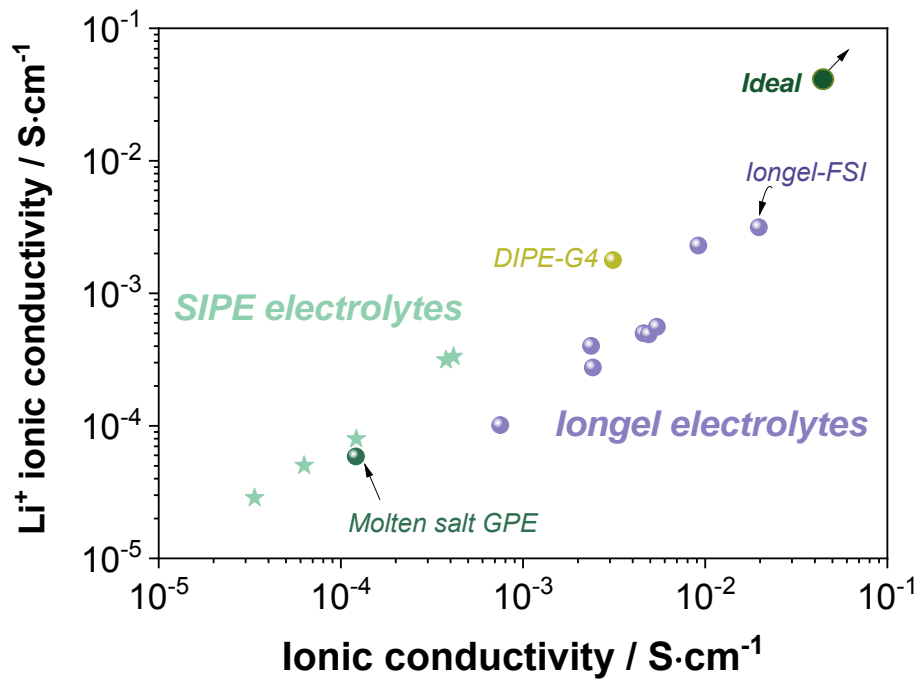
Figure 6. 2. Lithium ion ionic conductivity versus full electrolyte ionic conductivity.

The plot in Figure 6.2 revealed that, actually, the dual ions systems (either aprotic or ionic liquid based) presented a higher absolute ionic conductivity value carried by the lithium ions. For example, Iongel-FSI cell had an ionic conductivity of $1.97 \cdot 10^{-2}$ $S \cdot cm^{-1}$ at 60 °C and an (apparently) low t_{Li}^+ of 0.16. These results might lead to misleading conclusions as, eventually, the ionic conductivity carried by the Li^+ ions is $3.16 \cdot 10^{-3}$ $S \cdot cm^{-1}$ in this membrane, possibly a much higher value than other SIPE systems.

To explore this further we plotted the t_{Li}^+ and the lithium ionic conductivity against the *Critical Current Density* (CCD) of each polymer electrolyte (Figure 6.3). In this case the CCD was defined as the upper value of current density in which the polarization potential was still below 1 V (E_{WE} < 1 V vs Li^0/Li^+), all measured in lithium symmetrical cells.
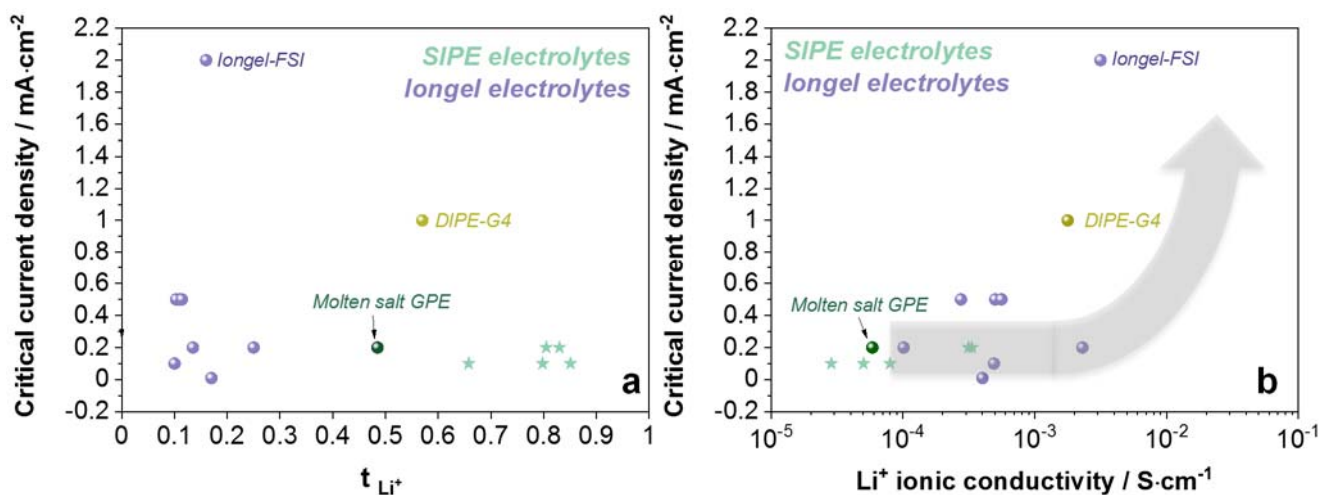
Figure 6. 3. CCD versus a) t_{Li^+}; and b) lithium ionic conductivity.

When looking at Figure 6.3a, it was challenging to find any trend between the CCD and t_{Li^+}, as lower or higher values did not seem to make a real difference in final polarization potentials. When plotted against the lithium ionic conductivity values, the data points re-ordered in a different way. It appeared that higher lithium conductivities led to an increased current rate stability.

Maybe, it would be a good exercise to present these type of plots when analyzing single and dual ion conductors. Systems that had a higher ionic conductivity carried by the lithium ions led to better results. Nonetheless, it appeared that it was not an exclusive property of single ion conductor cells; possibly limited by the remaining relatively low conductivities of SIPEs. Finally, this piece of information should never been taken alone, since many other properties or events involving the electrochemistry of the cell (i.e. SEI formation) are equally important.
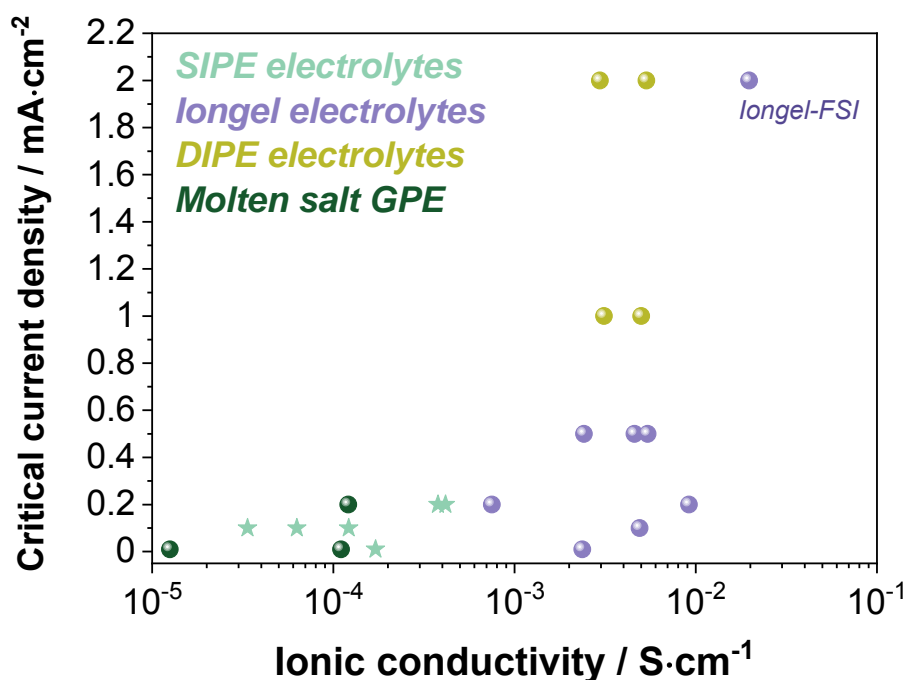
Figure 6. 4. CCD versus ionic conductivity of all the polymer-based electrolytes developed in this work.

Furthermore, all dual ion GPEs (plotted as *spheres*) and the SIGPEs and SIPEs (plotted as *stars*) developed in this work were plotted in Figure 6.4. This time, the CCD is presented against the ionic conductivity of the electrolyte. According to the results, there seem to be a correlation between ionic conductivity and performance against lithium metal. In this case, dual ion systems (Iongel-FSI, GPE-80G2 and GPE-80G4 electrolytes from Chapter 3) seemed to be the ones with a higher performance from this perspective.

To finalize, the influence of the t_{Li^+} in the results achieved in Li-O$_2$ cells was also evaluated. This time the selection of the comparative parameter was challenging as the systems presented in different chapters were discharged at different current densities and/or temperatures. One common test to the majority of them was the dynamic discharge (also called rate test in the manuscript). Thus, the current density achieved by the cell when the equilibrium potential was 2.5 V during the dynamic discharge, was taken as the reference parameter (in absolute value). Usually, from this point (2.5 V equilibrium potential), the potential started to fade more rapidly and

sharply in the majority of the cells analysed, indicating, amongst other things, a saturated positive electrode.
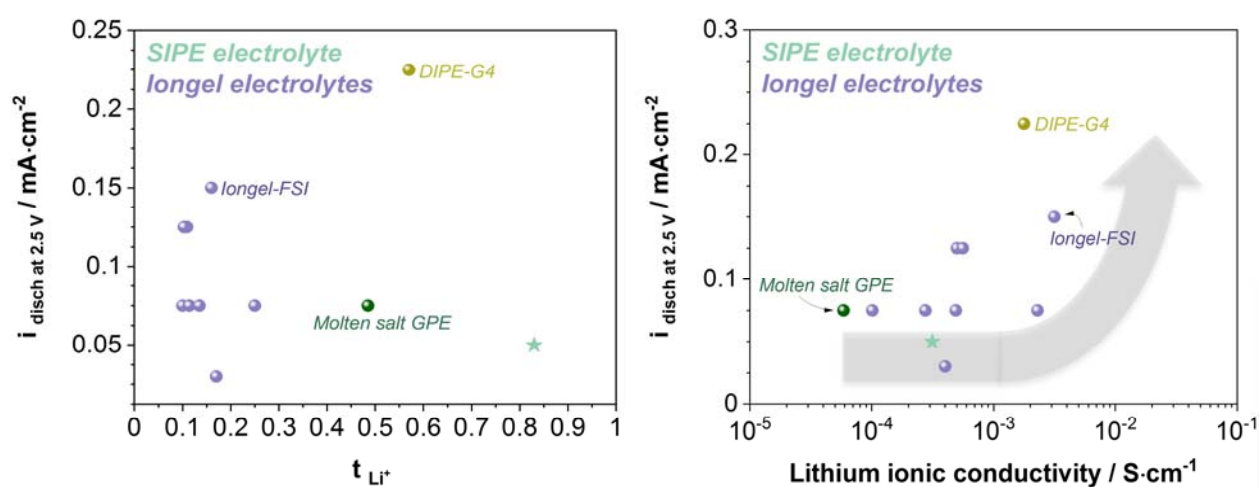
Figure 6. 5. Discharged current density value (absolute value) achieved at 2.5 V potential during dynamic discharged (rate test) versus: a) t_{Li^+}; and b) lithium ionic conductivity.

Likewise Figure 6.3, it was also puzzling to find no trend between the discharge current density value and the t_{Li^+} (Figure 6.5a). The two variables seemed to behave independently. However, when it was plotted against the lithium ionic conductivity values, the data points re-organized in a different manner. Now, a plausible trend seemed to appear, indicating that electrolytes with higher lithium conductivities (usually headed by dual ion systems in this work) led to more rapid and higher performance ionic systems. This final thought reinforces the idea of using this kind of plots for truly comparing different battery cells.

List of acronyms

[BETI]-	Bis(perfluoroethylsulfonyl)imide
[C₃F₉SO₃]-	Nanofluoro-1-butanesulfonate
[DEME]	N,N-Diethyl-N-methyl-N-(2-methoxyethyl) ammonium
[TFSI]	Bis(trifluoromethanesulfonyl)imide
[FSI]-	Bis(fluorosulfonyl)imide
ACN	Acetonitrile
AE	Air electrode
BEV	Battery electric vehicles
CCD	Critical current density
CE	Coulombic efficiency
COP	Conference of the Parties
CV	Cyclic voltammetry
DA	Diethylene glycol diacrylate
DMC	Dimethyl carbonate
DME	Dimethoxyethane
DMSO	Dimethyl sulfoxide
DMTA	Dynamic mechanical thermal analysis
DOL	1,3-dioxolane
DSC	Differential scanning calorimetry
EDS	Energy dispersive spectroscopy
EEA	European Economic Area
EIS	Electrochemical impedance spectroscopy
FCEV	Fuel cell electric vehicles
FD-TFSI	N,N-diethyl-N-methyl-N-((trifluoroethoxy) ethyl) ammonium bis(trifluoro methylsulfonyl)imide
FTIR	Fourier Transform Infrared Spectroscopy
G2, diglyme	Diethylene glycol dimethyl ether

G4, TEGDME, tetraglyme	Tetraethylene glycol dimethyl ether
GDL	Gas diffusion layer
GLMS	Gel containing lithium molten salt
GPE	Gel polymer electrolytes
HEV	Hybrid electric vehicles
IL	Ionic liquids
ILE	Ionic liquid electrolyte
LE	Liquid electrolyte
LIB	Lithium-ion batteries
LiMTFSI	Lithium 1-[3-(methacryloyloxy)-propylsulfonyl]-1-(trifluoromethylsulfonyl)imide
Li-O$_2$	Lithium oxygen batteries
LiTFSI	Lithium bis(trifluoromethanesulfonyl)imide
NASICON	Sodium (Na) Super Ionic CONductor
NiMH	Nickel-metal hydride
NMR	Nuclear magnetic resonance
OCV	Open-circuit voltage
OER	Oxygen-evolution reaction
ORR	Oxygen-reduction reaction
PC	Propylene carbonate
PDADMA-TFSI	Poly(diallyldimethylammonium) bis(trifluoro-methanesulfonyl)imide
PEGA	Poly(ethylene glycol) methyl ether acrylate
PEGDM	Poly(ethylene glycol) dimethacrylate
PHEV	Plug-in hybrid electric vehicles
PIL	Polymer ionic liquid
RT	Room temperature
SEI	Solid electrolyte interphase
SEM	Scanning electron microscopy
SIE	Solid inorganic electrolytes

SIGPE	Single-ion conducting gel polymer electrolytes
SIM	Single ion monomer
SIPE	Single-ion conducting polymer electrolytes
SPE	Solid polymer electrolytes
t_{Li^+}	Lithium transference number
TA	Glycerol propoxylate triacrylate
Tg	Glass transition temperature
TGA	Thermal gravimetrical analysis
THF	Tetrahydrofuran
TME	Toyota Motor Europe
TMP	1,2,3 – Trimethoxypropane
XPS	X-ray photoelectron spectroscopy
XRD	X-ray powder diffraction
σ	Ionic conductivity

List of patents, publications, conference presentations and collaborations

Patents

Cotte, S.; Gueguen, A.; Castro, L.; Vauthier, S.; **Alvarez-Tirado, M**.; Casado, N.; Mecerreyes, D. BINDERS FOR CATHODES OF LITHIUM SECONDARY BATTERY CELLS. EP21306763.0 filing number, December **2021**

Castro, L.; Gueguen, A.; Cotte, S.; **Alvarez-Tirado, M**.; Mecerreyes, D.; Vauthier, S.; Porcarelli, L.; Casado, N. LOW TOXICITY ETHER-BASED ELECTROLYTE COMPOSITION AND METAL-AIR BATTERY COMPRISING THE SAME. EP22305013.9 filing number, January **2022**.

An additional patent protecting part of the work developed in Chapter 4 is currently being drafted.

Publications

Alvarez-Tirado, M.; Castro, L.; Guzmán-González, G.; Porcarelli, L.; Mecerreyes, D. Single- Versus Dual-Ion UV-Cross-Linked Gel Polymer Electrolytes for Li-O$_2$ Batteries. *ACS Appl. Energy Mater.* **2021**, *4*, 295–302

Guzmán-González, G.; Vauthier, S.; **Alvarez-Tirado, M.**; Cotte, S.; Castro, L.; Guéguen, A.; Casado, N.; Mecerreyes, D. Single-ion Lithium Conducting Polymers with High Ionic Conductivity Based on Borate Pendant Groups. *Angew. Chemie Int. Ed.* **2021**, *202114024*.

Alvarez-Tirado, M.; Guzmán-González, G.; Vauthier, S.; Cotte, S.; Guéguen, A.; Castro, L.; Mecerreyes, D. Designing Boron-Based Single-Ion Gel Polymer Electrolytes for Lithium Batteries by Photopolymerization. *Macromol. Chem. Phys.* **2022**, *n/a* (n/a), 2100407.

Alvarez-Tirado, M.; Castro, L.; Guéguen, A.; Mecerreyes, D. Iongel soft solid electrolytes based on [DEME][TFSI] ionic liquid for low polarization Li-O$_2$ batteries. *Batteries & Supercaps* **2022**, e202200049.

Alvarez-Tirado, M.; Castro, L.; Qian, S.; Bara, J. E.; Di Genaro, M.; Gkagkas, K.; Guéguen, A.; Mecerreyes, D. 1,2,3 – Trimethoxypropane: a glycerol-derived glyme with low toxicity as electrolyte for Lithium-O$_2$ batteries. *Submitted.*

Alvarez-Tirado, M.; Castro, L.; Guzmán-González, G.; Guéguen, A.; Tomé, L. C.; Mecerreyes, D. Influence of anion and cation structure on the design of highly conductive iongel electrolytes suitable for Li-O$_2$ batteries. *In preparation*

Vauthier, S. †; **Alvarez-Tirado, M.** †; Guzmán-González, G.; Tomé, L.C.; Cotte, S.; Castro, L.; Guéguen, A.; Mecerreyes, D.; Casado, N. High performance pyrrolidinium-based poly(ionic liquid) binders for Li-ion and Li-air batteries. († These authors contributed equally to this work). *Submitted.*

Guzmán-González, G.; **Alvarez-Tirado, M.**; Castro, L.; Guéguen, A.; TBD; Forsyth, M.; Mecerreyes, D. Lithium molten salts at room temperature based on highly delocalized asymmetric borate groups. *In preparation.*

Conference presentations and training schools

Unfortunately, and due to COVID-19 pandemic most of the events on 2020 were cancelled. Since the pandemic started, all events attended during the PhD thesis have been online contributions.

Innovative POLYmers for Lithium Battery Technologies. **Alvarez-Tirado, M.;** Vauthier, S.; Lechartier, M.; Castro, L.; Mecerreyes, D. – *Poster presentation*
Grenoble Energy Conversion & Storage Winter School - ENGINE2019 (40 hours), Grenoble (France)
February 2019

Innovative POLYmers for Lithium Battery Technologies. **Alvarez-Tirado, M.;** Vauthier, S.; Lechartier, M.; Castro, L.; Mecerreyes, D. – *Poster presentation*

4th International Forum on Progress and Trend in Battery and Capacitor Technologies – Power our Future 2019, Vitoria-Gasteiz (Spain)
July 2019

Chemistry of Electric Storage Materials Summer School (5 ECTS credits), organized by Uppsala University (Sweden) – Online attendance
June 2021

Development of Effective, Safer and Fast UV-cured Solid Gel Polymer Electrolytes for Lithium-O_2 rechargeable batteries. **Alvarez-Tirado, M.;** Castro, L.; Guzmán-González, G.; Porcarelli, L.; Mecerreyes, D. – *Oral presentation (online)*
240th ECS Meeting in Orlando, Florida (USA)
October 2021

Framework of work

This thesis has been done as part of the European Industrial Doctorate programme POLYTE-EID (GA N°765828), hence there was a very close collaboration between UPV/EHU-POLYMAT (San Sebastián, Spain) and Toyota Motor Europe (Zaventem, Belgium). Actually, the polymer materials development and characterization was developed at UPV/EHU-POLYMAT labs, and all the electrochemical was undertaken at Toyota Motor Europe facilities. Half of the PhD duration was spent at each organization (1.5 years each).

The author would like to thank the simulation team at Toyota Motor Europe (Belgium) for their contribution in Chapter 3. I would also like to thank Prof Jason Bara and co-workers at Alabama University (USA) for the provision of 1,2,3 – TMP solvent and their valuable discussions on the topic as part of Chapter 3.

Finally, I would also like to give a big *gracias* to Dr Gregorio Guzmán-González for the synthesis of the monomers and molten salts of Chapter 2 and our invaluable discussions about electrochemistry.

TOYOTA

TOYOTA MOTOR EUROPE

POLYMAT

eman ta zabal zazu

Universidad del País Vasco
Euskal Herriko Unibertsitatea

POLYTE - EID

Innovative POLYmers for Lithium Battery TEchnologies

European Industrial Doctorate

Marie Skłodowska-Curie Actions

Resumen

La temperatura media mundial entre 2011 y 2020 fue ~1.20 °C más caliente que en el nivel preindustrial, convirtiéndola en la década más cálida registrada hasta la fecha. En Europa, este aumento fue aún más rápido durante este periodo (~2 °C). Debido a esta situación, los países miembros de la *Convención Marco De Las Naciones Unidas Sobre el Cambio Climático* (UNFCCC) se comprometieron en el Acuerdo de París a limitar el aumento de la temperatura global por debajo de los 2 °C por encima del nivel preindustrial e intentar limitar el aumento a 1.5 °C [1]. Sin embargo, sin recortes drásticos en las emisiones globales de gases de efecto invernadero, incluso el límite de 2 °C ya se superaría antes de 2050.
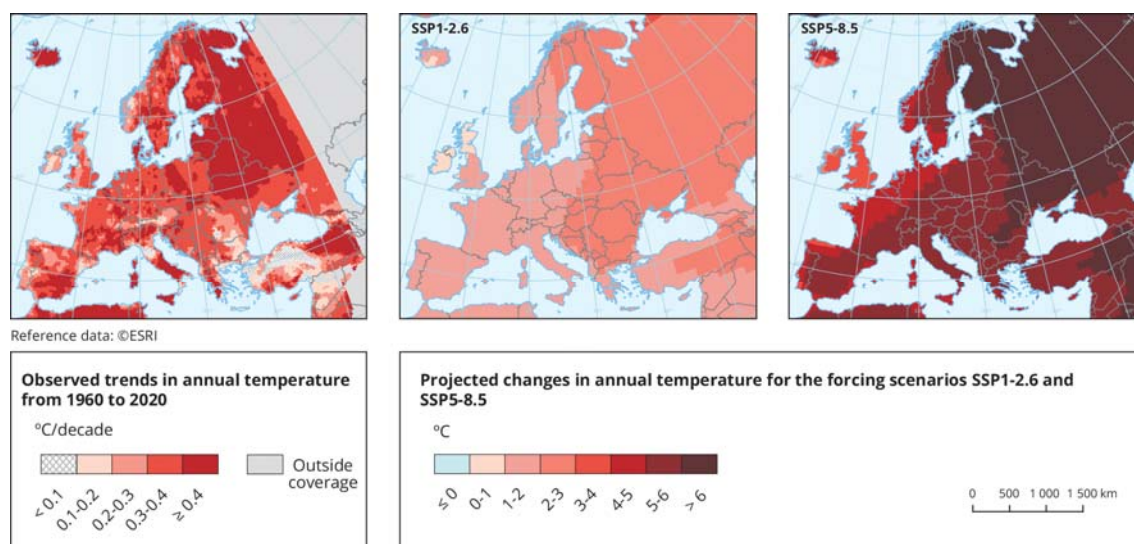

Figura S1. Tendencia de temperatura media anual observada de 1960 a 2020 (panel izquierdo) y cambio de temperatura proyectado para el siglo XXI bajo diferentes escenarios SSP (panel derecho) en Europa. Fuente: Agencia Europea de Medio Ambiente (https://www.eea.europa.eu/ims/global-and-european-temperatures)

Como parte de la estrategia de lucha contra el cambio climático, los 27 Estados miembros de la UE esbozaron el Pacto Verde Europeo (*European Green Deal*), una propuesta comprometida a convertir a la UE en un continente climáticamente neutro para 2050 [2]. Para lograrlo, las emisiones deben reducirse en al menos un 55 % para 2030 (en comparación con los niveles de 1990). De hecho, el transporte representa un ~25% de las emisiones de gases de efecto invernadero. Y dentro de este tipo de

emisiones, el transporte por carretera es responsable del 72 % (según datos de 2019 de todo el transporte nacional e internacional) [3].

En este contexto, los sistemas de almacenamiento de energía, y más en particular las baterías, son habilitadores tecnológicos clave para combatir el cambio climático. Para satisfacer esta enorme demanda, las baterías de litio-ión deben complementarse con otras tecnologías. Las baterías de $Li-O_2$ o de litio-aire son muy prometedoras desde el punto de vista de densidad de energía. Sin embargo, esta tecnología no está suficientemente madura para su comercialización y es necesario desarrollar nuevos materiales para que la tecnología sea más eficiente y segura.
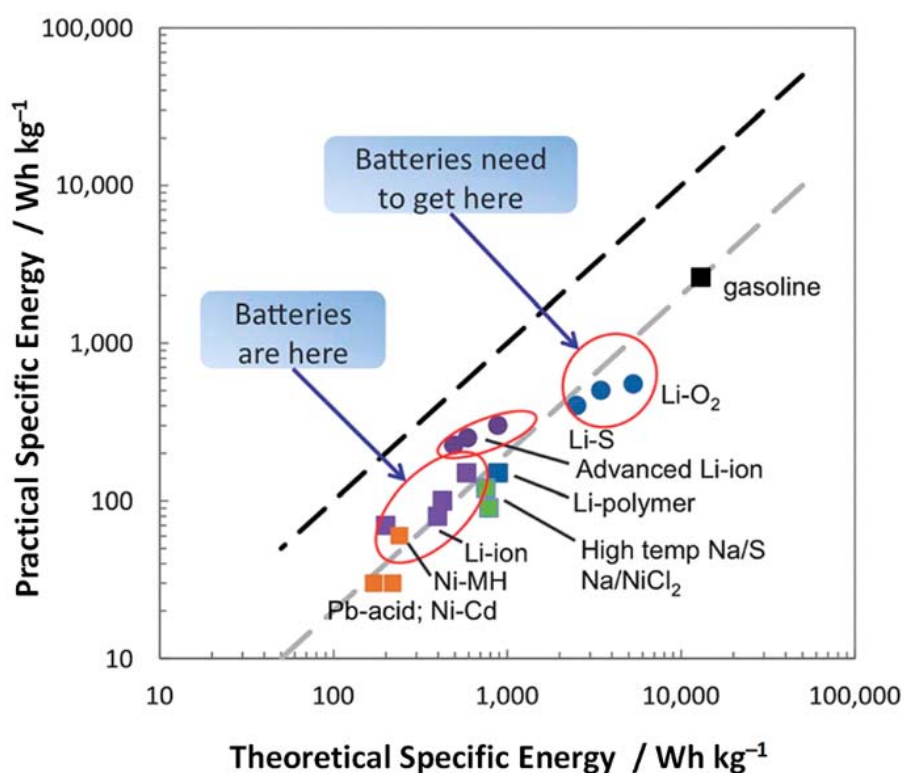

Figura S2. Energía específica versus densidad de energía teórica de baterías actuales y proyección de baterías avanzadas más allá de las baterías de litio-ión (LIB) de última generación en comparación con gasolina. Reproducido con permiso de la literatura [4].

En este contexto, el principal objetivo de esta tesis es desarrollar nuevos materiales poliméricos adecuados para baterías de $Li-O_2$ y conseguir baterías más ecológicas, seguras y de mayor rendimiento.

El trabajo se ha desarrollado dentro de una colaboración entre industria y academia. La síntesis, optimización y caracterización de los nuevos materiales poliméricos se ha llevado a cabo en POLYMAT - Universidad del País Vasco (San Sebastián, España). Por otro lado, la mitad del tiempo de esta tesis doctoral se ha desarrollado en Toyota Motor Europe (Zaventem, Bélgica), donde se ejecutó la caracterización electroquímica en celdas simétricas de litio y celdas de Li-O$_2$.

Nuestro trabajo se ha centrado en el desarrollo de electrolitos sólidos poliméricos y nuevos aglutinantes/ligantes poliméricos que sean adecuados para este tipo de baterías. En general, se proponen materiales y métodos que combinan procesos de polimerización escalables industrialmente, como la foto-polimerización por UV, desarrollo de electrolitos sólidos más seguros basados en geles o geles iónicos (iongeles), disolventes de baja toxicidad como glimas verdes o líquidos iónicos; así como nuevos compuestos iónicos o sales de litio líquidas a temperatura ambiente.

En la primera mitad del Capítulo 2 de este manuscrito, se presenta el diseño de electrolitos en gel (GPE) basados en materiales del estado del arte, usando, por ejemplo, éter dimetílico del tetraetilenglicol, TEGDME (un disolvente/plastificante común usado en Li-O$_2$) o (trifluorometano) sulfonimida metacrilato de litio, LiMTFSI (uno de los monómeros conductores (exclusivo) de iones de litio más conocidos). En primer lugar, geles conductores de iones de litio (SIGPE) se comparan por primera vez en celdas de Li-O$_2$ con sus geles homólogos conductores de aniones y cationes (GPE). La comparación se realizó mediante técnicas de caracterización electroquímica comunes y un nuevo método para evaluar el efecto de polarización durante la descarga. Sorprendentemente, ambos geles se comportaron de forma similar a sus electrolitos líquidos equivalentes, estimulando el potencial de estos geles como electrolitos sólidos. El enfoque propuesto en este capítulo se utilizó como base para la optimización de electrolitos en gel en los próximos capítulos.

En la segunda mitad de este Capítulo 2, se intenta reducir la cantidad de disolvente/plastificante utilizado en los geles incorporando cadenas de éter en la matriz polimérica. Para ello, se diseñan tres monómeros de boro funcionales (y conductores exclusivos de litio ión), combinándolos con TEGDME como plastificante y así obtener SIGPEs. Se analizaron como grupos funcionales grupos borato-fluorados o borato-etoxi, así como sus posibles combinaciones. Los hallazgos en este

capítulo muestran la versatilidad de esta química y, del mismo modo, también se evalúa por primera vez un nuevo conjunto de sales de litio líquidas a temperatura ambiente para baterías de litio metal.
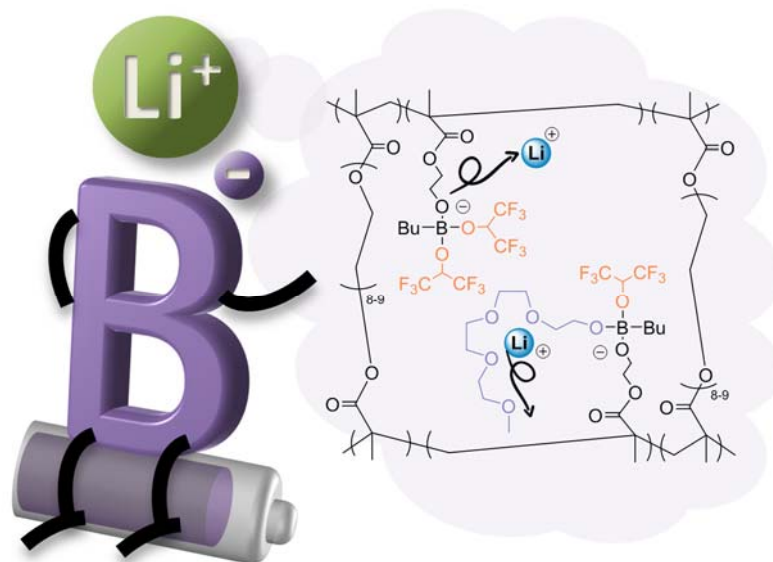

Figura S4. Geles funcionales y conductores exclusivos de iones de litio pasados en la química del boro.

En el Capítulo 3 se investigó por primera vez el uso de 1,2,3 – trimetoxipropano (TMP) como disolvente/plastificante alternativo a las glimas lineales tóxicas, usadas comúnmente en este tipo de baterías. El TMP es una glima más ecológica y de baja toxicidad derivada del glicerol (origen biológico). Adicionalmente, la formulación de los GPEs se mejoró mediante una combinación optimizada de acrilatos trifuncionales, difuncionales y monofuncionales, generando geles más robustos. Los GPEs que contenían TMP como plastificante (GPE-TMP) mostraron valores de conductividad iónica tan buenos como los GPEs que contenían diglimas lineales. En celdas simétricas de litio, el uso de GPE-TMP redujo las polarizaciones de potencial a corrientes de hasta 2 mA·cm^{-2}. Más allá de celdas de Li-O$_2$, este disolvente más ecológico podría usarse en otras tecnologías, como las baterías recargables de litio-metal o sodio metal/Na-O$_2$.
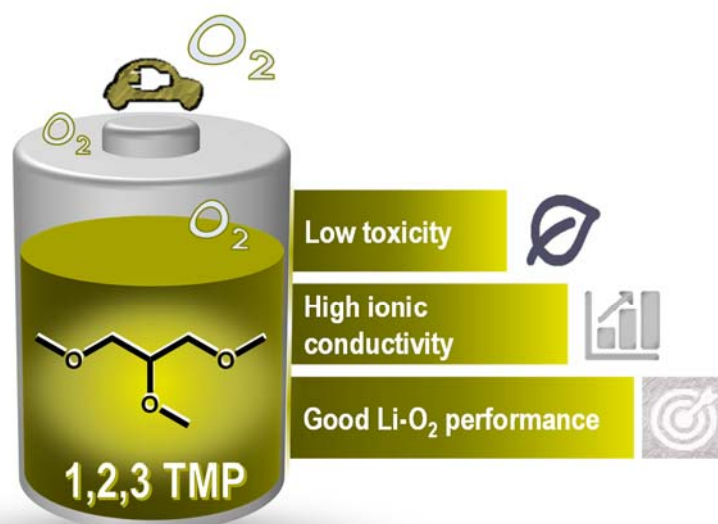
Figura S5. Geles funcionales usando 1,2,3 TMP como plastificante, un disolvente orgánico más ecológico y de baja toxicidad.

Siguiendo el espíritu del tercer capítulo, en el Capítulo 4 también se persiguió el uso de plastificantes más amigables con el medio ambiente. Para ello, se evaluaron líquidos iónicos a base de tetraalquilamonio como plastificante para preparar iongeles, electrolitos iónicos sólidos blandos en los que se usan líquidos iónicos como plastificantes.

En primer lugar, se presenta un estudio de optimización para el desarrollo de iongeles basados en DEME-TFSI (bis(trifluorometilsulfonil)imida de dietilmetilamonio), un líquido iónico de baja polarización. Este proceso de optimización permitió encontrar iongeles con una conductividad iónica cercana a celdas con electrolito líquido, una estabilidad térmica excepcional y una gran capacidad de ciclado en celdas de Li-O$_2$.

Posteriormente, en la segunda mitad del Capítulo 4, se presenta toda una nueva familia de iongeles basados en líquidos iónicos usando DEME-TFSI como base. Así, se demuestra la versatilidad del proceso de foto-polimerización por UV para preparar iongeles. La búsqueda de materiales alternativos permitió reportar una de las conductividades iónicas más altas observadas en literatura utilizando iongeles como electrolitos. Además, este iongel también pudo ralentizar el crecimiento dendrítico de manera más eficiente. La adición de grupos funcionales fluorados dentro de la

estructura del líquido iónico mejoró en gran medida algunas de las propiedades de los iongeles; pero se concluyó que debían emplearse estrategias alternativas para optimizar aún más el rendimiento en el electrodo positivo de las celdas de Li-O_2.
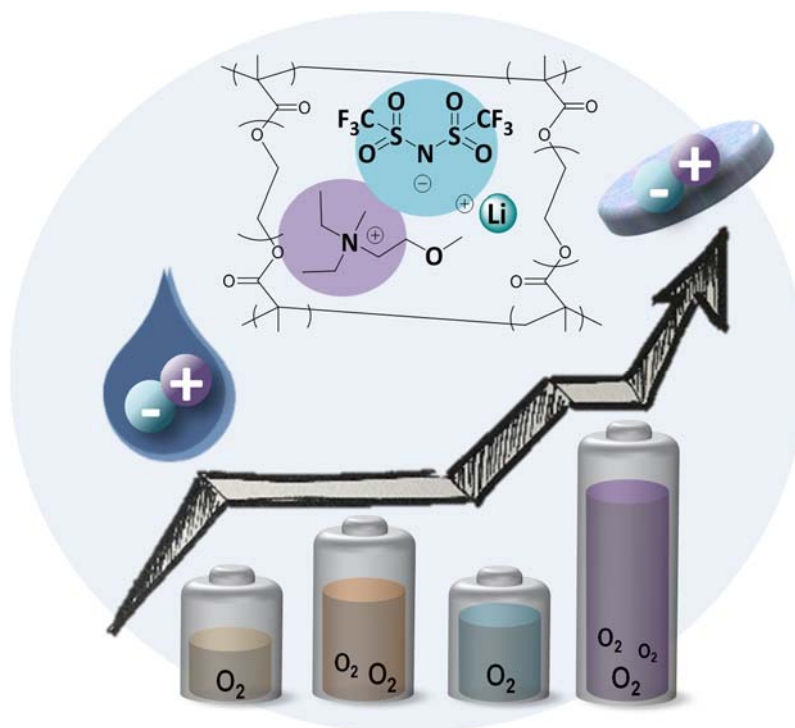

Figura S6. Iongeles basados en un líquido iónico de baja polarización.

Por último, en el Capítulo 5 se evalúa por primera vez un set de 4 polímeros iónicos basados en poli(dialildimetilamonio) (PIL). Esta familia de polímeros se caracteriza por ser funcionales y flexibles en su química. Es este caso se evaluaron como aglutinantes/ligantes en el electrodo positivo de celdas de Li-O_2. Se evaluaron hasta cinco electrodos diferentes (cuatro de ellos con los nuevos PIL propuestos; y uno de ellos utilizando Nafion[TM] como referencia) en cuatro tipos de electrolitos (dos líquidos y dos de base polimérica). Independientemente del electrolito utilizado, los electrodos basados en los PIL pudieron mejorar de manera clara y efectiva la capacidad y la ciclabilidad de las celdas analizadas en comparación con Nafion[TM]. Debido a este rendimiento, esta nueva familia de ligantes podría explorarse en otras tecnologías de baterías más allá de litio-O_2.

Referencias

(1)   Nations, U. COP26 - A pivotal moment in the fight against climate change.

(2)   European Commission. Energy and the Green Deal | European Commission https://ec.europa.eu/info/strategy/priorities-2019-2024/european-green-deal/energy-and-green-deal_en (accessed Jan 12, 2022).

(3)   European Environment Information and Observation Network (Eionet). Greenhouse gas emission intensity of fuels and biofuels for road transport in Europe https://www.eea.europa.eu/data-and-maps/indicators/greenhouse-gas-emissions-intensity-of-1/assessment.

(4)   Kwak, W.-J.; Rosy; Sharon, D.; Xia, C.; Kim, H.; Johnson, L. R.; Bruce, P. G.; Nazar, L. F.; Sun, Y.-K.; Frimer, A. A.; Noked, M.; Freunberger, S. A.; Aurbach, D. Lithium–Oxygen Batteries and Related Systems: Potential, Status, and Future. *Chem. Rev.* **2020**, *120* (14), 6626–6683.

Universidad
del País Vasco

Euskal Herriko
Unibertsitatea

Marta Alvarez Tirado | PhD Thesis 2022